

Material tests for the characterisation of replicated solid clay brick masonry

Jafari, Samira; Esposito, Rita

Publication date

2017

Document Version

Final published version

Citation (APA)

Jafari, S., & Esposito, R. (2017). *Material tests for the characterisation of replicated solid clay brick masonry*. Delft University of Technology.

Important note

To cite this publication, please use the final published version (if applicable).
Please check the document version above.

Copyright

Other than for strictly personal use, it is not permitted to download, forward or distribute the text or part of it, without the consent of the author(s) and/or copyright holder(s), unless the work is under an open content license such as Creative Commons.

Takedown policy

Please contact us and provide details if you believe this document breaches copyrights.
We will remove access to the work immediately and investigate your claim.

<i>Project number</i>	C31B67
<i>File reference</i>	C31B67WP1-12
<i>Date</i>	August 16, 2017
<i>Corresponding author</i>	Samira Jafari (s.jafari@tudelft.nl)

TU Delft Large-Scale Testing Campaign 2016

MATERIAL TESTS FOR THE CHARACTERISATION OF REPLICATED SOLID CLAY BRICK MASONRY

*Authors: Samira Jafari, Rita Esposito
Collaborators: Iren Frana, Jakub Pawlowicz, Edwin Meulman*

Cite as: Jafari, S., Esposito, R. *Material tests for the characterisation of replicated solid clay brick masonry.* Report No. C31B67WP1-12, August 16 2017. Delft University of Technology.

This document is made available via the website 'Structural Response to Earthquakes' and the TU Delft repository. While citing, please verify if there are recent updates of this research in the form of scientific papers.

All rights reserved. No part of this publication may be reproduced, stored in a retrieval system of any nature, or transmitted, in any form or by any means, electronic, mechanical, photocopying, recording or otherwise, without the prior written permission of TU Delft.

TU Delft and those who have contributed to this publication did exercise the greatest care in putting together this publication. This report will be available as-is, and TU Delft makes no representations of warranties of any kind concerning this Report. This includes, without limitation, fitness for a particular purpose, non-infringement, absence of latent or other defects, accuracy, or the presence or absence of errors, whether or not discoverable. Except to the extent required by applicable law, in no event will TU Delft be liable for on any legal theory for any special, incidental consequential, punitive or exemplary damages arising out of the use of this report.

This research work was funded by NAM Structural upgrading stream.

Table of Contents

1	Introduction.....	4
2	Nomenclature	6
2.1	Symbols.....	6
2.2	Abbreviations.....	8
3	Construction of the samples	9
4	Flexural and compressive strength of mortar.....	10
4.1	Testing procedure.....	10
4.2	Experimental results.....	10
5	Compression strength of masonry unit	13
5.1	Testing procedure.....	13
5.2	Experimental results.....	14
6	Flexural strength of masonry unit.....	16
6.1	Testing procedure.....	16
6.2	Experimental results.....	17
7	Density of clay brick masonry	19
8	Compression properties of masonry	20
8.1	Testing procedure.....	20
8.2	Experimental results.....	23
9	Flexural strength of masonry	37
9.1	Testing procedure.....	37
9.2	Experimental results.....	39
10	Bond strength of masonry.....	48
10.1	Testing procedure.....	48
10.2	Experimental results.....	48
11	Shear strength of masonry.....	51
11.1	Testing procedure.....	51
11.2	Experimental results.....	52
11.3	Comparison between the properties of standard triplet and modified triplet.....	57
12	Comparison with values proposed by standards.....	58
12.1	Characteristic compressive strength of masonry.....	58
12.2	Elastic modulus of masonry.....	59
12.3	Stress-strain relationship for masonry in compression.....	59
12.4	Characteristic out-of-plane flexural strengths of masonry.....	60
12.5	Characteristic shear properties of masonry	60
12.6	Comparison with Table F.2 in NPR 9998:2017.....	61
13	Comparison between the properties of single and double wythe specimens.....	62
14	Summary and properties overview.....	65
	References	68

Appendix A.....	70
-----------------	----

1 Introduction

The detached houses built before 1945 in the Netherlands were commonly made of either single or double wythe walls, having solid clay bricks and general purpose mortar. Despite the widespread application of double wythe masonry walls, knowledge regarding the seismic response of these structures at material level is relatively limited in the literature. Therefore, an experimental study was conducted within the "NAM Structural Upgrading Project" developed at TU Delft in 2016, aiming to pursue the dual purpose of providing a complete characterisation of solid clay brick masonry, both single and double wythe, as well as serving as companion tests for the large-scale component tests, developed in WP3 [1]. Moreover, a secondary aim was to compare the properties of the clay brick masonry with respect to the number of wythe, since this information is limited in the literature.

The current research study aims to extensively characterise the mechanical properties of solid clay brick masonry as well as serve as input for the assessment tools such as numerical and analytical models. By using well-designed displacement-control testing set-ups, the compression, bending and shear properties of masonry specimens were measured, indicating strength, stiffness and softening post-peak behaviour of solid clay brick masonry. A set of required input masonry properties pursued within this research is listed in Table 1. The two types of the solid clay brick masonry used are as follows:

- Single wythe specimens having thickness of 100 mm and "Running" bond pattern (Figure 1a).
- Double wythe specimens having thickness of 210 mm and "Dutch cross" bond pattern (Figure 1b).

More detailed information regarding the dimensions of the specimens can be found on the dedicated report [1].

A comprehensive overview of the behaviour of masonry constituents (brick and mortar) and masonry at material level is reported in this document. The flexural and compressive strength of mortar and masonry unit (brick) is provided from Section 4 to Section 6. The density of masonry is reported in Section 7. The compression, bending and shear properties of single and double wythe masonry are reported from Section 8 to Section 11. A comparison between the results obtained from tests and those values proposed in the standards is reported in Section 12. An Analysis of the compression and the shear properties of masonry with respect to the number of wythe is conducted in Section 13. Eventually, a summary and an overview of the material properties are reported in Section 14.

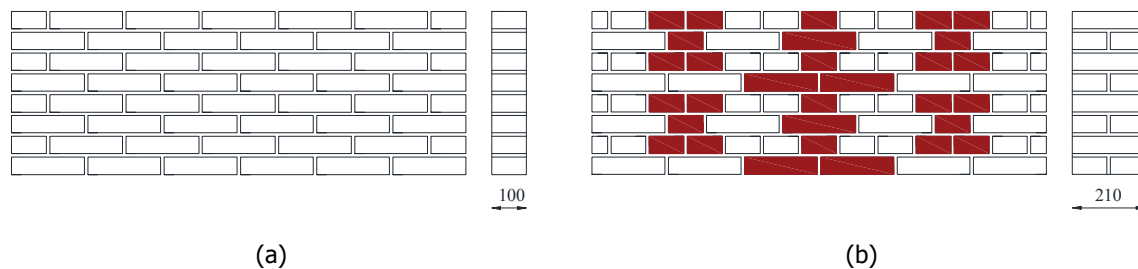


Figure 1 – Adopted bond pattern: (a) Running bond pattern for the single wythe wall specimens; (b) Dutch cross bond pattern for the double wythe wall specimens (dimensions are in mm).

Table 1 – Destructive material tests for the characterisation of masonry.

Type of test			Material property
Mortar	Compression		Compressive strength of masonry mortar
	Bending		Flexural strength of masonry mortar
Masonry units	Compression	Single unit	Compressive strength of brick Stress-strain relationship in compression
		Stacked units	Young's modulus of brick Stress-strain relationship in compression
	Bending		Flexural strength of brick Elastic modulus Stress-strain relationship in bending
Masonry	Compression	Vertical	Compressive strength Young's modulus Fracture energy in compression Poisson ratio Stress-strain relationship in compression (pre- and post-peak)
		Horizontal	
	Bending	Out-of-plane	Vertical Flexural strength with plane of failure parallel to bed joints Stress-strain relationship Fracture energy in bending
			Horizontal Flexural strength with plane of failure perpendicular to bed joints Stress-strain relationship Fracture energy in bending
		In-plane	Vertical Flexural strength with the moment vector perpendicular to the plane of the wall Stress-strain relationship Fracture energy in bending
	Shear test	Standard triplets	Initial and residual shear strength Initial and residual shear friction coefficient Mode-II fracture energy
		Modified triplets with head joints	Shear stress vs. shear displacement relationship (pre- and post-peak)
	Bond wrench		Flexural bond strength

2 Nomenclature

2.1 Symbols

This report adopts mainly the nomenclature used in Eurocode 6 [2]. In addition, symbols used in the codes for testing are adopted.

α	Masonry (bed joint) angle of internal friction
α_{res}	Masonry (bed joint) residual angle of internal friction
α_k	Characteristic masonry (bed joint) angle of internal friction
ν	Poisson ratio of masonry
μ	Masonry (bed joint) shear strength coefficient
μ_{res}	Masonry (bed joint) residual shear strength coefficient
μ_{ik}	Masonry (bed joint) characteristic coefficient of friction
ε_p	Strain associated with peak strength in vertical compression test
$\varepsilon_{p,h}$	Strain associated with peak strength in horizontal compression test
d_1	Distance between bearing supports
d_2	Distance between loading supports
d_3	Distance between the loading and bearing supports (four-point bending test)
f_b	Normalised compressive strength of masonry unit
f_{bs}	Normalised compressive strength of masonry unit from test on stacked masonry units
f_b^*	Compressive strength of masonry unit
f_{bs}^*	Compressive strength of masonry unit from test on stacked masonry units
f_{bt}	Flexural strength of masonry unit
f_{ik}	Characteristic value of the i -th property
$f_{ik,EC6}$	Characteristic value of the i -th property as prescribed by Eurocode 6
$f_{ik,NPR}$	Characteristic value of the i -th property as prescribed by NPR 9096-1-1:2012
$f_{ik,NPR9998}$	Characteristic value of the i -th property as prescribed by NPR 9998:2017
f_m	Compressive strength of masonry mortar
f_{mt}	Flexural strength of masonry mortar
f_m'	Compressive strength of masonry in the direction perpendicular to the bed joints
$f_{m,h}'$	Compressive strength of masonry in the direction parallel to the bed joints
f_p	Applied lateral pre-compression stress
f_{x1}	Masonry flexural strength with the moment vector parallel to the bed joints and in the plane of the wall, which generates a plane of failure parallel to the bed joints
f_{x2}	Masonry flexural strength with the moment vector orthogonal to the bed joints and in the plane of the wall, which generates a plane of failure perpendicular to the bed joints
f_{x3}	Masonry flexural strength with the moment vector orthogonal to the plane of the wall

f_{v0}	Masonry (bed joint) initial shear strength
$f_{v0,res}$	Masonry (bed joint) residual initial shear strength
f_w	Masonry uniaxial bond strength between the masonry unit and the mortar
l_j	Length of the mortar bed joint in a masonry specimens
l_m	Length of the mortar specimen
l_s	Length of the masonry specimen as built
l_p	Length of the loading plate for compression tests on mortar specimens
l_u	Length of the masonry unit as used in the construction of masonry
h_m	Height of the mortar specimen
h_s	Height of the masonry specimen as built
h_u	Height of the masonry unit as used in the construction
t_s	Thickness of the masonry specimen as built
t_m	Thickness of the mortar specimen
t_u	Thickness of the masonry unit as used in the construction of masonry
v_{el}	Vertical displacement corresponding to the load F_{el}
A_s	Cross sectional area of the specimen parallel to the bed joints (shear test)
E_b	Chord elastic modulus of stacked masonry unit subjected to compression load
E_1	Secant elastic modulus of masonry subject to a compressive loading perpendicular to the bed joints, evaluated at 1/3 of the maximum stress
E_2	Secant elastic modulus of masonry subject to a compressive loading perpendicular to the bed joints, evaluated at 1/10 of the maximum stress
E_3	Chord elastic modulus of masonry subject to a compressive loading perpendicular to the bed joints, evaluated at between 1/10 and 1/3 of the maximum stress
$E_{1,h}$	Secant elastic modulus of masonry subject to a compressive loading parallel to the bed joints, evaluated at 1/3 of the maximum stress
$E_{2,h}$	Secant elastic modulus of masonry subject to a compressive loading parallel to the bed joints, evaluated at 1/10 of the maximum stress
$E_{3,h}$	Chord elastic modulus of masonry subject to a compressive loading parallel to the bed joints, evaluated at between 1/10 and 1/3 of the maximum stress
E_{bt}	Chord elastic modulus of masonry unit subjected to the bending load
E_{fx1}	Chord elastic modulus of masonry in bending parallel to the bed joints evaluated between 1/10 and 1/3 of the maximum force
E_{fx2}	Chord elastic modulus of masonry in bending perpendicular to the bed joints evaluated between 1/10 and 1/3 of the maximum force
E_{fx3}	Chord elastic modulus of masonry subjected to bending load with the moment vector orthogonal to the plane of the wall evaluated between 1/10 and 1/3 of the maximum force
F_1	Applied vertical load (bond-wrench test)
F_2	Vertical load due to the weight of the top clamping system (bond-wrench test)
F_3	Vertical load due to the top masonry unit (bond-wrench test)
F_{el}	Selected vertical load value in the linear elastic stage (flexural test of masonry unit)
F_{max}	Maximum vertical load
F_p	Applied lateral pre-compression force (shear test)

G_{f-c}	Fracture energy in compression for loading perpendicular to the bed joints
$G_{f-c,h}$	Fracture energy in compression for loading parallel to the bed joints
G_{fII}	Mode II fracture energy in shear
G_{fx1}	Fracture energy in out-of-plane bending for loading direction parallel to the bed joints
G_{fx2}	Fracture energy in out-of-plane bending for loading direction perpendicular to the bed joints
G_{fx3}	Fracture energy in bending for loading with the moment vector orthogonal to the plane of the wall
M_{max}	Maximum bending moment
W	Section modulus
I	Moment of inertia of the masonry unit along the cross-section

2.2 Abbreviations

Avg.	Average
C.o.V.	Coefficient of variation
CS	Calcium silicate
LVDT	Linear variable differential transformer
St. dev.	Standard deviation
SCF	Slenderness correction factor

3 Construction of the samples

The masonry specimens were built in the Stevin II laboratory at Delft University of Technology. The masonry was made of clay bricks and cement based mortar. The declarations of performance of the materials are reported in Appendix A.

Figure 2 shows the adopted masonry unit. The dimensions are defined considering the orientation of the masonry unit as used in the construction of the masonry. This definition is consistently adopted in this report despite the position of the specimen in the test set-up. A similar consideration is applied to describe the dimensions of masonry specimens.

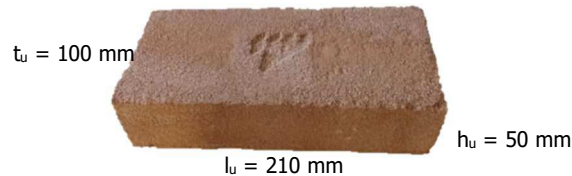


Figure 2 – Mean dimensions of the clay bricks.

In order to ensure quality control, the construction followed the prescription as reported in the construction protocol [3]:

- The bags of mortar mix were stored dry and separated from the soil;
- The mortar mix was used within 18 months after production;
- The mortar was mixed with clean water;
- The mortar was prepared using a fixed water content;
- The flow of the mortar was determined in agreement with EN 1015-3:1999 [4].
- At least three samples of mortar (size 160x40x40-mm) were made at every start of the day during construction of masonry for testing the properties. The samples were tested under flexural and compressive loading in agreement with EN 1015-11:1999 [5];
- The mortar was prepared and used between 5 and 25 degrees;
- The mortar was used within 2 hours after preparation;
- No additives were mixed after preparation of the mortar;
- Bricks were covered against moisture;
- Bricks were clean before use;
- Bricks were not wetted before use;

The mortar was prepared with fixed water content per bag of mix (25 kg): 3.7 l/bag for clay brick masonry.

4 Flexural and compressive strength of mortar

During the masonry construction, mortar samples were collected and cast in moulds to be tested for the flexural and compressive strength in agreement with EN 1015-11:1999 [5]. The consistency of the mortar was determined in accordance with EN 1015-3:1999 [4].

4.1 Testing procedure

During each day of construction, at least three mortar specimens having a length of $l_m = 160$ mm, a height of $h_m = 40$ mm and thickness of $t_m = 40$ mm were collected. The samples were stored in controlled conditions. The first two days they were placed in a fog room ($T = 20 \pm 2$ °C, $RH = 95 \pm 5\%$) with the moulds. After two days, they were unmoulded and kept for other five days in the fog room. Eventually, they were placed in a conditioning room with a temperature of 20 ± 2 °C and a relative humidity of 50 ± 5 % until testing. The test was performed after at least 28 days from construction.

The flexural strength was determined by three-point bending test (Figure 3a). The test set-up is composed by two steel bearing rollers having a diameter of 10 ± 0.5 mm and spaced $d_l = 100 \pm 0.5$ mm. A third roller is centrally placed on top of the sample to apply the load.

The compression test was performed on the broken pieces obtained from the flexural test, which have at least a length of 40 mm. The specimen is placed between two steel plates with a length of $l_p = 40$ mm. For the interpretation of the results the specimens considered to be 40x40x40-mm (Figure 3b).

For both test, the load was applied without shock at a uniform rate so that failure occurred within a period of 30 to 90 s. The maximum load was recorded.



Figure 3 – Test on masonry mortar specimens: (a) three-point bending test; (b) compression test.

4.2 Experimental results

The flexural strength f_{mt} of the mortar was calculated as [5]:

$$f_{mt} = \frac{3}{2} \frac{F_{\max} d_l}{t_m h_m^2} \quad (1)$$

where F_{\max} is the maximum load, d_l is the distance between the supports ($100 \text{ mm} \pm 0.5 \text{ mm}$), h_m is the height of the mortar specimen (40 mm) and t_m is the thickness of the mortar specimen (40 mm).

The compressive strength f_m of the mortar was calculated as [5]:

$$f_m = \frac{F_{\max}}{t_m l_p} \quad (2)$$

where F_{\max} is the maximum load, t_m is the thickness of the mortar specimen (40 mm) and l_p is the length of the loading plate (40 mm).

During the masonry construction, the slump test was performed after the preparation of every batch of mortar. The diameter of the cone was obtained in agreement with the slump test described in EN 1015-3:1999 [4]. The measured diameter varied between 166 to 197 mm (see Table 2).

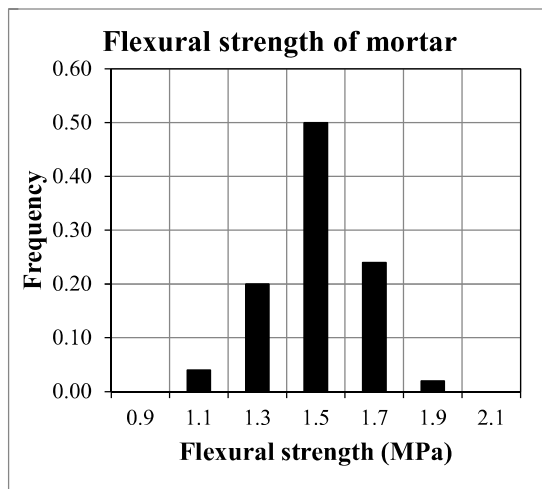
Table 2 – Consistency of mortar for the clay brick masonry.

Date of construction	Number of batch	Companion sample	Flow (mm)
26-10-2016	1	COMP-27 MAT-35 MAT-36A MAT-36B	192
	2		188
	3		192
	4		191
27-10-2016	1	COMP-27	192
	2		188
	3		192
	4		191
01-11-2016	1	Comp-23 MAT-42	191
	3		182
	4		190
	5		197
02-11-2016	1	Comp-23 MAT-42	189
	3		185
	4		184
	5		191
03-11-2016	1	Comp-22	184
	3		180
	4		182
	5		185
	6		191
04-11-2016	1	Comp-21 MAT-42	194
	2		193
	3		191
	4		193
07-11-2016	1	MAT-32 MAT-33	189
	2		195
	3		194
08-11-2016	1	MAT-33 MAT-34 MAT-42 MAT-44	190
	2		191
	3		192
	4		196
09-11-2016	1	MAT-43 MAT-31	189
	2		184
	6		166
10-11-2016	2	MAT-31 MAT-35 MAT-44	180
	4		185
	5		195
11-11-2016	1	MAT-31 MAT-43 MAT-44	190
	2		195
	3		190
Average			188

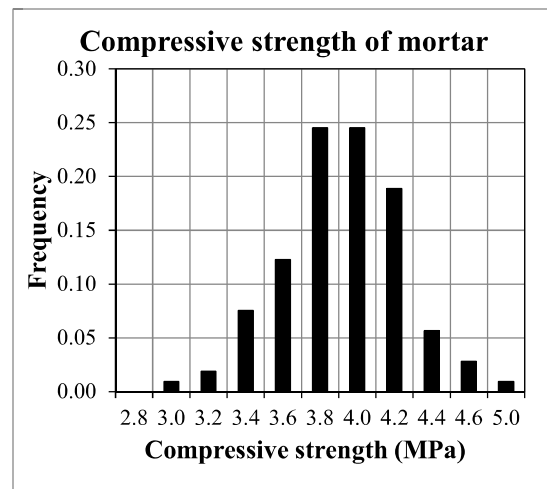
The flexural and compression tests on the hardened mortar were performed at least after 28 days. Table 3 lists the results for the three-point bending tests and compression tests. Three-point bending tests were performed on 54 mortar bars and compressive tests were conducted on 108 broken pieces obtained from the flexural tests. The values of the flexural strength and compressive strength for each batch are obtained from performing tests on the three mortar bars. The mortar has a compressive strength of 3.8 MPa and flexural strength of 1.4 MPa. These values are obtained considering the average of all the tested specimens. In both cases, the coefficient of variation is limited to less than 15%.

Table 3 – Flexural and compressive strength of clay brick masonry mortar.

Date of construction	Batch	Density (Kg/m ³)	Flexural tests			Compression test		
			f_{mt} (MPa)	St. dev.	C.o.V.	f_m (MPa)	St. dev.	C.o.V.
18-10-2016	3	1657	1.4	0.14	0.10	3.7	0.17	0.05
19-10-2016	2	1708	1.6	0.07	0.05	3.9	0.14	0.04
20-10-2016	1	1669	1.3	0.24	0.18	3.6	0.13	0.04
21-10-2016	1	1661	1.3	0.04	0.03	3.3	0.15	0.05
24-10-2016	1	1692	1.2	0.08	0.06	3.3	0.21	0.06
25-10-2016	1	1727	1.4	0.06	0.05	4.1	0.17	0.04
25-10-2016	5	1699	1.4	0.04	0.03	3.9	0.21	0.05
26-10-2016	4	1714	1.4	0.25	0.18	4.0	0.14	0.04
27-10-2016	1	1687	1.6	0.07	0.05	3.7	0.19	0.05
27-10-2016	4	1700	1.6	0.05	0.03	3.6	0.41	0.12
28-10-2016	1	1711	1.3	0.17	0.13	3.9	0.18	0.04
28-10-2016	7	1702	1.2	0.37	0.30	3.6	0.27	0.07
31-10-2016	1	1708	1.4	0.03	0.02	3.8	0.27	0.07
31-10-2016	4	1695	1.4	0.01	0.01	3.9	0.17	0.04
01-11-2016	5	1711	1.4	0.16	0.11	4.1	0.25	0.06
02-11-2016	4	2630	1.4	0.14	0.10	3.8	0.20	0.05
03-11-2016	4	1701	1.6	0.24	0.15	4.3	0.45	0.10
03-11-2016	6	1679	1.3	0.19	0.14	4.1	0.18	0.04
Average		1747	1.40			3.81		
Standard deviation		382	0.17			0.34		
Coefficient of variation		0.22	0.12			0.09		



(a)



(b)

Figure 4 – Statistical distribution of mortar strength: (a) flexural strength; (b) compressive strength.

5 Compression strength of masonry unit

The compressive strength of a masonry unit (brick) is determined in agreement with EN 772-1:2000 [6]. In addition, the Young's modulus is determined by compressing the stacked masonry units.

5.1 Testing procedure

The compressive test of masonry unit was performed on two specimen types: single unit and stacked masonry units. In the previous experimental campaign it was observed that direct compression tests on a single masonry unit did not provide a good estimation of the Young's modulus [7]. Therefore, in the current study the Young's modulus was calculated considering the method adopted by Vermeltfoort [8].

To estimate the compressive strength of masonry unit a single masonry unit having a length l_u , a height h_u and thickness t_u was subjected to compression load in agreement with EN 772-1:2000 [6], Figure 5a.

To estimate the Young's modulus of the masonry unit, a compressive test on a prism was performed as suggested by Vermeltfoort [8]. The prism consisted of units stacked together using the glue "Sikadur 30" which has an high compressive strength. The dimensions of the specimen were chosen such that the ratio between the height and the thickness (h_s/t_s) ranges between 4 and 5, see Figure 5b.



(a)



(b)

Figure 5 – Compressive test: (a) specimen composed of a single unit; (b) specimen composed of 8 stacked masonry units.

The test was carried out through a displacement-controlled apparatus including a hydraulic jack with 300-ton capacity. The hydraulic jack lifts a steel plate, the active side, and there is a passive load plate at the top. A hinge between the load cell and the top steel plate reduces possible eccentricities during loading. A load cell that measures the applied force is attached to the top steel plate. Both single unit and stacked masonry units specimens were tested with its bed joint plane perpendicular to the loading direction.

Since the small height of the single brick did not allow attaching LVDTs in this dimension, four vertically oriented LVDTs were attached to the machine platens in order to measure relative vertical displacements. Their measuring range was 10 mm with an accuracy of 0.1%. To reach the failure load within 2 min [6], the rate of the jack displacement was set to 0.01 mm/s.

The specimen composed of stacked masonry units was instrumented with 4 LVDTs (3 longer ones on the sides and 1 smaller on one brick) both on the front and the back sides (see Figure 5b). The rate of the jack displacement was set to 0.003 mm/s.

5.2 Experimental results

The compressive strength of the masonry unit f_b^* can be determined from test on single masonry unit as:

$$f_b^* = \frac{F_{\max}}{l_u \cdot t_u} \quad (3)$$

where F_{\max} is the maximum load, l_u and t_u are the length and thickness of the masonry unit respectively. Following the Annex A of standard EN 772-1 [6], the normalised compressive strength of the masonry unit f_b is determined as:

$$f_b = \delta \cdot f_b^* \quad (4)$$

where δ is the shape factor determined in agreement with Table A.1 in Ref. [6].

Table 4 lists the compressive strength of the bricks as well as the normalised compressive strength obtained by tests on the single masonry unit.

Table 4 – Compressive strength of the clay masonry unit.

Clay brick – 210x101x45-mm			
Sample name	f_b^*	δ	f_b
	MPa	-	MPa
TUD_ B32a	40.92	0.727	29.75
TUD_ B32b	42.02	0.725	30.46
TUD_ B32c	41.12	0.721	29.63
TUD_ B32d	40.82	0.722	29.48
TUD_ B32e	32.08	0.727	23.32
TUD_ B32f	31.97	0.7255	23.20
TUD_ B32g	42.71	0.721	30.77
TUD_ B32h	40.39	0.725	29.26
TUD_ B32i	40.05	0.722	28.92
Average	39.12	0.724	28.31
Standard deviation	4.10	0.002	2.92
Coefficient of variation	0.10	0.003	0.10

The compressive strength of stacked masonry units can be determined assuming that the confining effects of the loading plates did not disturb the stress distribution in the middle of stacked masonry units and the stress was constant over the cross-section of the specimen, as follows:

$$f_{bs}^* = \frac{F_{\max}}{l_u \cdot t_u} \quad (5)$$

where F_{\max} is the maximum load, l_u and t_u are the length and thickness of the masonry unit respectively.

Following the Annex A of standard EN 772-1 [6], the normalised compressive strength of the masonry unit f_b is determined as:

$$f_b = \delta \cdot f_{bs}^* \quad (6)$$

where δ is the shape factor determined in agreement with Table A.1 in Ref. [6].

During the test the displacements and the force were measured continuously allowing the determination of the stress-strain relationship along the loading direction, which is defined as normal direction. Considering the readings of the LVDTs' attached on the samples, the chord modulus was calculated between 1/10 and 1/3 of the maximum stress. Table 5 lists the results of the samples tested. Similarly, the same values of the normalised compressive strength from tests on the single bricks and tests on the stacked masonry unit are found.

Table 5 – Compression properties of the clay masonry unit from tests on stacked units.

Clay brick – Stacked masonry units				
Sample name	f_{bs}	δ	f_{bs}	E_b
	MPa	-	MPa	MPa
TUD_ B33a	19.54	1.45	28.3	8348
TUD_ B33b	18.12	1.45	26.3	7750
Average	18.83	-	27.3	8049
Standard deviation	1.00	-	1.41	423
Coefficient of variation	0.05	-	0.05	0.05

6 Flexural strength of masonry unit

The flexure strength of the masonry unit was determined with the three-point bending test following NEN 6790:2005 [9]. The test was also used to determine the elastic modulus of the masonry unit.

6.1 Testing procedure

The masonry units were tested by having the bed joint plane parallel to the loading direction (Figure 6). The specimen was supported by two roller bearings, which were placed 10 mm from the end of the specimen. A third roller was used to apply load to the specimen at mid-span. Table 6 lists the dimensions of the masonry units and the distance between the supports.

The test was carried out by a displacement controlled apparatus including a hydraulic jack with 100 kN capacity. A spherical joint, between the upper roller and hydraulic jack, was used to minimise load eccentricity. To obtain the failure of the specimen in 30 to 90 s, a displacement rate of 0.02 mm/s was adopted. The applied load was recorded from the load cell attached to the hydraulic jack.

Two LVDTs were attached to the specimens to measure horizontal and vertical displacements. On the front side the vertical displacement at mid-span of the masonry unit, relative to its supports, was measured. On the back side, a horizontal LVDT measured the elongation between two points on the masonry unit. The LVDTs had a measuring range of 10 mm with an accuracy of 0.1%.

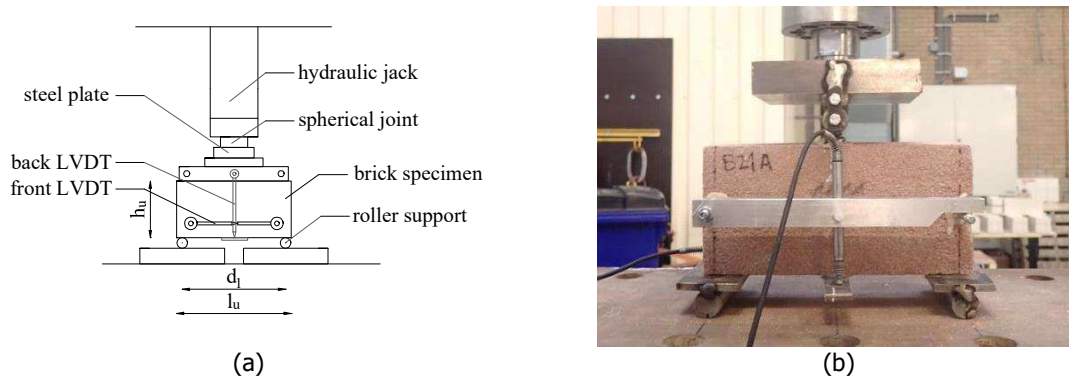


Figure 6 – Three-point bending test on masonry unit.

Table 6 – Dimensions of the masonry units and distance d_1 between the bearing supports.

Masonry type	Sample name	l_u	t_u	h_u	d_1
		mm	mm	mm	mm
Clay bricks	TUD_ B31a	208	100	47	189
	TUD_ B31b	208	100	48	188
	TUD_ B31c	209	100	48	189
	TUD_ B31d	209	100	48	189
	TUD_ B31e	209	100	48	189
	TUD_ B31f	209	100	48	189
	TUD_ B31g	209	100	48	189
	TUD_ B31h	209	100	48	189
	TUD_ B31i	209	100	48	189

6.2 Experimental results

The flexural strength of the masonry unit f_{bt} was determined as:

$$f_{bt} = \frac{3}{2} \frac{F_{\max} d_1}{h_u t_u^2} \quad (7)$$

where F_{\max} is the maximum load, d_1 is the distance between the supports, h_u is the height of the masonry unit, t_u is the thickness of the masonry unit.

Assuming a linear stress distribution over the height of the brick's cross-section, the elastic modulus E_b of the masonry units can be determined as follows:

$$E_{bt} = \frac{F_{el} d_1^3}{48 v_{el} I} \quad (8)$$

where F_{el} and v_{el} are the load and vertical displacement in the linear elastic stage, respectively and I is the moment of inertia of the masonry unit along the cross-section.

Figure 7 shows the displacement-force diagram for the clay bricks. The bricks presented a brittle failure when the maximum force was reached. The behaviour was linear approximatively until 90% of the peak load, while some nonlinearity occurs just before the peak.

Table 7 lists the results in terms of flexural strength and elastic modulus. The clay bricks showed a low variation in strength and elastic modulus.

A symmetric crack pattern for all the samples was observed, except TUD_MAT-B31h that showed an asymmetric crack pattern, see Figure 8. Therefore, the test results of this sample were excluded from the average.

The result of flexural strength in the form of histogram is shown in Figure 9.

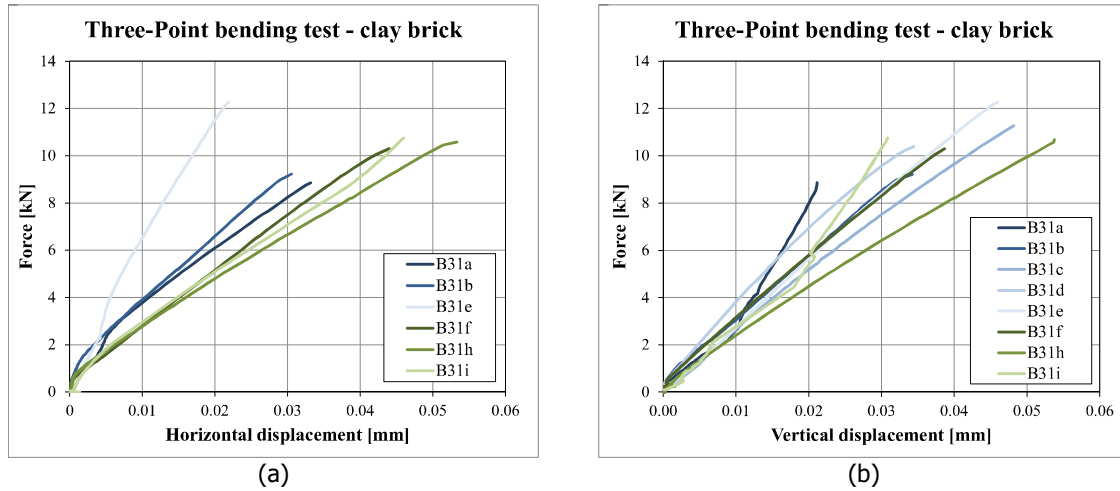


Figure 7 – Force-displacements curves (LVDTs readings) of three-point bending test on clay brick: (a) horizontal displacement; (b) mid-span displacement.

Table 7 – Flexural strength and elastic modulus for clay bricks.

Clay bricks		
Sample name	f_{bt}	E_{bt}
	MPa	MPa
TUD_B31a	5.34	9963
TUD_B31b	5.41	10538
TUD_B31c	6.66	14185
TUD_B31d	6.14	12913
TUD_B31e	7.25	-
TUD_B31f	6.08	12080
TUD_B31g	7.22	-
TUD_B31h*	6.43	8035
TUD_B31i	6.35	9029
Average	6.31	11451
Standard deviation	0.72	1945
Coefficient of variation	0.11	0.17

* Excluded from the average due to the asymmetric crack pattern



(a)



(b)

Figure 8 – Crack pattern for clay brick: (a) symmetric crack pattern; (b) asymmetric crack pattern.

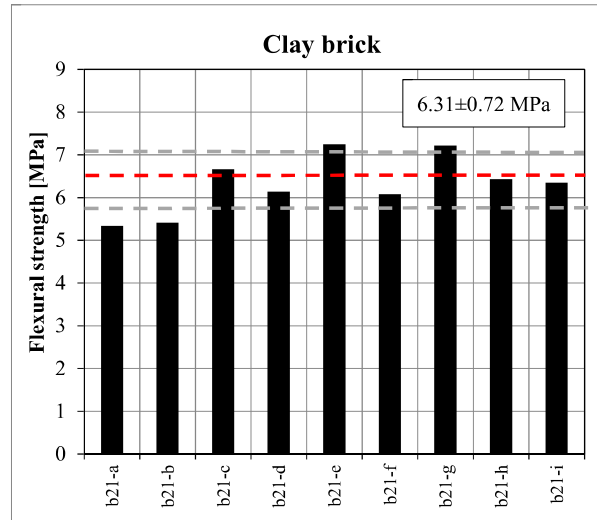


Figure 9 – Flexural strength values of clay brick: histogram representation.

7 Density of clay brick masonry

To measure the density of solid clay brick masonry, weight and dimensions of the specimens adopted for the bond wrench test were measured prior to testing. The average value of the density for the clay brick masonry is reported as 1708 kg/m³, see Table 8.

Table 8 – Density of clay brick masonry.

h_s	L_s	t_s	Weight	Density
mm	mm	mm	kg	Kg/m ³
104	208	99	3.72	1735
105	210	100	3.63	1644
106	208	99	3.68	1686
105	209	99	3.68	1694
106	209	99	3.67	1671
109	208	99	3.76	1673
108	207	99	3.67	1656
105	209	98	3.66	1702
106	208	100	3.66	1660
106	209	100	3.70	1670
106	210	99	3.62	1643
106	209	99	3.72	1694
105	209	99	3.73	1717
104	208	99	3.66	1709
106	209	100	3.69	1663
106	210	99	4.14	1876
106	209	99	4.19	1908
105	209	99	3.77	1735
104	208	99	3.70	1725
Average				1708
Standard deviation				71
Coefficient of variation				0.04

8 Compression properties of masonry

The compression strength and elastic modulus of the masonry were determined in agreement with EN 1052-1:1998 [10]. Additional test configurations were adopted to investigate the orthotropic behaviour of the masonry and the cyclic response of the material.

8.1 Testing procedure

The compression strength and elastic modulus of the masonry were determined in two orthogonal directions with respect to the bed joints. Two configurations were used: a *vertical configuration* in which the loading was perpendicular to the bed joints and a *horizontal configuration* in which the loading was parallel to the bed joint. The former is prescribed by the standard EN 1052-1:1998, while the latter is additionally used to investigate the orthotropic behaviour of the material.

The dimensions of the single wythe specimens as well as LVDT's location for both vertical and horizontal compression tests are reported in Figure 10.

Two types of the double wythe samples were adopted for the compression tests:

- Specimens conforming to the standard prescriptions [10], having dimensions 540x650x210-mm. These specimens tested only under vertical configuration, see Figure 12.
- Specimens having a 1:1 ratio between the length and height. The specimens were subjected to vertical and horizontal compressive load aiming to study the orthotropic behaviour, see Figure 11. The length-to-height ratio of 1 was selected in agreement with previous experimental investigations on replicated masonry carried out at TU Delft in 2015 [11].

Four LVDTs (two for each side) were attached to the specimen to register vertical relative displacements over the height of the specimen. They were installed as closely as possible to the surface of the specimen to reduce possible errors caused by rotation of the contact points to which they were attached. To monitor the vertical deformation the length of the LVDTs were increased with respect to the one suggested by the standard. A longer length was used in order to capture the entire behaviour of the wallets, with attention in particular to the estimation of the fracture energy. The measuring range of the LVDTs was 10 mm with an accuracy of 0.1%. Additionally, two LVDTs (one for each side) were attached to the specimen to register the horizontal relative displacement over the length of the specimen. Their measuring range was 10 mm with an accuracy of 0.1%.

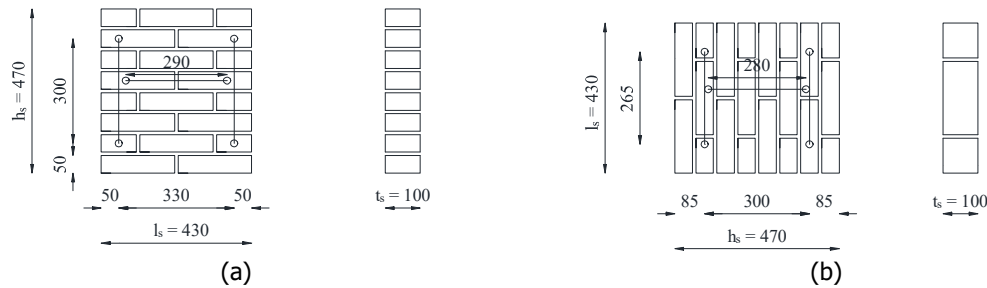


Figure 10 – Dimensions of the clay single wythe specimens (TUD-MAT-31): (a) vertical compression test; (b) horizontal compression test.

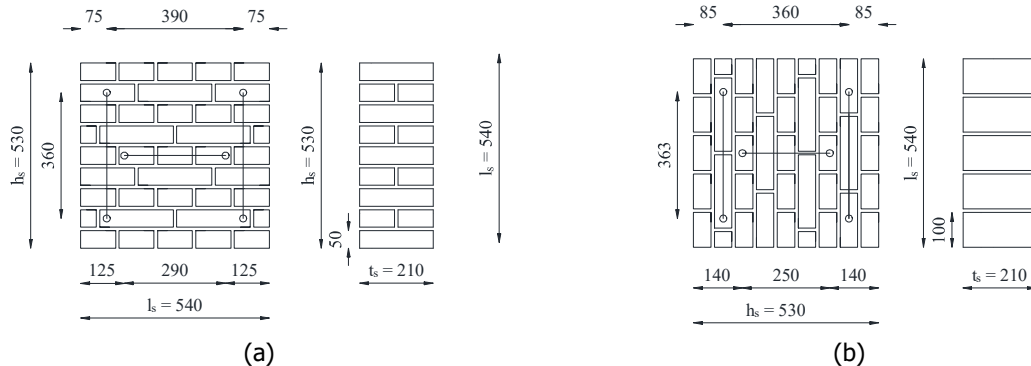


Figure 11 – Dimensions of the clay double wythe specimens aiming to investigate the orthotropic behaviour (TUD-MAT-41B): (a) vertical compression test; (b) horizontal compression test.

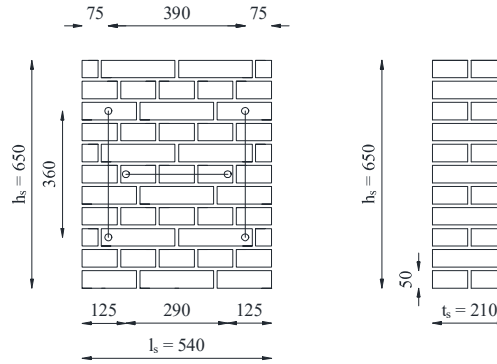


Figure 12 – Dimensions of the clay double wythe specimens (TUD-MAT-41A): vertical compression test.

A 10-mm thick layer of gypsum was applied to faces in contact with the loading plates, to ensure that the loaded faces of the specimens were levelled and parallel to one another. This was done to prevent additional stresses in the specimens.

The specimens with different height were adopted; therefore, two testing apparatuses were employed. The specimens having a height less than 550 mm (both TUD-MAT-31 and TUD-MAT-41B) were tested using an apparatus provided with a 3000 kN hydraulic jack. The jack is positioned at the bottom. The hydraulic jack lifts a steel plate, the active side, and there is a passive load plate at the top. A hinge between the load cell and the top steel plate reduces possible eccentricities during loading. The hydraulic jack is operated in deformation control, using the displacement of the jack as control variable. A load cell that measures the applied force is attached to the top steel plate (Figure 13).

A displacement-control set-up (Figure 14) was designed to compress the double-wythe masonry specimens higher than 550 mm (TUD-MAT-41A). The set-up is composed of two identical steel frames positioned parallel to each other, connected on top and bottom. Each of the contrast frames is composed of two HEB300 columns and two HEB1000 beams. Bottom steel beam acts as a support for the tested specimen, while the top one holds the load cell. The testing apparatus is provided with a hydraulic jack of approximately 200-ton capacity. The load is applied through two spreading beams, which are connected to the load cell by a hinge to reduce possible eccentricities during loading (Figure 14). A load cell that measures the applied force is attached to the top steel plate.

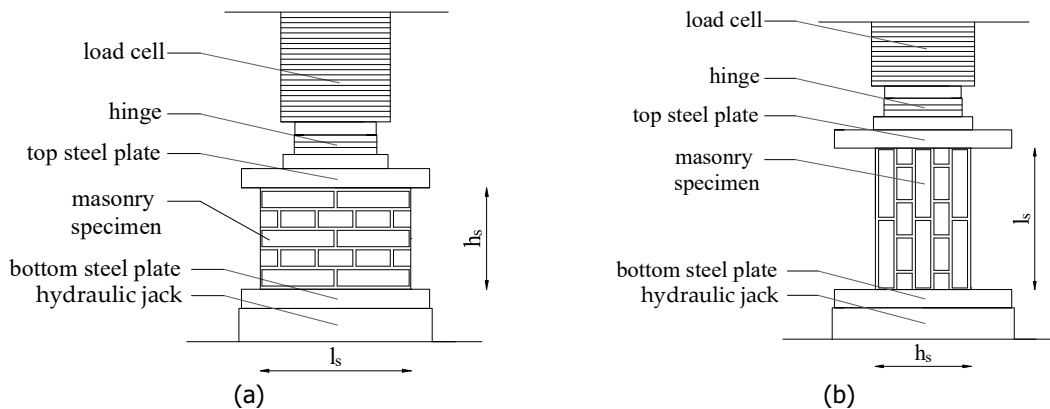


Figure 13 – Test set-up used to compress TUD-MAT-31 and TUD-MAT-41B specimens: (a) vertical configuration; (b) horizontal configuration.

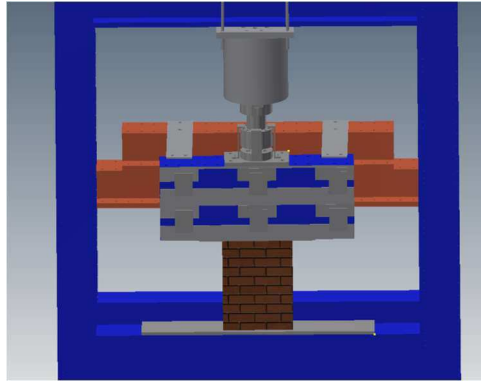


Figure 14 – Test set-up used to compress the TUD-MAT-41A specimens.

For the two configurations, three specimens were tested by applying a *monotonic loading* as prescribed by the EN 1052-1:1998 [10] (Figure 15). Half of the expected maximum compression force was applied in three equal steps and was kept constant for 2 ± 1 min. Afterwards, the maximum stress was reached monotonically. Subsequently, the test was continued to explore the post-peak behaviour. The load was applied with a rate of 0.003 mm/s to reach the peak stress in 15 to 30 min. The deformation and the force were registered, including the post-peak softening regime.

For both configurations, three specimens were tested by applying a *cyclic loading* (Figure 15). This loading scheme gives additional information regarding the loading-unloading behaviour. Three cycles of three runs were applied at approximately 1/4, 1/2 and 3/4 of the expected maximum strength. The load was applied with a rate of 0.01 mm/s to reach the peak stress in approximately 30 min. The deformation and the force were registered.

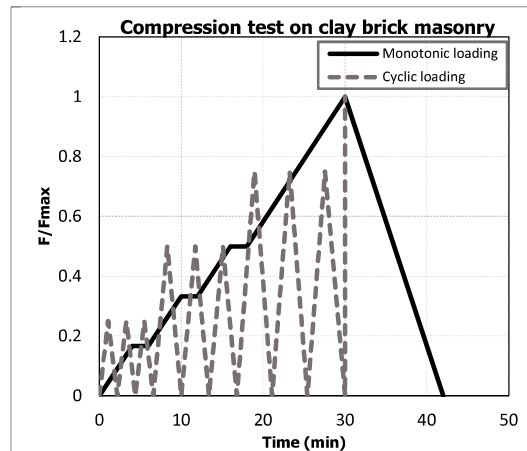


Figure 15 – Monotonic and cyclic loading scheme for compression test on masonry specimen.

8.2 Experimental results

Assuming that the stress is constant over the cross-section of the specimen, the compressive strength of masonry for the vertical, f'_{m_v} and horizontal, f'_{m_h} configuration can be determined as follows:

$$f'_m = \frac{F_{\max}}{t_s l_s} \quad (9)$$

$$f'_{m,h} = \frac{F_{\max}}{t_s h_s} \quad (10)$$

where F_{\max} is the maximum load, l_s , h_s and t_s are the dimensions of the masonry specimen as built (Figure 13).

During the test the displacements and the force were measured continuously allowing the determination of the stress-strain relationship along the loading direction, which was defined as normal direction. From this relation was possible to determine the elastic modulus of masonry. Three estimates of the elastic modulus were adopted (Figure 16a):

- E_1 ($E_{1,h}$) is the secant elastic modulus evaluated at 1/3 of the maximum stress;
- E_2 ($E_{2,h}$) is the secant elastic modulus evaluated at 1/10 of the maximum stress;
- E_3 ($E_{3,h}$) is the chord elastic modulus evaluated between 1/10 and 1/3 of the maximum stress.

The first estimate was consistent with the prescription of EN 1052-1:1998. The third estimate aimed to exclude the initial start-up of the stress-strain diagram, which would unrealistically affects the other two secant estimates with the initial lower slope.

The Poisson ratio ν is determined in the elastic phase as the ratio between the lateral strains, which are evaluated in the direction perpendicular to the loading one, and the normal strains (Figure 16 b).

The displacement control procedure of the test allowed determining the post-peak behaviour of the material. The fracture energy in compression G_{fc} ($G_{fc,h}$) was determined as the area underneath the normal stress versus normal strain diagram, taking the height of the specimen into account. This concept was introduced by van Mier [12] for concrete material and subsequently applied to masonry by Lourenco [13]. In the case of cyclic loading, the envelope curve was considered for the calculation of the fracture energy.

The strain obtained by LVDTs' readings and by the jack's readings resulted similar in the post-peak phase. Consequently, the former were used to evaluate the pre-peak phase, while the latter were used to describe the post-peak phase, in which LVDTs may be detached from the specimen due to extensive cracking. The elastic modulus and the Poisson ratio were calculated on the basis of the LVDTs readings, while the fracture energy was calculated on the basis of the LVDTs' reading in the pre-peak and jack's reading in the post-peak phase.

The strain associated with peak strength, which is called peak strain, ϵ_p ($\epsilon_{p,h}$), is reported in the current document.

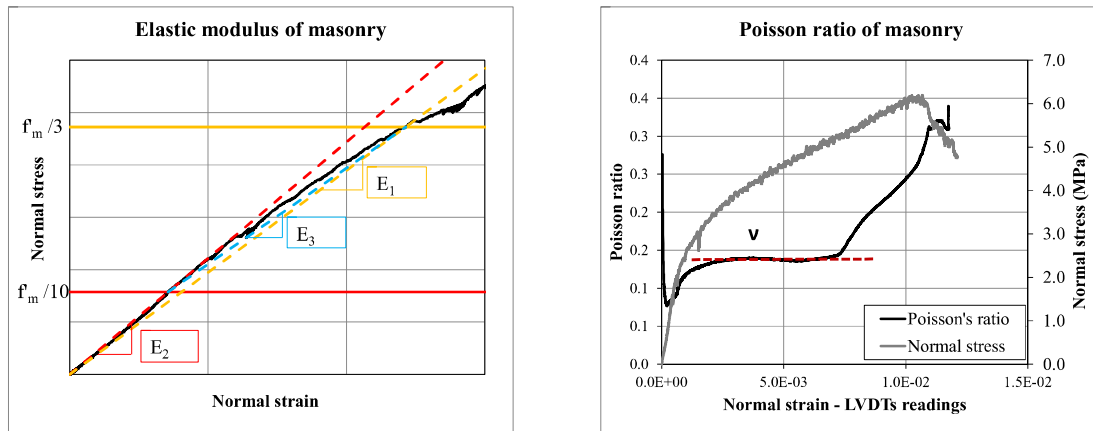


Figure 16 – Compression test on masonry: (a) three estimates of the elastic modulus; (b) evaluation of Poisson ratio.

Figure 17 and Figure 18 show the stress-strain diagram for the single wythe clay brick masonry for the vertical and horizontal configurations, respectively. The graphs refer to the normal direction that is defined as the one parallel to the loading direction.

For both configurations the stress-strain relationship in the normal direction presents a similar trend. The pre-peak stage was characterised by linear-elastic followed by an hardening behaviour until the peak. In the case of the vertical configuration, the non-linearity started at approximatively 1/3 of peak stress, while in the case of the horizontal configuration the nonlinear behaviour occurred already at lower stress level between 1/10 and 1/3 of the maximum stress. After the peak stress was reached, an exponential softening behaviour was observed for both configurations. In the case of cyclic loading, the masonry showed an elastic unloading in the pre-peak phase, for both configurations.

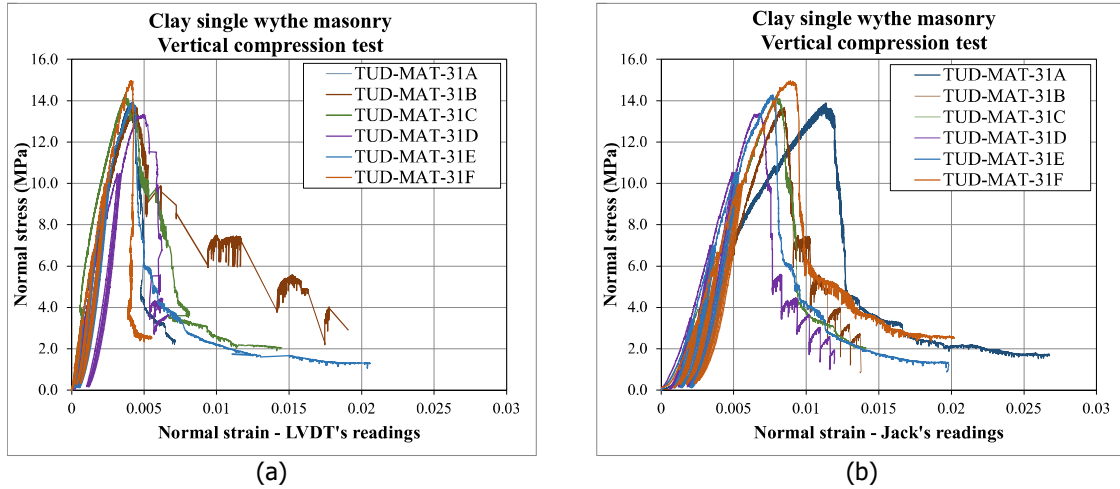


Figure 17 – Vertical compression tests on single wythe clay brick masonry specimens: (a) normal strain obtained by LVDT's reading; (b) normal strain obtained by jack's reading.

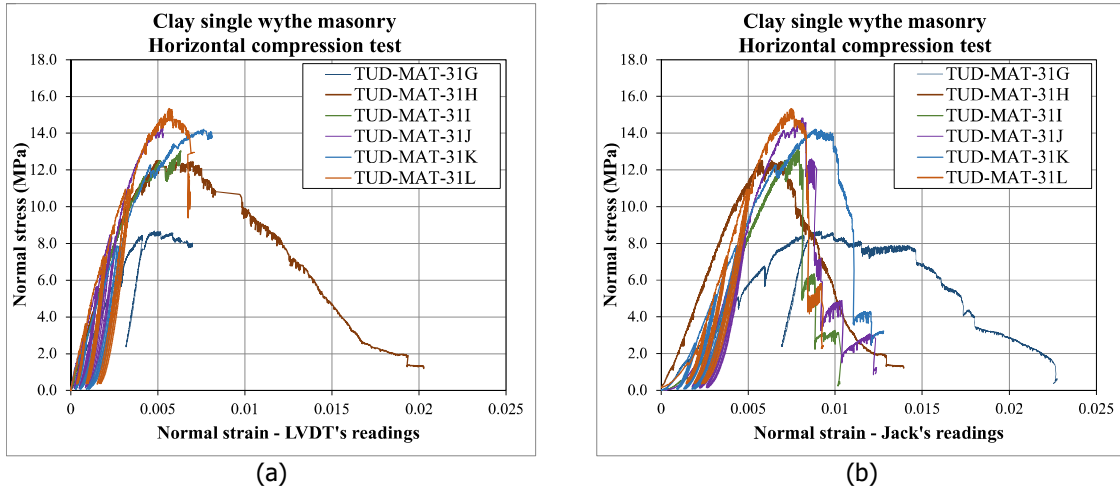


Figure 18 – Horizontal compression tests on single wythe clay brick masonry specimens: (a) normal strain obtained by LVDT's reading; (b) normal strain obtained by jack's reading.

Figure 19 and Figure 20 analyse the development of cracks in the two specimens tested under vertical and horizontal compression test, respectively. In both cases splitting cracks started in the bricks. In the case of vertical compression tests, the cracks mainly occurred in the central part of the specimens (Figure 19b). On the contrary, for the horizontal configuration the damage was concentrated in the bottom or upper part, where half bricks were located (Figure 20b). In the case of horizontal compression, cracks also formed at the mortar-brick interface for the joints parallel to the loading direction (Figure 20a).

In the post-peak phase, the specimens tested under the two configurations showed different behaviour. For the case of vertical configuration, the vertical cracks mainly occurred along the thickness of the specimens, by splitting it in two parts (Figure 19c, Figure 19d). For the horizontal configuration, spalling of the bricks was observed and the cracks developed through the thickness of the specimen, rather than through the length, creating a buckling mechanism (Figure 20c, Figure 20d). The cracking was observed to occur in a distributed manner over the height of the specimen; no localisation of the cracking at the boundary was observed.

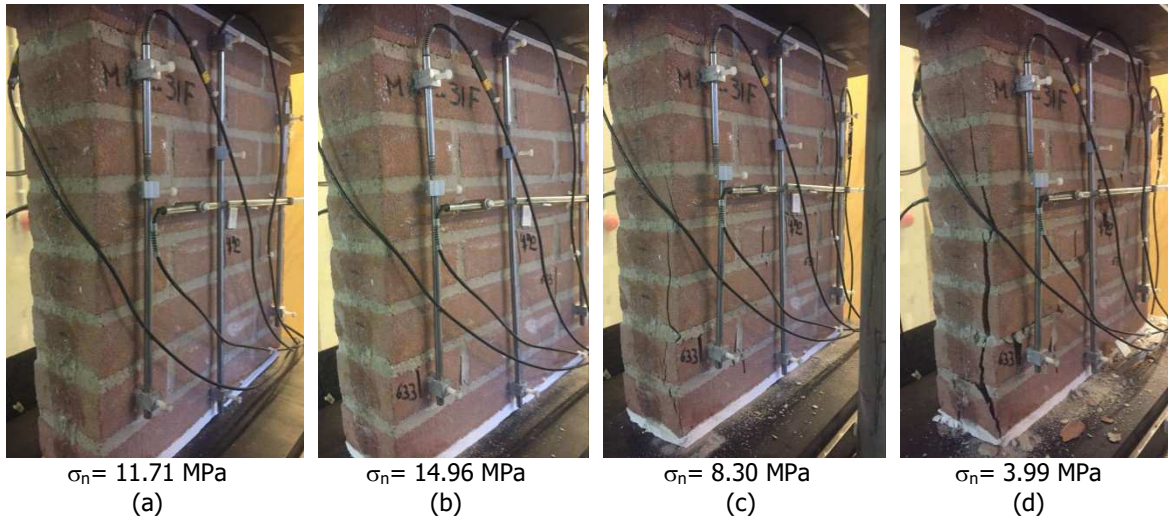


Figure 19 – Crack pattern of single wythe specimen TUD-MAT-31F tested under vertical compression: (a) first crack; (b) maximum stress; (c)-(d) post-peak phase.

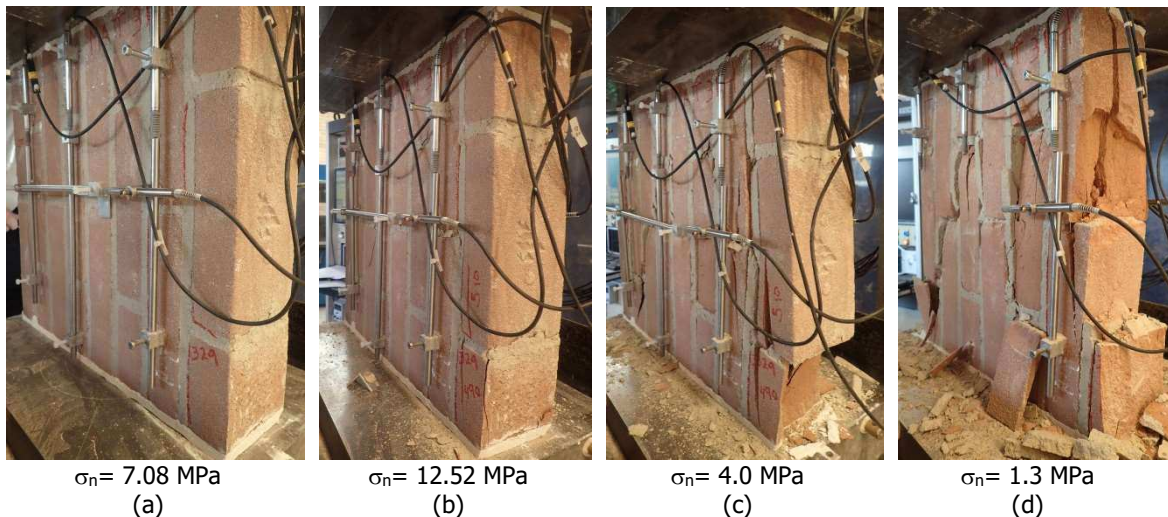


Figure 20 – Crack pattern of single wythe specimen TUD-MAT-31H tested under horizontal compression: (a) first crack; (b) maximum stress; (c)-(d) post-peak phase.

Table 9, Table 10 and Table 11 list the main experimental results for the single wythe clay brick masonry specimens. No noticeable variation in terms of compressive strength in the two orthogonal directions was found ($f'_m / f'_{m,h} = 1.1$). However, higher peak strain in the horizontal direction was observed than the vertical direction ($\epsilon_p / \epsilon_{p,h} = 0.74$). As a result, lower stiffness ($E_3 / E_{3,h} = 1.4$) and higher values of fracture energy ($G_{f-c} / G_{f-c,h} = 0.81$) in the horizontal direction can be expected. By analysing the crack pattern, it was possible to note that when the masonry specimen was rotated and the direction of the bed joints coincided with the loading direction, bricks and head joints formed small columns that were subjected to buckling rather than cracking in the bricks.

Figure 21 and Figure 22 show the results with the histogram representation.

Table 9 – Vertical compression test results of clay single wythe masonry specimens.

Specimen name	Test type	f'_m	E_1	E_2	E_3	ϵ_p	G_{f-c}	ν
		MPa	MPa	MPa	MPa	‰	N/mm	
TUD_MAT-31A	monotonic	13.89	4535	3861	4969	4.0	32.31	0.14
TUD_MAT-31B	monotonic	13.68	3724	3089	4151	4.5	29.59	-
TUD_MAT-31C	monotonic	14.30	5289	4885	5553	3.7	25.24	0.13
TUD_MAT-31D	cyclic	13.34	3683	3377	3857	5.0	28.56	0.12
TUD_MAT-31E	cyclic	13.95	4424	4173	4561	4.3	23.82	-
TUD_MAT-31F	cyclic	14.96	4627	5023	4451	4.1	31.58	0.16
Average		14.02	4380	4068	4590	4.3	28.52	0.14
Standard deviation		0.56	605	783	603	0.4	3.40	0.02
Coefficient of variation		0.04	0.14	0.19	0.13	0.10	0.12	0.11

Table 10 – Horizontal compression test results of clay single wythe masonry specimens.

Specimen name	Test type	$f'_{m,h}$	$E_{1,h}$	$E_{2,h}$	$E_{3,h}$	$\epsilon_{p,h}$	$G_{f-c,h}$	ν_h
		MPa	MPa	MPa	MPa	‰	N/mm	-
TUD_MAT-31G	monotonic	8.68	2480	2519	2462	4.8	42.21	-
TUD_MAT-31H	monotonic	12.52	3362	3493	3301	5.0	34.82	-
TUD_MAT-31I	monotonic	13.11	3168	3438	3049	-	28.28	-
TUD_MAT-31J	cyclic	14.82	3759	4532	3465	5.8	32.87	-
TUD_MAT-31K	cyclic	14.21	3109	3997	2797	7.6	43.70	-
TUD_MAT-31L	cyclic	15.34	4115	4008	4170	5.6	28.47	-
Average		13.11	3332	3664	3207	5.8	35.06	-
Standard deviation		2.41	565	689	592	1.0	6.63	-
Coefficient of variation		0.18	0.17	0.19	0.18	0.19	0.19	-

Table 11 – Orthotropic behaviour of clay single wythe masonry.

	f'_m	E_1	E_2	E_3	ϵ_p	G_{f-c}	ν
	$f'_{m,h}$	$E_{1,h}$	$E_{2,h}$	$E_{3,h}$	$\epsilon_{p,h}$	$G_{f-c,h}$	
	MPa	MPa	MPa	MPa	‰	N/mm	-
Vertical configuration	14.02	4380	4068	4590	4.3	28.52	-
Horizontal configuration	13.11	3332	3664	3207	5.8	35.06	-
Ratio Vertical/Horizontal	1.07	1.31	1.11	1.43	0.74	0.81	-

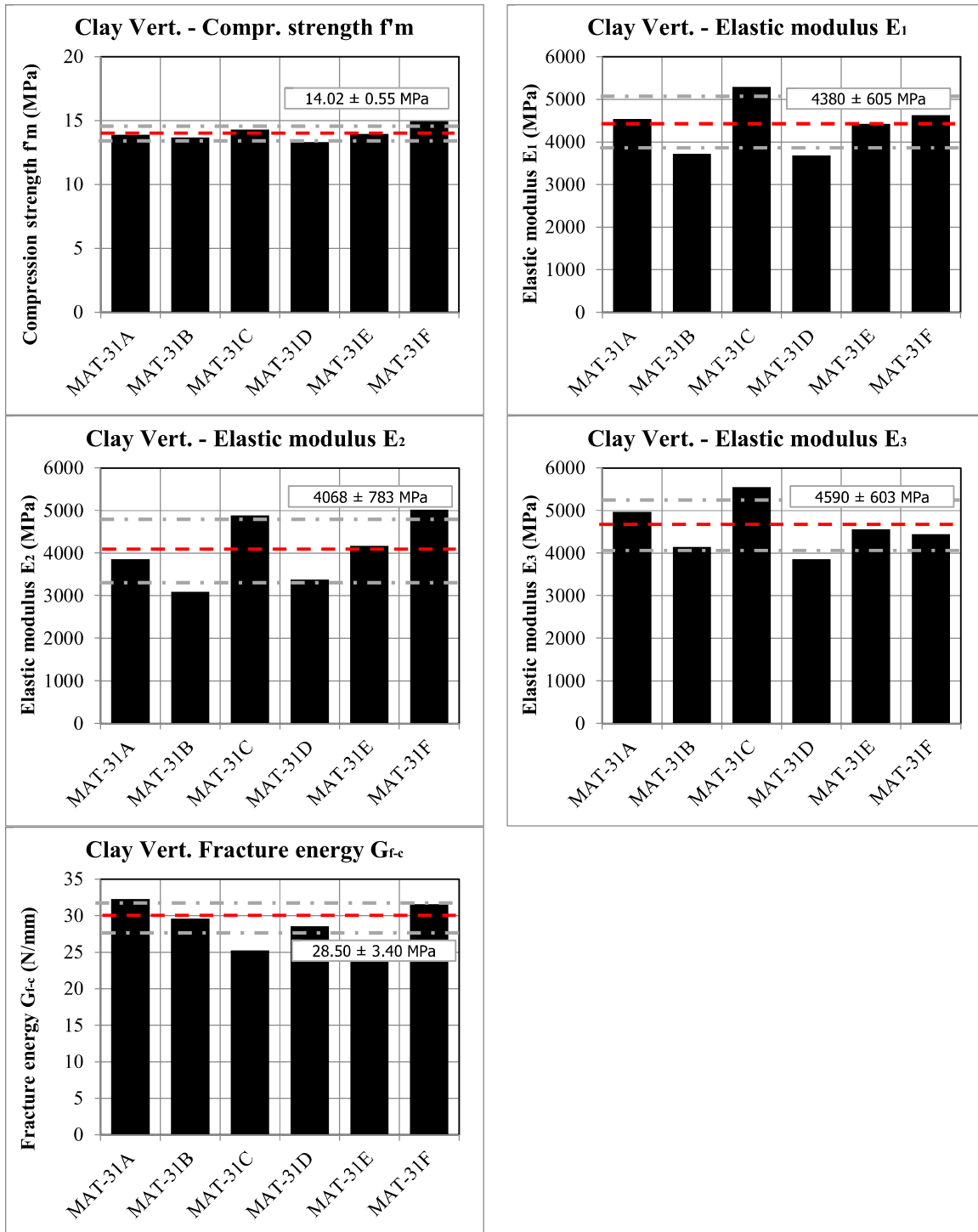


Figure 21 – Vertical compression tests on single wythe clay brick masonry specimens: histogram representation.

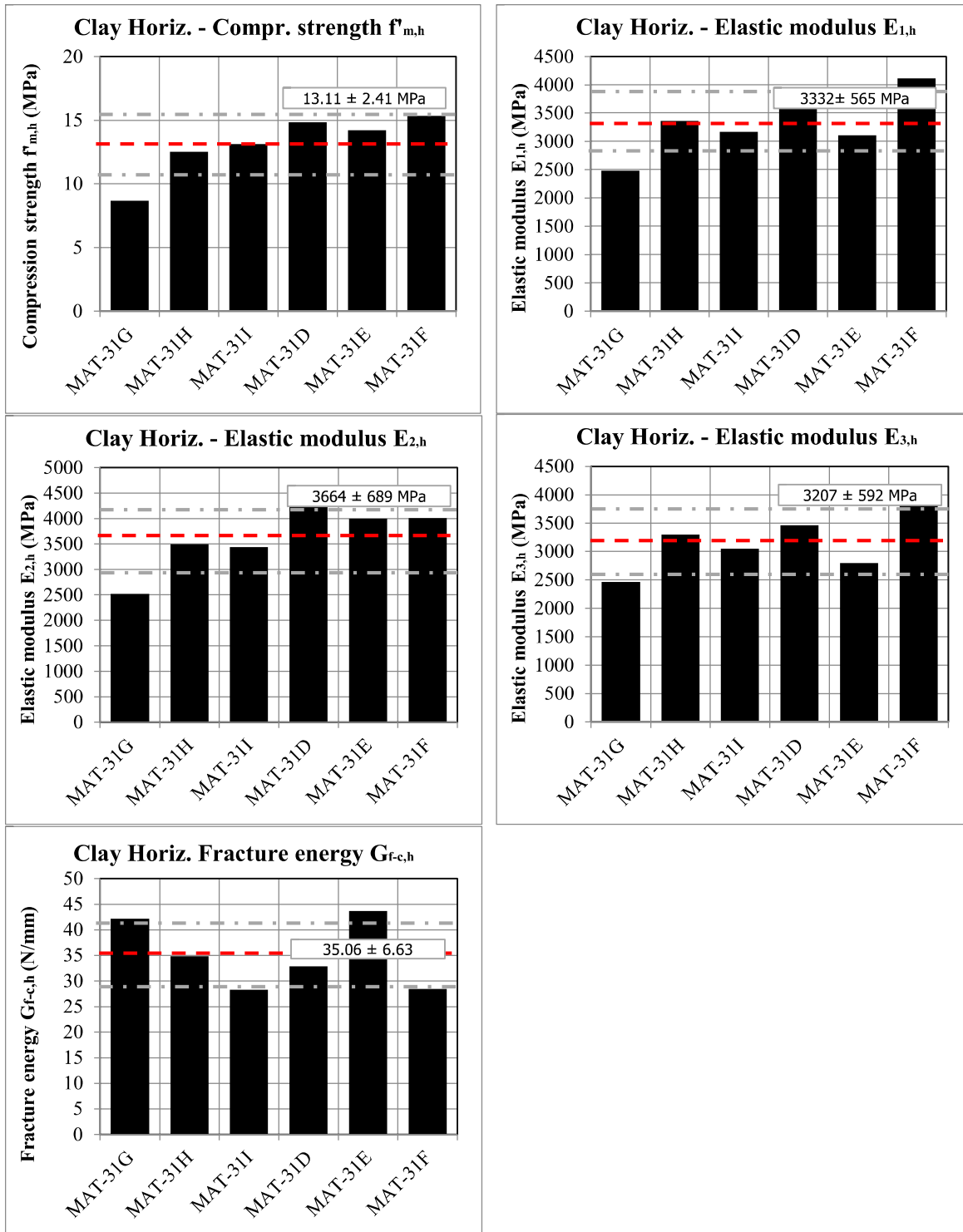


Figure 22 – Horizontal compression tests on single wythe clay brick masonry specimens: histogram representation.

Figure 23 and Figure 24 show the stress-strain diagram for the clay double wythe masonry subjected to vertical load, for the two types of the adopted specimens (TUD-MAT41A and TUD-MAT41B). For both types of the specimens subjected to vertical loading, the stress-strain relationship in the normal direction presents a similar trend. The pre-peak stage was characterised by linear-elastic followed by an hardening behaviour until the peak. The nonlinearity started at approximately 1/3 of peak stress. After the peak stress was reached, an exponential softening behaviour was observed for both types of the specimens. In the case of cyclic loading, the masonry showed an elastic unloading for both configurations.

Figure 25 shows the stress-strain diagram for the horizontal configuration. The graphs refer to the normal direction that is defined as the one parallel to the loading direction. In the case of the horizontal configuration the nonlinear behaviour occurred already at lower stress level between 1/10 and 1/3 of the maximum stress. After the peak stress was reached, an exponential softening behaviour was observed. In the case of cyclic loading, the masonry showed an elastic unloading.

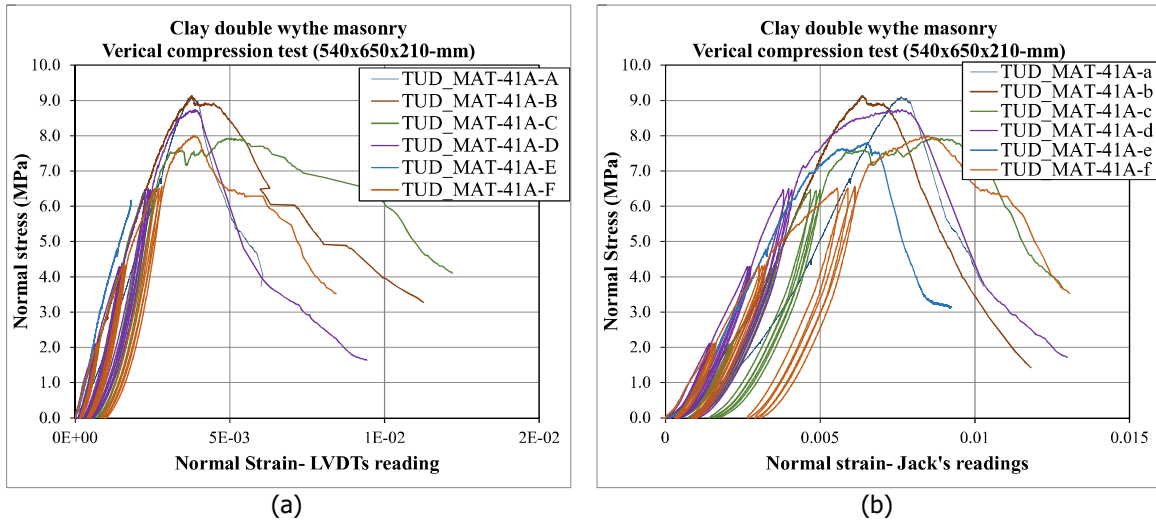


Figure 23 – Vertical compression tests on double wythe clay brick masonry specimens having dimensions 540x650x210-mm (TUD-MAT-41A): (a) normal strain obtained by LVDTs reading; (b) normal strain obtained by jack's reading.

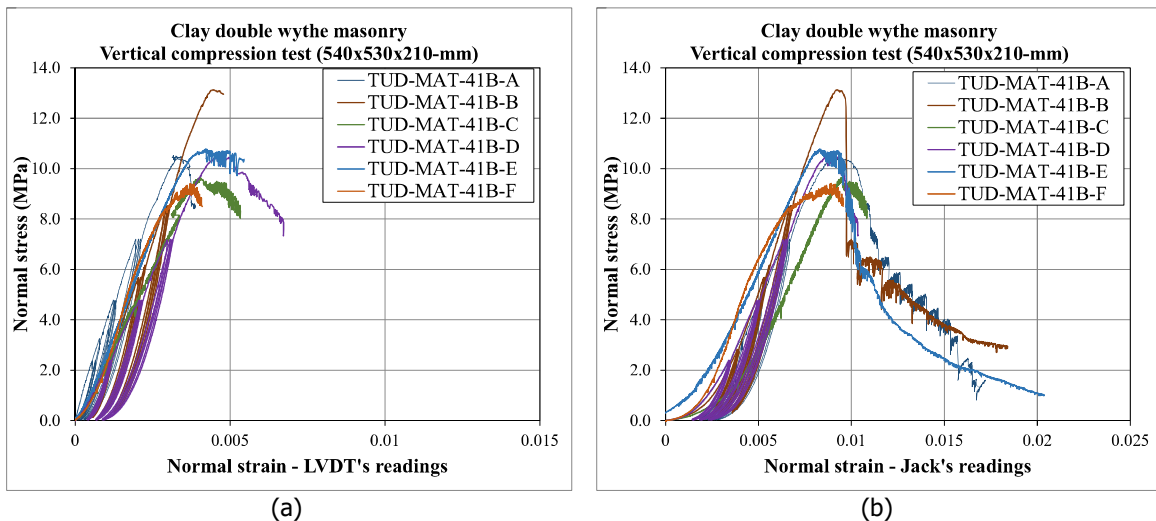


Figure 24 – Vertical compression tests on double wythe clay brick masonry specimens having dimensions 540x530x210-mm (TUD-MAT-41B): (a) normal strain obtained by LVDTs reading; (b) normal strain obtained by jack's reading.

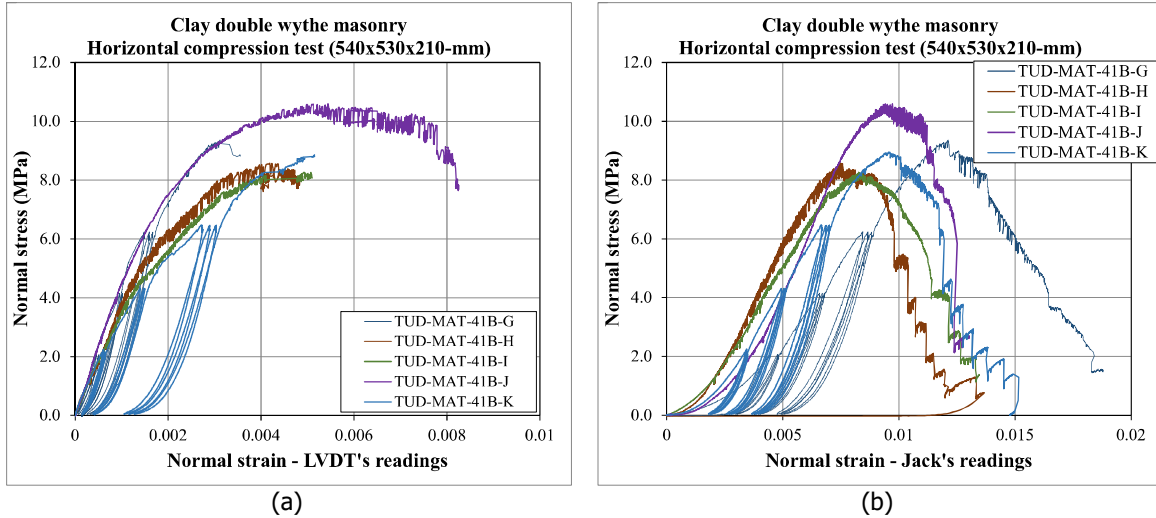


Figure 25 – Horizontal compression tests on double wythe clay brick masonry specimens having dimensions 540x530x210-mm (TUD-MAT41B): (a) normal strain obtained by LVDTs reading; (b) normal strain obtained by jack's reading.

Figure 26 and Figure 27 show the development of cracks in the two specimens having dimensions 540x650x210-mm (TUD-MAT-41A-F) and 540x530x210-mm (TUD-MAT-41B-B) tested under vertical loads. In both cases, splitting cracks started in the bricks and were oriented parallel to the loading direction (Figure 26a, Figure 27a). The cracks were mainly distributed at the extremities (Figure 27b). In the post-peak phase, the vertical cracks mainly developed through the length of the specimen, by splitting it in several parts (Figure 26c, Figure 27c). In addition, on the width face of the specimen a vertical crack propagated over the height of the specimen. The crack propagated until the specimen split in the two leaves Figure 27d).

For the case of horizontal compression tests, cracks started at the brick-mortar interface parallel to the loading direction (Figure 28a). The cracks later developed in the bricks and the external surface of the bricks was spalled off (Figure 28b). In the post-peak phase, the cracks developed through the thickness and through the length, creating a buckling mechanism (Figure 28d). The cracking occurred in a distributed manner over the height of the specimen; no localisation of the cracking at the boundary was observed.

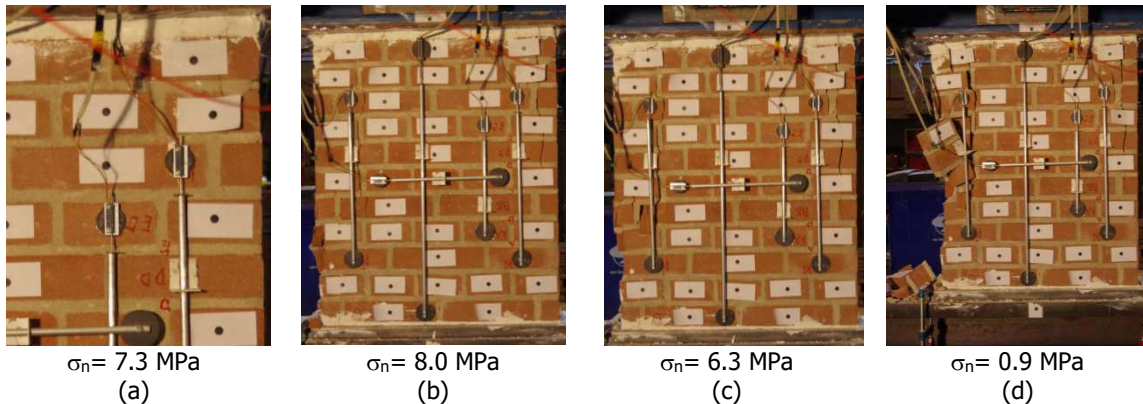


Figure 26 – Crack pattern of double wythe specimen TUD-MAT-41A-F having dimensions (540x650x210-mm) tested under vertical compression: (a) first crack; (b) maximum stress; (c)-(d) post-peak phase.

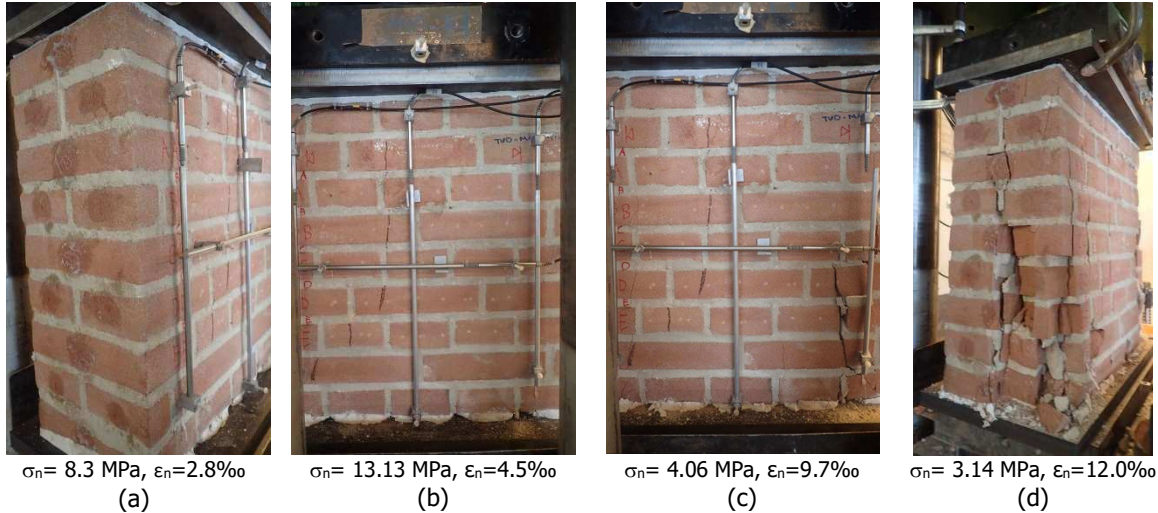


Figure 27 – Crack pattern of double wythe specimen TUD-MAT-41B-B having dimensions (540x530x210-mm) tested under vertical compression: (a) first crack; (b) maximum stress; (c)-(d) post-peak phase.

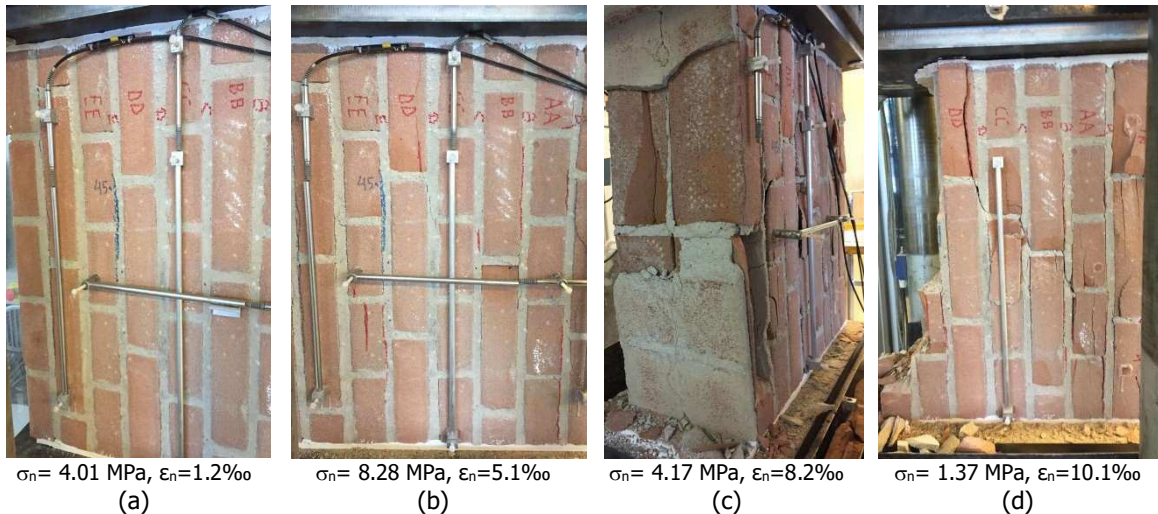


Figure 28 – Crack pattern of double wythe specimen TUD-MAT-41B-I having dimensions (540x530x210-mm) tested under vertical compression: (a) first crack; (b) maximum stress; (c)-(d) post-peak phase.

Table 12 and Table 13 list the compression properties for the clay double wythe specimens having dimensions 540x530x210-mm subjected to vertical and horizontal compressive load.

Table 14 lists the main experimental results for the conforming specimens having dimensions 540x650x210-mm (TUD-MAT-41A) subjected to vertical compressive load.

Table 12 - Vertical compression test results of double wythe clay brick masonry specimens having dimensions 540x530x210-mm.

Specimen name	Test type	f'_m	E_1	E_2	E_3	ϵ_p	G_{f-c}	ν
		MPa	MPa	MPa	MPa	‰	N/mm	
TUD_MAT-41B-A	cyclic	10.53	3868	4628	3584	3.2	30.15	-
TUD_MAT-41B-B	cyclic	13.13	2581	1963	3064	4.5	49.57	-
TUD_MAT-41B-C	monotonic	9.65	2352	1956	2607	4.0	33.74	0.12
TUD_MAT-41B-D	cyclic	10.49	2233	1888	2455	4.5	31.63	0.13
TUD_MAT-41B-E	monotonic	10.79	2693	2126	3110	4.2	35.09	0.13
TUD_MAT-41B-F	monotonic	9.41	2367	1611	3090	3.7	23.88	0.13
Average		10.67	2682	2362	2985	4.0	34.01	0.13
Standard deviation		1.32	605	1123	404	0.5	8.56	0.00
Coefficient of variation		0.12	0.23	0.48	0.14	0.13	0.25	0.03

Table 13 – Horizontal compression test results of double wythe clay brick masonry specimens having dimensions 540x530x210-mm.

Specimen name	Test type	$f'_{m,h}$	$E_{1,h}$	$E_{2,h}$	$E_{3,h}$	$\epsilon_{p,h}$	$G_{f-c,h}$	ν
		MPa	MPa	MPa	MPa	‰	N/mm	-
TUD_MAT-41B-G	cyclic	9.36	4793	3065	6839	3.1	21.59	-
TUD_MAT-41B-H	monotonic	8.58	3682	4154	3487	4.2	28.66	-
TUD_MAT-41B-I	monotonic	8.28	3614	3983	3453	5.1	27.67	-
TUD_MAT-41B-J	monotonic	10.60	4674	4372	4842	5.4	31.21	-
TUD_MAT-41B-K	cyclic	8.95	3299	4195	2976	5.2	32.55	-
Average		9.15	4012	3954	4319	4.6	28.34	-
Standard deviation		0.91	676	516	1571	0.9	4.25	-
Coefficient of variation		0.10	0.17	0.13	0.36	0.21	0.15	-

Table 14 – Vertical compression test results of double wythe clay brick masonry specimens having dimensions 540x650x210-mm.

Specimen name	Test type	f'_m	E_1	E_2	E_3	ϵ_p	G_{f-c}	ν
		MPa	MPa	MPa	MPa	‰	N/mm	-
TUD_MAT-41A-A	monotonic	9.11	2197	1645	2641	3.5	24.21	0.12
TUD_MAT-41A-B	monotonic	9.13	2766	3163	2603	3.9	32.99	0.13
TUD_MAT-41A-C	cyclic	7.93	2807	2959	2736	5.9	46.11	0.10
TUD_MAT-41A-D	cyclic	8.74	3234	3948	2966	3.9	33.92	0.06
TUD_MAT-41A-E	monotonic	7.80	3295	2524	3890	-	-	-
TUD_MAT-41A-F	cyclic	8.00	2861	3342	2669	3.4	41.26	-
Average		8.54	2860	2930	2917	4.1	35.7	0.10
Standard deviation		0.61	395	785	493	1.1	8.39	0.03
Coefficient of variation		0.07	0.14	0.27	0.17	0.26	0.24	0.3

Table 15 lists the properties of the specimens having dimensions 540x530x210-mm aiming to investigate the orthotropic behaviour. The clay brick masonry showed an orthotropic behaviour, having a higher compressive strength in the direction perpendicular to the bed joints ($f_m / f_{m,h} = 1.2$). A similar ratio was observed in terms of fracture energy ($G_{f-c} / G_{f-c,h} = 1.2$). Similar to the single wythe specimens the strain at peak increased when the loading direction was coincided with the bed joint ($\epsilon_p / \epsilon_{p,h} = 0.87$). In contrast to single wythe specimens, the double wythe specimens resulted to be stiffer in the direction parallel to the bed joints ($E_1 / E_{1,h} = 0.7$ and $E_3 / E_{3,h} = 0.7$).

Table 15 – Orthotropic behaviour of double wythe clay brick masonry having dimensions 540x530x210-mm.

Orthotropic behaviour	f'_m	E_1	E_2	E_3	ϵ_p	G_{f-c}	ν
	$f'_{m,h}$	$E_{1,h}$	$E_{2,h}$	$E_{3,h}$	$\epsilon_{p,h}$	$G_{f-c,h}$	-
Vertical configuration	10.67	2682	2362	2985	4.0	34.01	-
Horizontal configuration	9.15	4012	3954	4319	4.6	28.34	-
Ratio Vertical/Horizontal	1.17	0.67	0.60	0.69	0.87	1.20	-

An analysis on the influence of the specimen size on the evaluation of the compression properties of masonry is made in Table 16, where the experimental results obtained on specimens having size 540x650x210-mm (TUD-MAT-41A) and 540x530x210-mm (TUD-MAT-41B) are compared. By comparing the results, the following observations can be made:

- lower values of compressive strength was obtained by increasing the height of the specimen
- no significant variation in the compression properties in terms of the Young's modulus, strain at peak strength and fracture energy was reported for the specimens having different heights.

The experimental results are in line with information reported in literature [14], which provides a scaling factor only for the compressive strength. According to the literature information, the compressive strength of a specimen with certain dimensions should be normalised to the strength of a reference sized specimen by using a slenderness correction factor (scf). Figure 29 shows the correction factors versus slenderness of the specimen (h_s / t_s). According to different references, variation can be obtained in the estimation of slenderness correction factor (scf). In this case, the slenderness correction factor has been defined as the average value obtained from the graph in Figure 29. Although the compressive strength of the specimens having dimensions of 540x530x210-mm is normalised with respect to the dimensions of the specimens with 540x560x210-mm, the compressive strength has not been changed significantly. It should be mentioned the results reported in this study are based on a limited number of specimens, additionally; limited information is available in the literature regarding the effect of masonry size on the properties. Figure 30, Figure 31 and Figure 32 show the results with the histogram representation.

Table 16 – An overview of the vertical compression properties of specimens having different dimensions: TUD-MAT-41A (540x650x210-mm) and TUD-MAT-41B (540x530x210-mm).

Size of the specimens	h_s / t_s	scf	f'_m	f'_{mod}	E_1	E_2	E_3	ε_p	G_{f-c}
		-	MPa	MPa	MPa	MPa	MPa	‰	N/mm
540x650x210-mm (MAT- 41A)	3.1	1	8.45	8.45	2860	2930	2917	3.8	35.7
540x530x210-mm (MAT- 41B)	2.5	0.94	10.67	10.03	2682	2362	2985	4.0	34.0
Ratio between results of MAT-41A/MAT41B			0.8	0.8	1.1	1.2	1.0	1.0	1.0
Including all the results of MAT-41A specimens and MAT- 41B specimens	Avg.		9.56	9.26	2771	2646	2951	4.1	34.8
	St.dev.		1.52	1.26	496	970	431	0.76	8.1
	C.o.V.		0.16	0.14	0.18	0.37	0.15	0.19	0.23

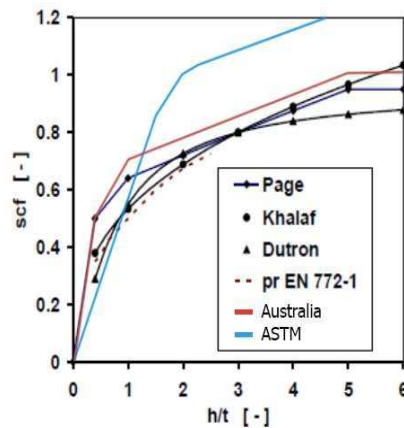


Figure 29 – Correction factors for compressive strength as a function of slenderness (h/t) based on [14].

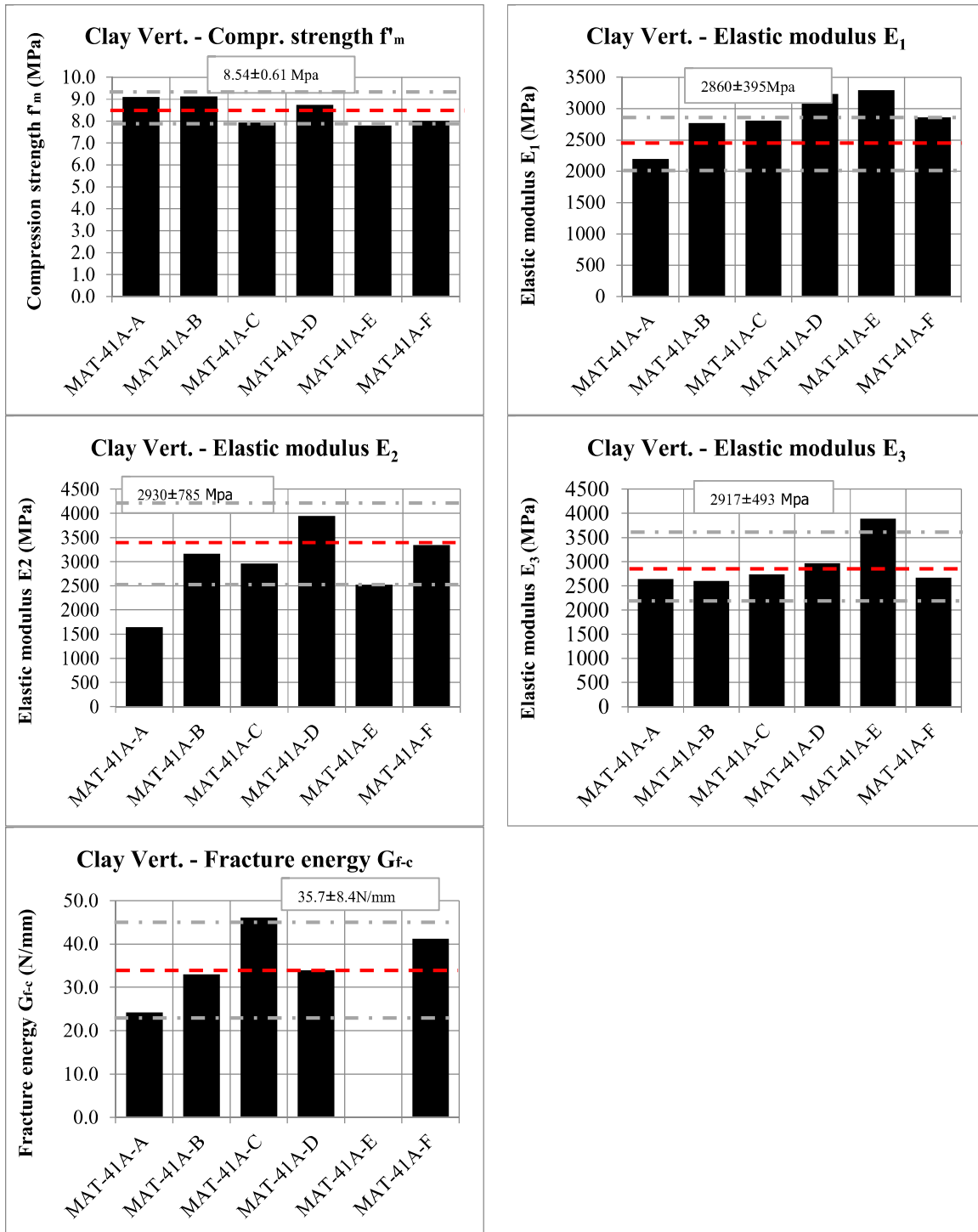


Figure 30 – Vertical compression tests on clay double wythe masonry specimens (TUD-MAT-41A): histogram representation.

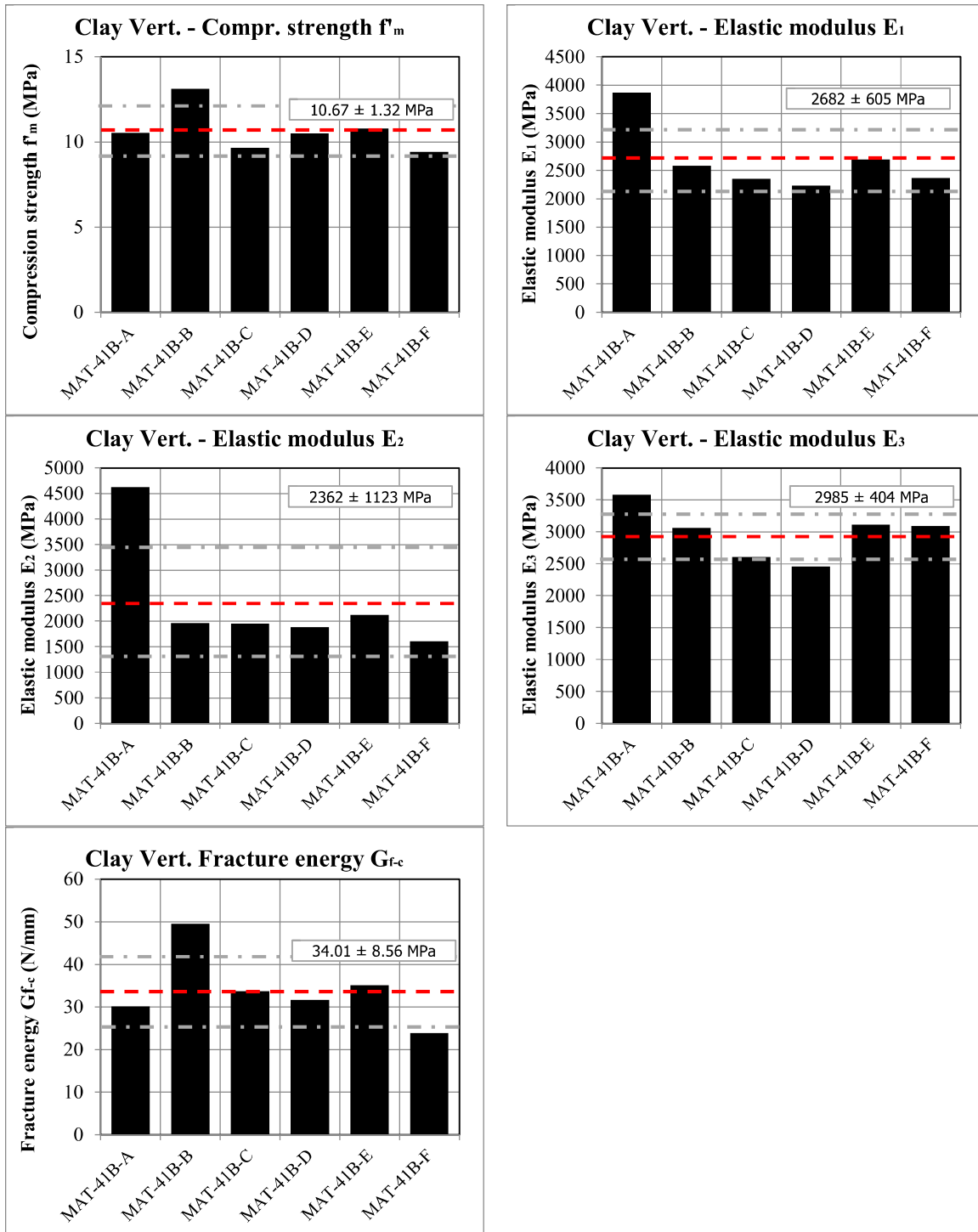


Figure 31 – Vertical compression tests on double wythe clay brick masonry specimens (TUD-MAT-41B): histogram representation.

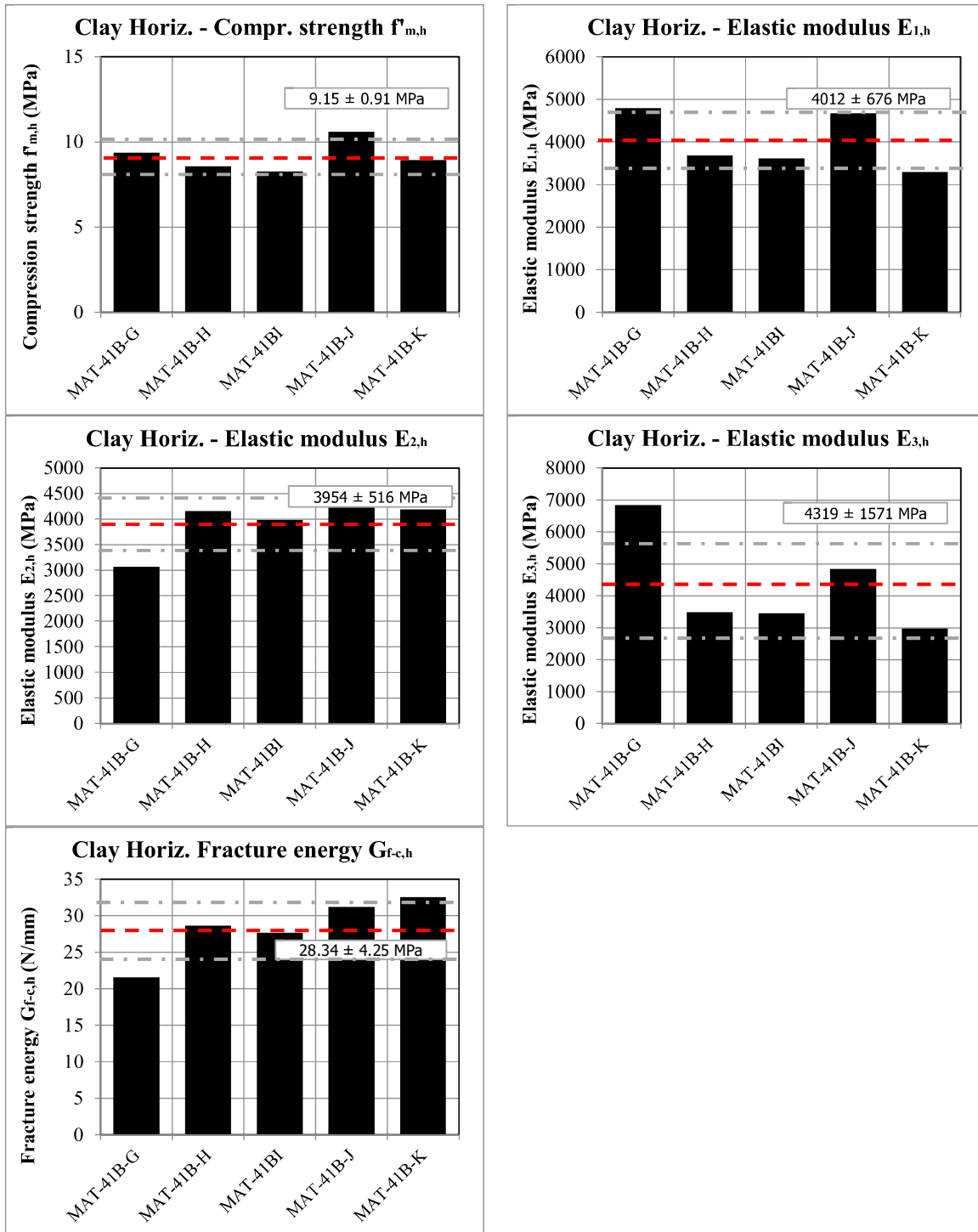


Figure 32 – Horizontal compression tests on double wythe clay brick masonry specimens (TUD-MAT-41B): histogram representation.

9 Flexural strength of masonry

The flexural strength of masonry was determined for three configurations:

- Four-point bending test with the moment vector parallel to the bed joints and in the plane of the wall, which generates a plane of failure parallel to the bed joints (denoted as vertical out-of-plane bending test OOP1);
- Four-point bending with the moment vector orthogonal to the bed joints and in the plane of the wall, which generates a plane of failure perpendicular to the bed joints (denoted as horizontal out-of-plane bending test OOP2);
- Four-point bending with the moment vector orthogonal to plane of the wall (denoted as in-plane vertical bending test IP).

The first two tests were performed in agreement with EN 1052-2:1999 [15], while the third one was a non-standardized test.

9.1 Testing procedure

The masonry specimens tested with the moment vector in the plane of the wallets were designed in agreement with EN 1052-2:1999 [15]. An overview of dimensions of the tested specimens both single and double wythe is listed in Table 17. The masonry type, the dimensions and the distance between the bearing supports d_1 and loading supports d_2 are listed. More information regarding the size of the specimens can be found on Ref. [1].

Table 17 – Overview of dimensions of specimens adopted for bending tests.

Test type	Masonry wythe	l_s (mm)	h_s (mm)	d_1 (mm)	d_2 (mm)
Bending test with moment vector parallel to the bed joints and in the plane of the wall (OOP1)	Single	430	590	420	220
	Double	760	890	720	360
Bending test with moment vector orthogonal to the bed joints and in the plane of the wall (OOP2)	Single	870	290	660	360
	Double	1200	650	1100	600
Bending test with moment vector orthogonal to the bed joints and in the plane of the wall (IP)	Single	870	290	660	360
	Double	1420	350	990	410

In the current testing campaign, a new testing set-up for the out-of-plane bending tests was designed, as shown in Figure 33. In the improved set-up, the specimens were placed vertically and loaded in such a way that the bending axis was always horizontal. Consequently, the contribution of the masonry self-weight was excluded.

The load was applied via cylindrical roller bearings mounted to steel hollow profiles with springs which enabled them to easily move. A counterweight was used to minimise the friction forces between the specimen and the loading support, the loading support was suspended using steel wire. The bearing rollers were mounted to the test rig with springs. The distance between the loading, d_l , and bearing rollers, d_b , was chosen according to the standard (Table 17). At the base, the specimen was supported by a steel plate positioned on top of flat ball bearings.

The load was applied in displacement control by a spherical joint attached to a hydraulic jack with 100 kN capacity. The applied load was recorded from the load cell attached to the hydraulic jack. For each side, a maximum of five LVDTs was attached to measure the vertical and horizontal displacements in the constant moment zone (Figure 33). The LVDTs had a measuring range of 10 mm with an accuracy of 0.1%. Apart from the test set-up, the measuring system was also improved, by which a better understanding on the softening post-peak behaviour of masonry could be gained. In this view, two vertical LVDTs were installed on the back face of the specimen to measure the crack opening. The average crack opening value obtained by these LVDTs was used as a control parameter.

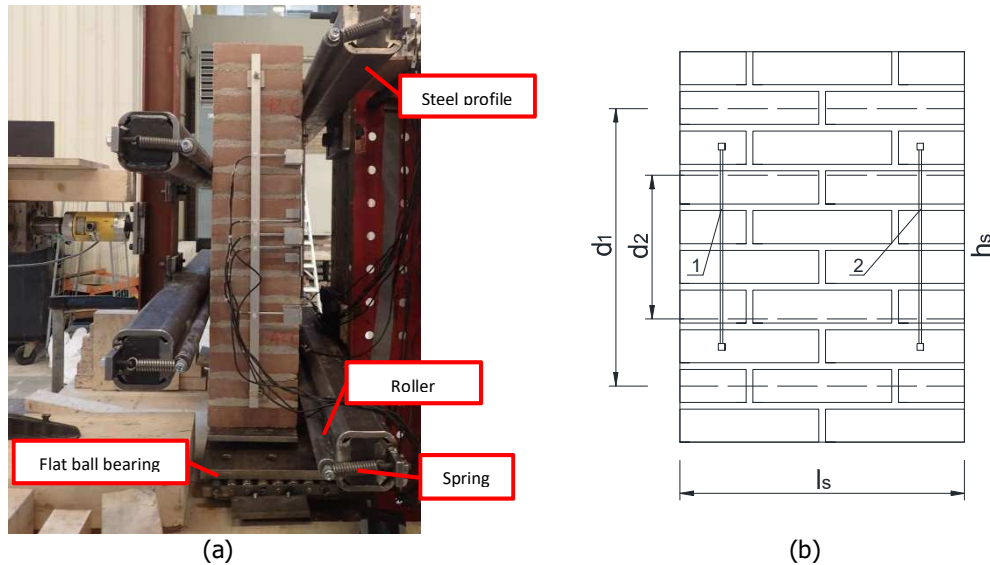


Figure 33 – Out-of-plane bending: (a) testing set-up; (b) average of LVDTs reading used as control parameter.

Figure 34 shows the in-plane bending test set-up. The load was applied in displacement control by a spherical joint attached to a hydraulic jack with 100 kN capacity. The applied load was recorded from the load cell attached to the hydraulic jack.

The deflection of the specimen in the constant moment zone was measured using five vertical LVDTs on each side. In addition, the crack opening was measured using the horizontal LVDTs; one on each side. The crack opening, obtained as the average value of the two horizontal LVDTs readings, was used as a parameter to control the applied load. Consequently, the horizontal load was imposed in order to provide a gradual increase in crack opening at the centre of the wallet.

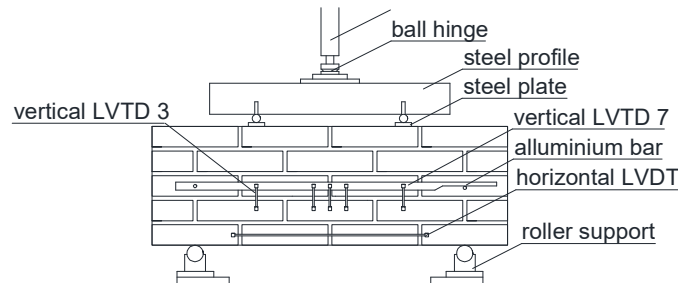


Figure 34 – In-plane bending test (IP): testing set-up.

In order to gather additional information, samples to be used for material tests were extracted from large-scale walls to be tested as component (code TUD_COMP) under in-plane and out-of-plane loading (WP3 in Ref. [1]). The wall TUD_COMP-22 made of single wythe clay brick masonry was used to saw-cut the samples for the material tests, such as shear, bond wrench and in-plane bending tests, see Figure 35. Two samples (4x5x1-brick) to be subjected to the in-plane bending were extracted from this wall. These samples in the current document were denoted as TUD-MAT-C34f and TUD-MAT-C34g.



Figure 35 – Sample extraction from wall TUD_COMP-22: (a) wall after the test; (b) selection of samples to be sawn-cut for the in-plane bending.

9.2 Experimental results

The flexural strength of the out-of-plane tests can be determined as follows:

$$f_{x1} = \frac{3F_{\max}d_3}{l_s t_s^2} \quad (11)$$

$$f_{x2} = \frac{3F_{\max}d_3}{h_s t_s^2} \quad (12)$$

where F_{\max} is the maximum load at failure, d_3 is the distance between the loading and the bearing support, l_s is the length of masonry specimen as built, h_s is the height of masonry specimen as built and, t_s is the thickness of masonry specimen as built.

The flexural strength of the in-plane tests f_{x3} can be determined as follows:

$$f_{x3} = \frac{M_{\max}}{W} = \frac{(F_{\max}d_3/2 + pd_1^2/8)}{W} \quad (13)$$

where M_{\max} is the maximum bending moment, F_{\max} is the maximum load at failure, d_3 is the distance between the loading and the bearing support, d_1 is the distance between the bearing support, p is the masonry self-weight uniform load (calculated assuming a density of 1700 kg/m³ as described in Section 7) and W is the section modulus.

Assuming a linear stress distribution over the height of the specimen's cross-section, the elastic modulus of the masonry can be determined as follows:

$$E_{f_{xi}} = \frac{\frac{F_{el}}{2} \times \frac{(d_1 - d_2)}{2} \times (3d_1^2 - 4(\frac{(d_1 - d_2)^2}{2}))}{24v_{el}I} \quad (14)$$

where F_{el} and v_{el} are the load and mid-span vertical displacement in the linear elastic stage, respectively, I is the moment of inertia of the masonry along the cross-section, d_1 and d_2 are the distance between the loading and bearing loading, respectively. The chord elastic modulus of masonry was calculated between 1/10 and 1/3 of the maximum force.

The concept of fracture energy associated with tensile cracking has already been used for the steel and concrete. Subsequently, this concept was applied to masonry as introduced by Van der Pluijm [16]. Thanks to using improved set-up, the fracture energy determined from the four-point bending test can be calculated as the sum of the areas underneath the two point loads versus the deflection diagram corresponding to these loads, taking into account the cross-section of the specimen. The fracture energy for the vertical out-of-plane bending, G_{fk1} , horizontal out-of-plane bending, G_{fk2} , and in-plane bending is calculated, G_{fk3} .

Figure 36 shows the point load versus the load point deflection for the clay brick masonry subjected to bending tests used for the calculation of the fracture energy. The position of the LVDTs is shown in Figure 34. In some case, especially for the out-of-plane tests, a plateau was found in the post-peak phase, which might be attributed to the weight of the specimen as well as formation of mixed cracks propagated along multiple joints. In the case that a constant force was achieved at the end of the post-peak phase, the stress-strain relationship adopted for the estimation of the fracture energy was modified by extending the softening branch up to zero force and thus excluding the plateau. The slope of the post-peak curve, calculated between the maximum load and approximately 10% reduction in the maximum load, was used as a basis for prolonging the softening branch, as shown in Figure 36b.

Figure 37 shows the force-displacement curve for clay single wythe specimens subjected to bending tests. In the case the installation of a central LVDT was not possible, the mid-span displacement has been calculated from the readings of the other vertical LVDTs, by applying a linear interpolation. A post-peak softening behaviour could be observed for almost all the tested specimens.

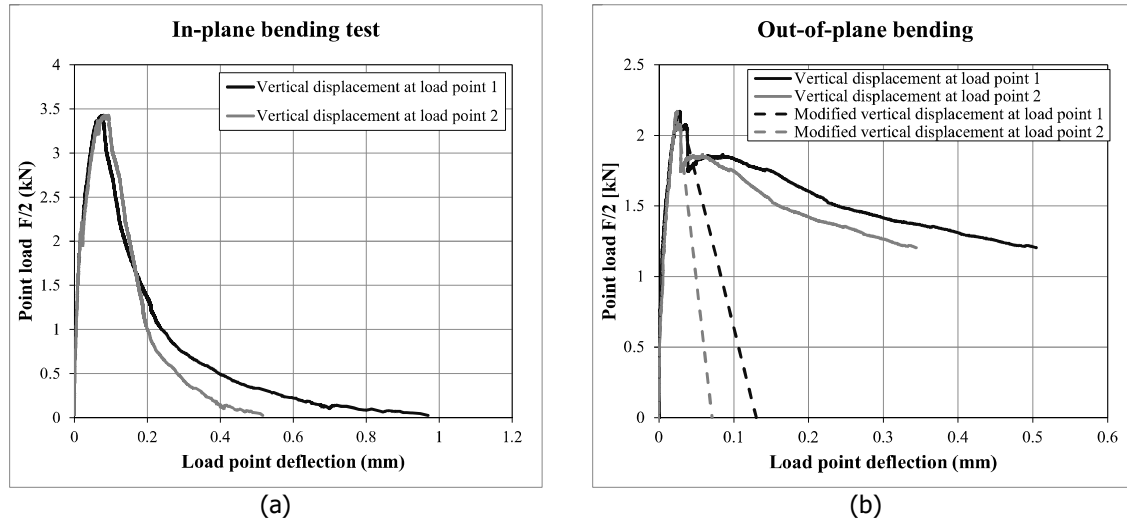


Figure 36 – Load point versus load point deflection curve for clay brick masonry used to calculate the fracture energy: (a) in-plane bending; (b) out-of-plane bending in which the curve is modified in the post-peak phase.

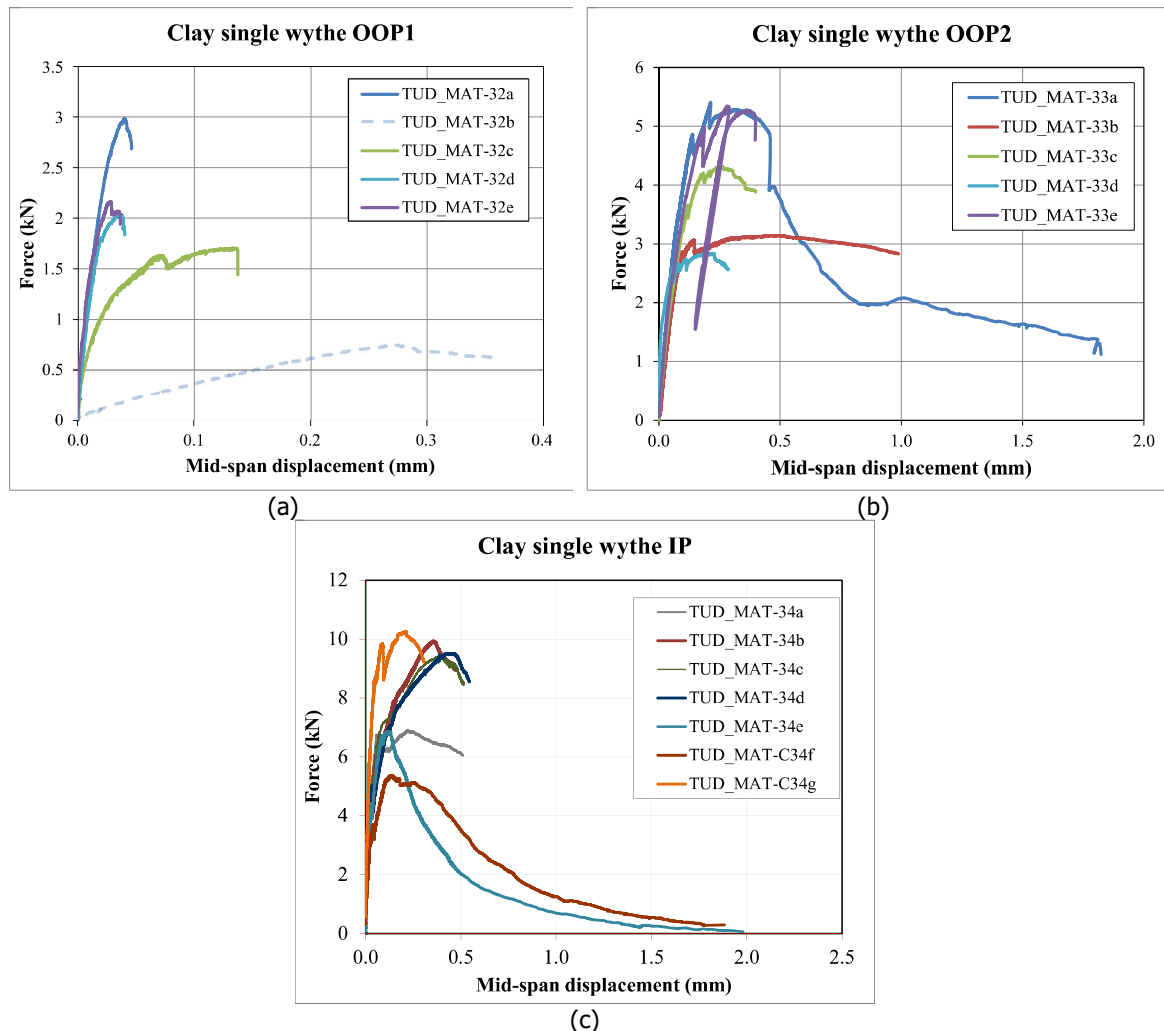


Figure 37 – Force-displacement curve for clay single wythe masonry specimens subjected to: (a) vertical out-of-plane bending test; (b) horizontal out-of-plane bending test; (c) in-plane bending.

The crack patterns of single wythe specimens for the bending tests are shown in Figure 38 to Figure 40.

For the vertical out-of-plane test, the observed crack pattern was as follows:

- Straight crack in the constant moment zone along one bed joint (MAT-32a and MAT-32b), see Figure 38a.
- Straight crack developed in the constant moment zone and then alternating to the upper row through the head joint (MAT-32c and MAT-32e), see Figure 38b.
- Mixed crack including straight crack in the constant moment zone along one bed joint which was also alternating to another row via head joint (MAT-32d).

A brittle failure mechanism was observed.

In the case of horizontal out-of-plane bending tests, alternating crack appeared running through the head joints and bed joints. The crack pattern of the tested specimen is shown in Figure 39. A quasi-brittle failure mechanism was observed.

For the in-plane bending test a brittle or quasi-brittle behaviour was reported. The cracking occurred in both bed and head joints, creating a stepwise pattern outside the constant moment zone. The cracking of the brick near to the applied load was observed in two specimens. The observed crack pattern for tested specimens is shown in Figure 40.

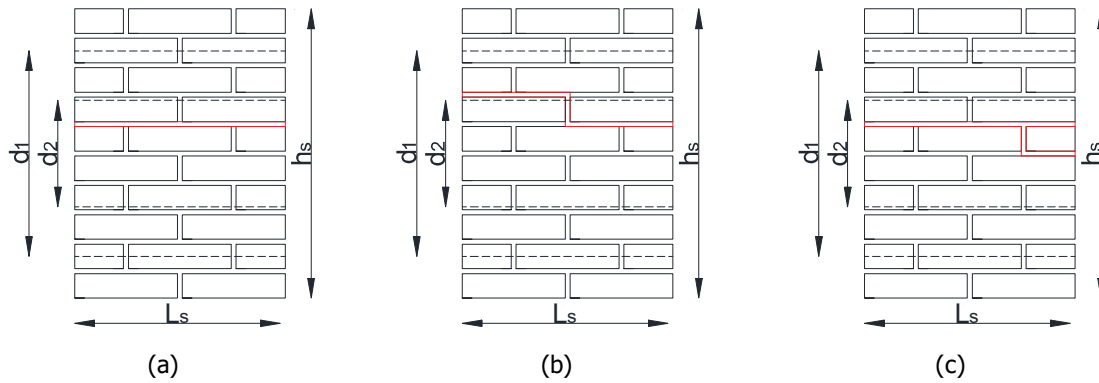
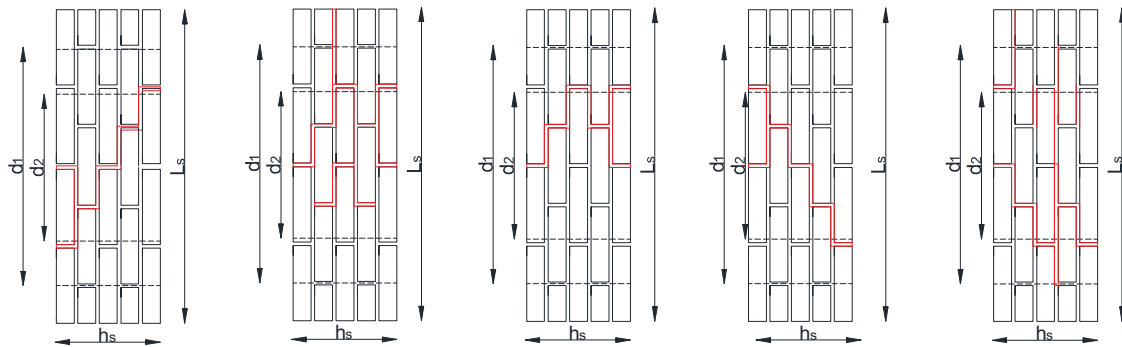


Figure 38 - Crack pattern for single wythe masonry specimens subjected to vertical out-of-plane bending (OOP1): (a) MAT-32a and MAT-32b; (b) MAT-32c and MAT-32e; (c) MAT-32d.



TUD-MAT-33a TUD-MAT-33b TUD-MAT-33c TUD-MAT-33d TUD-MAT-33e
Figure 39 - Crack pattern for single wythe masonry specimens subjected to horizontal out-of-plane bending (OOP2).

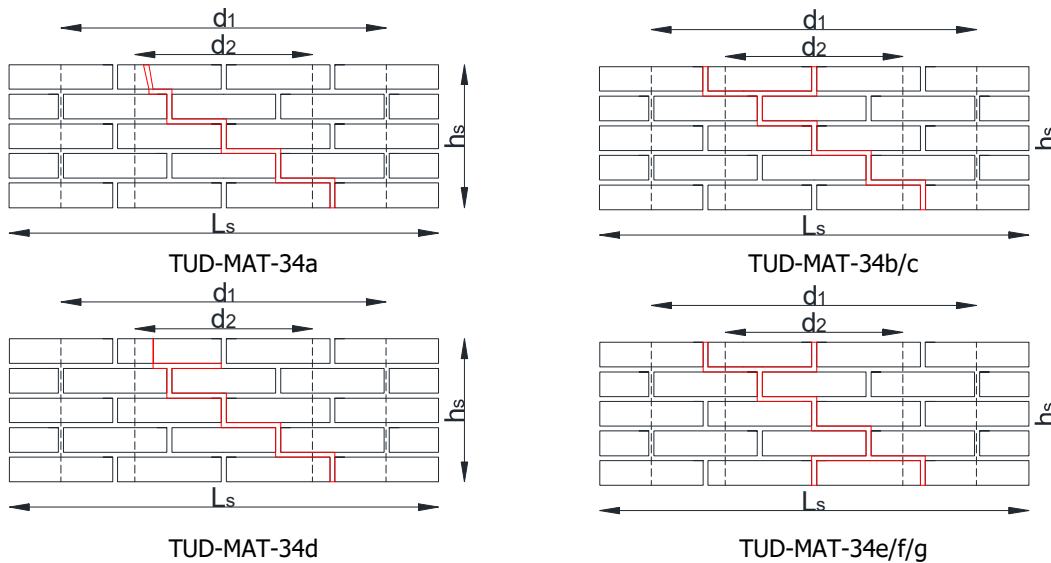


Figure 40 - Crack pattern for single wythe masonry specimens subjected to in-plane bending (IP).

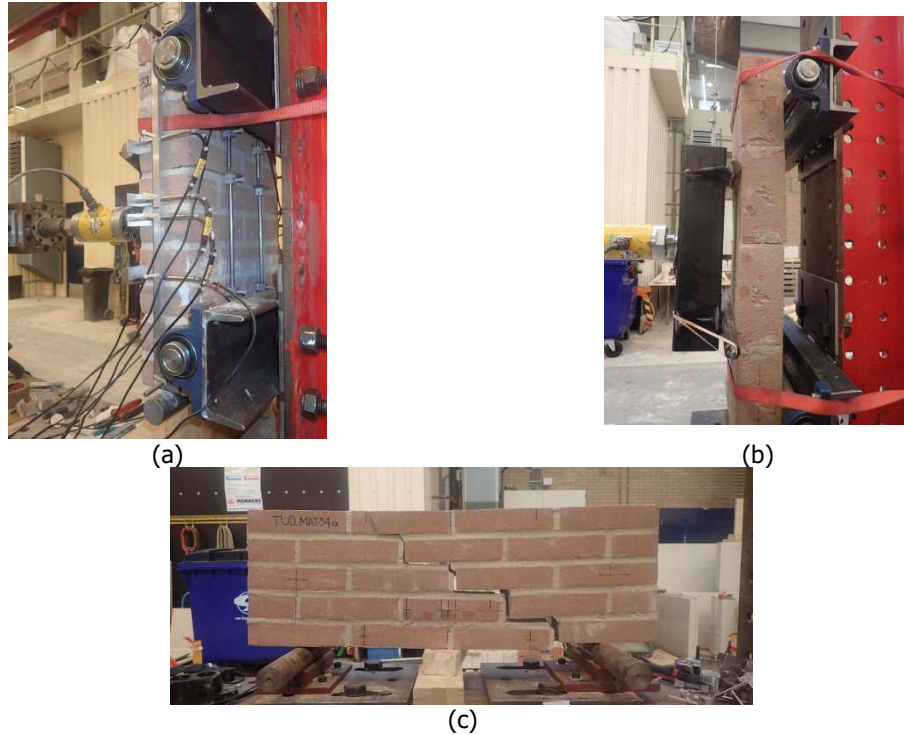


Figure 41 – Crack pattern for single wythe specimens subjected to four-point bending: (a) vertical out-of-plane bending; (b) horizontal out-of-plane bending; (c) in-plane bending.

The bending properties of the single wythe clay specimens in terms of flexural strength, elastic chord modulus calculated between 10% and 30% of the maximum load and the fracture energy are listed in Table 18. The horizontal out-of-plane flexural strength resulted approximatively 4 times higher values than the vertical out-of-plane flexural strength ($f_{x2} / f_{x1} = 4.1$). The in-plane strength is approximatively two times higher than the vertical out-of-plane flexural strength ($f_{x3} / f_{x1} = 2.4$). The mean value of the in-plane flexural strength obtained from testing the wallets constructed for this purpose (MAT-34) is relatively higher than the mean value obtained from those specimens extracted from the TUD-COMP-22 wall (MAT-C34).

Table 18 – Bending properties of single wythe clay brick masonry specimens.

Specimen name	f_{x1} MPa	E_{fx1} MPa	G_{fx1} N/mm	Specimen name	f_{x2} MPa	E_{fx2} MPa	G_{fx2} N/mm	Specimen name	f_{x3} MPa	E_{fx3} MPa	G_{fx3} N/mm
MAT-32a	0.21	3758	0.0045	MAT-33a	0.84	7746	0.24	MAT-34a	0.39	-	0.31
MAT-32b	0.06	-	-	MAT-33b	0.49	6608	0.26	MAT-34b	0.54	3039	0.20
MAT-32c	0.13	4120	0.0068	MAT-33c	0.67	-	0.10	MAT-34c	0.52	3454	0.21
MAT-32d	0.15	3390	0.0029	MAT-33d	0.44	-	0.06	MAT-34d	0.53	2485	0.17
MAT-32e	0.16	-	0.0027	MAT-33e	0.83	6887	0.18	MAT-34e	0.39	3276	0.08
								MAT-C34f	0.31	2365	0.21
								MAT-C34g	0.57	-	0.18
Average	0.16	3756	0.0042	Average	0.65	7080	0.17	Average	0.46	2924	0.19
St. dev.	0.03	365	0.0019	St. dev.	0.19	593	0.09	St. dev.	0.10	480	0.07
C.o.V	0.21	0.10	0.45	C.o.V	0.28	0.08	0.52	C.o.V	0.22	0.16	0.35
				f_{x2} / f_{x1}	4.06			f_{x3} / f_{x1}	2.44		
				Average of the MAT specimens					0.47	3064	0.19
				Average of the MAT-C specimens					0.44	2365	0.20

Figure 42 shows the force-displacement curve for clay double wythe specimens subjected to bending tests. Thanks to using an improved set-up post-peak softening branch was found.

The crack patterns for each bending test are shown in Figure 43 to Figure 45.

For the vertical out-of-plane test, the observed crack pattern was as follows:

- Straight crack in the constant moment zone along one bed joint (MAT-42a and MAT-42b), see Figure 43.
- Straight crack developed outside the constant moment zone along one bed joint (MAT-42c), see Figure 43.
- Straight crack developed in the constant moment zone and then alternating to the lower row through the head joint (MAT-42d and MAT-42e).

In the case of horizontal out-of-plane bending tests, cracking appeared both in the head joints and in the bed joints (see Figure 44). In addition, for all the tested specimens, no splitting of the unit was reported. A quasi-brittle failure mechanism was observed.

For the in-plane bending test a brittle or quasi-brittle behaviour was reported. The cracking occurred in both bed and head joints in the constant moment zone, creating a stepwise pattern. Only for specimen TUD-MAT-44a, cracks developed outside the constant moment zone; consequently the data of this test are excluded from the average value.

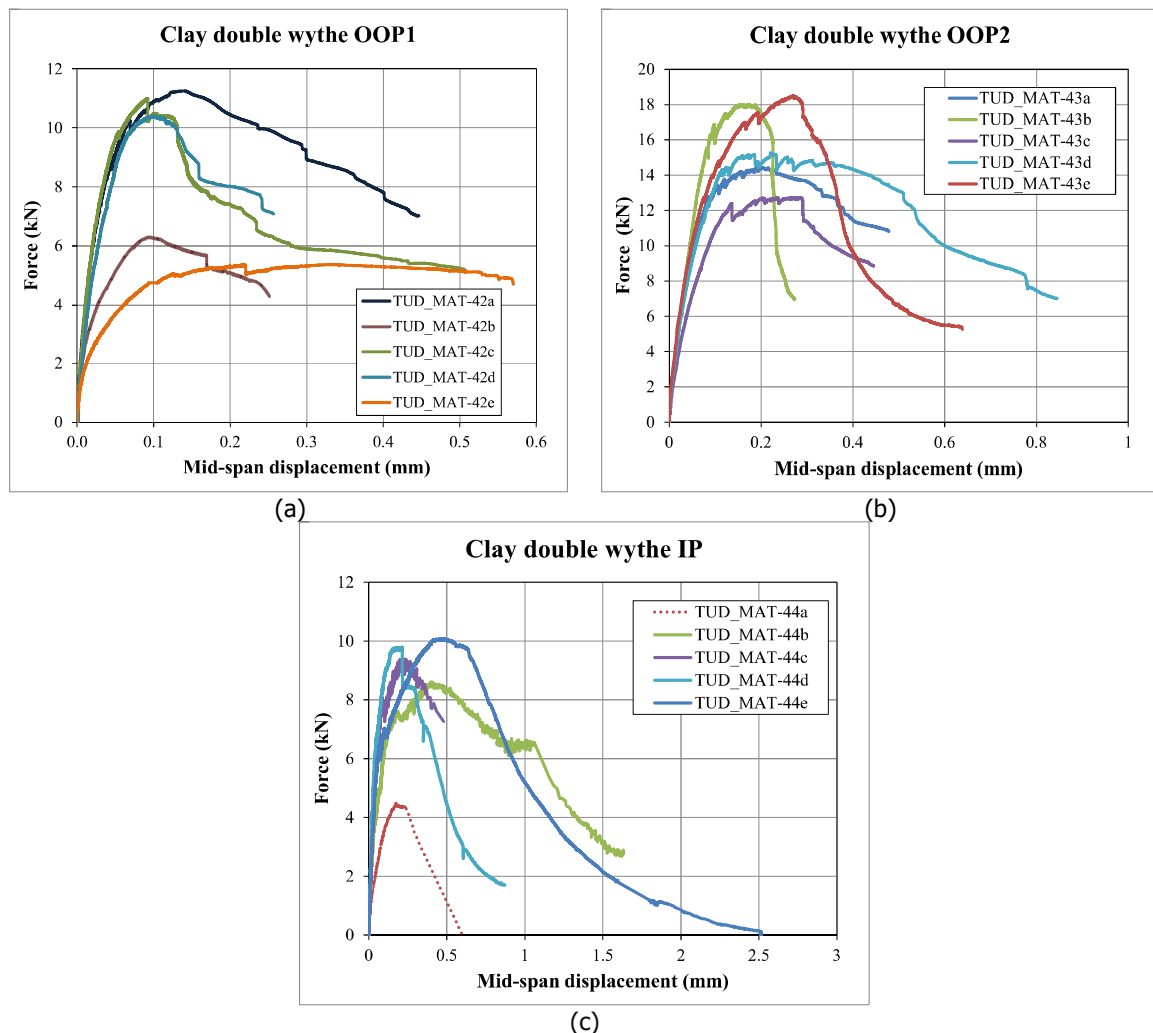
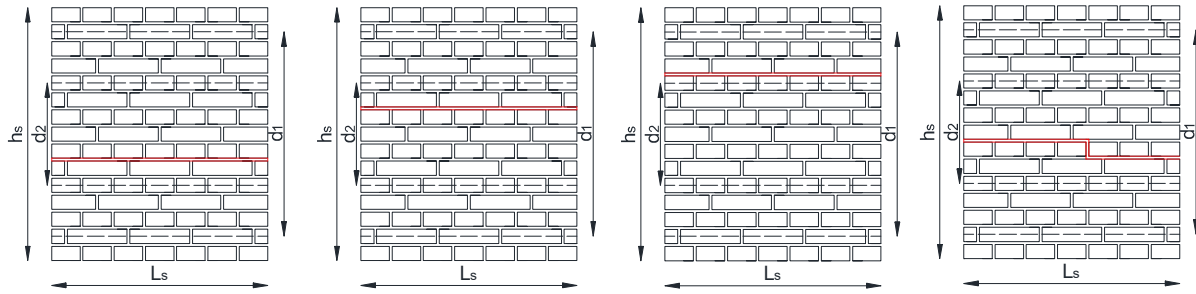


Figure 42 – Force-displacement curve for double wythe clay brick masonry specimens subjected to: (a) vertical out-of-plane bending test; (b) horizontal out-of-plane bending test; (c) in-plane bending.



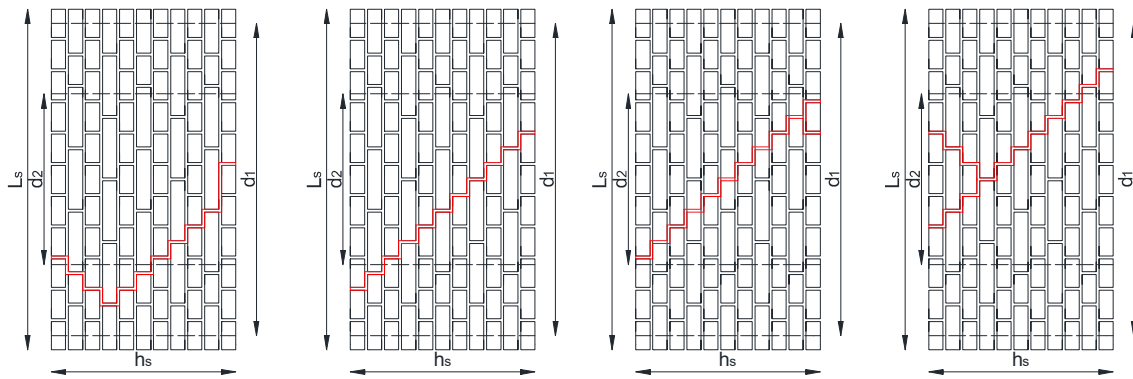
TUD-MAT-42a

TUD-MAT-42b

TUD-MAT-42c

TUD-MAT-42d/e

Figure 43 – Crack pattern for double wythe masonry specimens subjected to vertical out-of-plane bending test (OOP1).



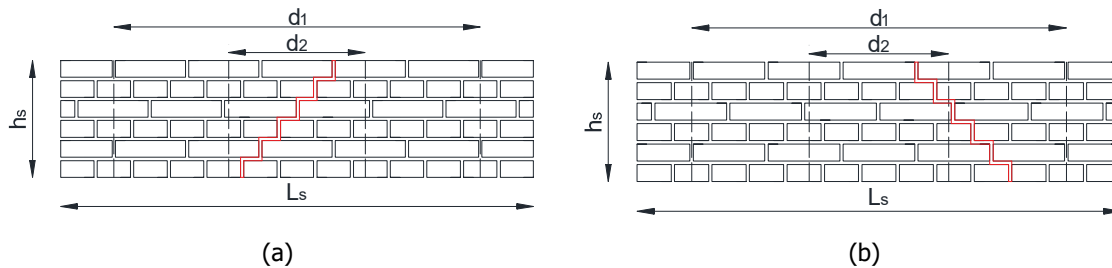
TUD-MAT-43a

TUD-MAT-43b/e

TUD-MAT-43c

TUD-MAT-43d

Figure 44 – Crack pattern for double wythe masonry specimens subjected to horizontal out-of-plane bending test (OOP2).



(a)

(b)

Figure 45 – Crack pattern for double wythe masonry specimens subjected to in-plane bending test (IP): (a) stepwise crack formed in the constant moment zone; (b) crack developed outside the constant moment zone.

The bending properties of the double wythe clay brick masonry specimens in terms of the flexural strength, elastic chord modulus calculated between 10% and 30% of the maximum load and fracture energy are listed in Table 19. The horizontal out-of-plane flexural strength resulted approximately 3 times higher values than the vertical out-of-plane flexural strength ($f_{x2} / f_{x1} = 2.9$). The vertical in-plane strength is 3 times higher than the vertical out-of-plane flexural strength ($f_{x3} / f_{x1} = 3.0$).

Table 19 – Bending properties of double wythe clay brick masonry specimens.

Specimen name	f_{x1} MPa	E_{fx1} MPa	G_{fx1} N/mm	Specimen name	f_{x2} MPa	E_{fx2} MPa	G_{fx2} N/mm	Specimen name	f_{x3} MPa	E_{fx3} MPa	G_{fx3} N/mm
MAT-42a	0.18	3059	0.016	MAT-43a	0.38	-	0.056	MAT-44a*	0.20	-	-
MAT-42b	0.10	1935	0.006	MAT-43b	0.47	7357	0.053	MAT-44b	0.39	3020	0.13
MAT-42c	0.18	3286	0.013	MAT-43c	0.33	5727	0.022	MAT-44c	0.43	2015	0.09
MAT-42d	0.17	2833	0.012	MAT-43d	0.40	7231	0.097	MAT-44d	0.43	2278	0.04
MAT-42e	0.09	1737	0.012	MAT-43e	0.48	8305	0.036	MAT-44e	0.44	2229	0.14
Average	0.14	2570	0.012	Average	0.41	7155	0.053	Average	0.42	2385	0.101
St. dev.	0.05	692	0.004	St. dev.	0.06	1066	0.028	St. dev.	0.02	438	0.05
C.o.V	0.31	0.27	0.30	C.o.V	0.15	0.15	0.54	C.o.V	0.05	0.18	0.47
				f_{x2} / f_{x1}	2.9			f_{x3} / f_{x1}	3.0		

* Excluded from the average, due to the formation of crack outside the constant moment zone.

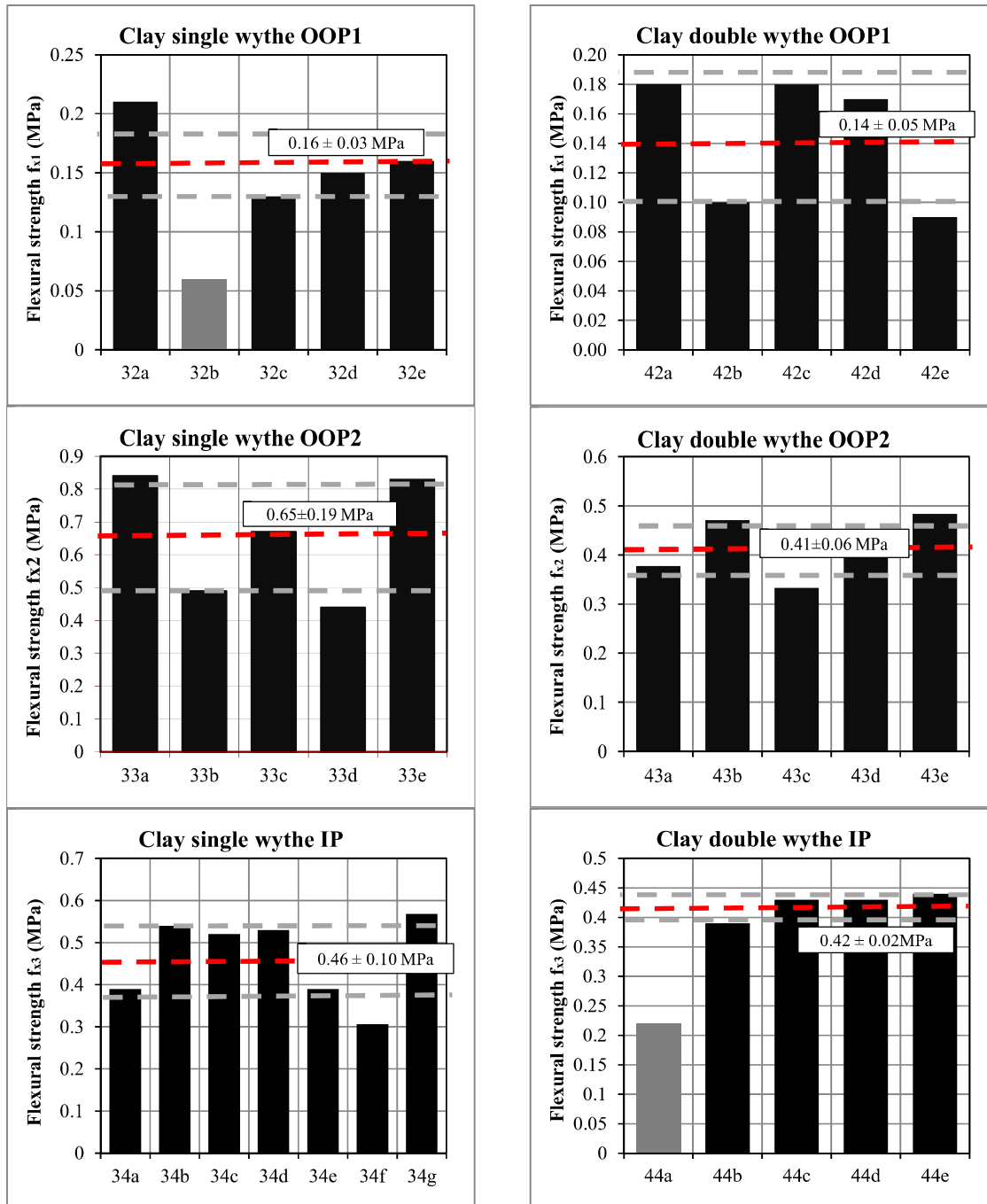


Figure 46 – Bending properties of the clay single wythe and double wythe specimens: histogram representation (value in grey excluded from mean value).

10 Bond strength of masonry

The bond strength between masonry unit and mortar was determined in agreement with the bond wrench test proposed by EN 1052-5:2002 [17].

10.1 Testing procedure

The improved test set-up used in this campaign as shown in Figure 47a. The specimen was rigidly held by a support frame that holds the specimen in accordance with EN 1052-5:2005 [17]. A clamp, with a lever attached, was applied to the masonry unit above the tested. The lever was used to apply a bending moment to the brick-mortar interface. The load was applied by a jack operated manually and a load cell attached to the jack measured the applied force. Therefore, the improved set-up provided the possibility for recording the applied load continuously.

Fifteen couplet specimens were adopted for the bond wrench tests (Figure 47b).



(a)



(b)

Figure 47 – Bond wrench tests: (a) improved set-up; (b) couplet specimen.

10.2 Experimental results

The bond wrench strength f_w is calculated on the assumption that the stress distribution is linear over the width of the top masonry unit [17]:

$$f_w = \frac{F_1 e_1 + F_2 e_2 - \frac{2}{3} t_u \left(F_1 + F_2 + \frac{F_3}{4} \right)}{l_j w_j^2 / 6} \quad (15)$$

where F_1 is the failure load, measured and applied by the jack. F_2 is the normal force as a result of the weight of the bond wrench apparatus. F_3 is the weight of the masonry unit pulled off the specimen, including the weight of adherent mortar. Furthermore, e_1 is the distance from the applied load to the tension face of the specimen, e_2 is the distance from the centre of gravity of the clamp to the tension face of the specimen, l_j is the mean length of the bed joint, and w_j is the mean width of the bed joint. Figure 48 shows the set-up and the definition of the various quantities.

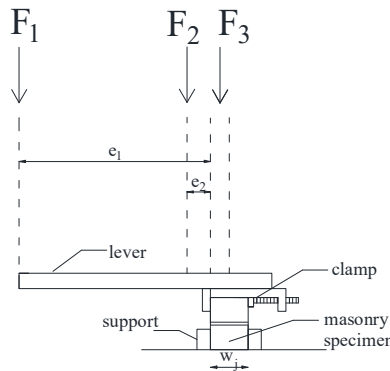


Figure 48 – Test set-up for the bond wrench test.

Figure 49 reports the classification of the type of failures [17], while Figure 50 shows the observed failure mechanisms.

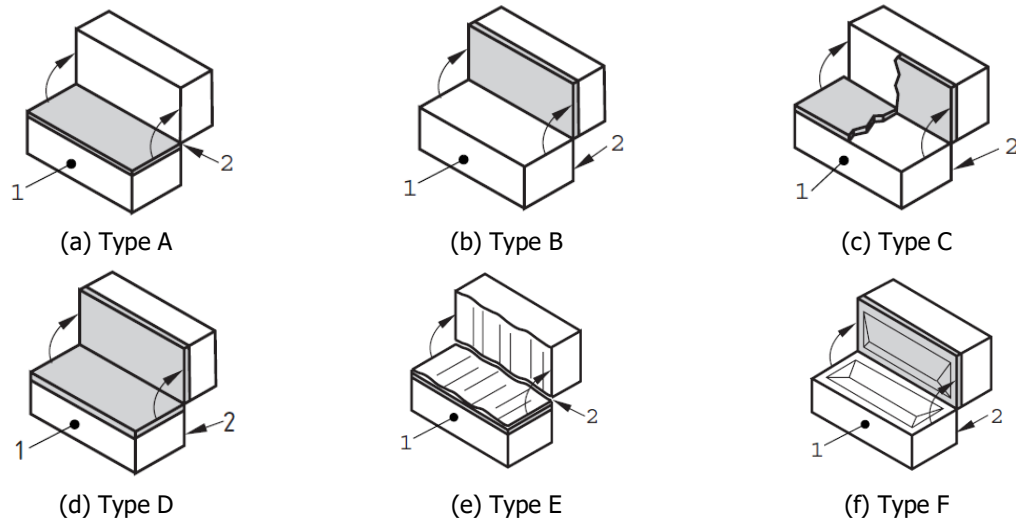


Figure 49 – Classification of failure modes in agreement with EN-1052-5:2005 (1 tension face, 2 compression face).



(a)



(b)

Figure 50 – Observed failure mechanisms: (a) *type A*; (b) *type B*.

Figure 51 shows the applied load (F_I) versus time. The specimens showed brittle behaviour.

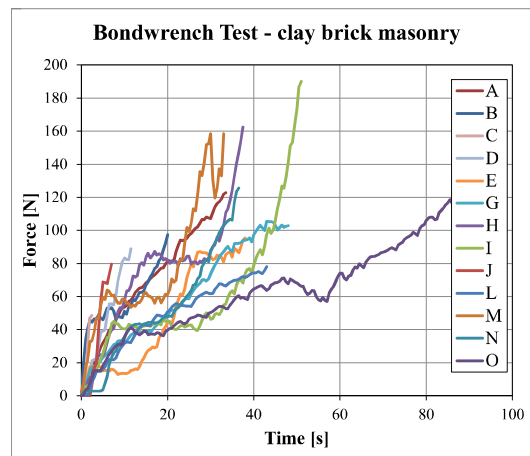


Figure 51 – Time versus force (F_I) applied by manually controlled jack.

Table 20 lists the results of bond wrench test on the clay brick masonry. The bond strength values of specimens in terms of histogram are shown in Figure 52.

From a physical point of view, it may be expected that there is a correlation between the flexural bond tensile strength, f_w , and flexural masonry strength. This correlation depends on loading direction so that the crack plane occurs along the brick to mortar interface in the bed joint plane, f_{x1} . One reason might be the fact that these parameters depend on the adhesion between mortar and brick. A ratio between the bond strength and the vertical flexural strength obtained from testing of the single wythe masonry specimens, is found close to 1 in the current study.

Table 20 – Bond strength of clay brick masonry samples.

Specimen Name	l_j	w_j	F_3	F_1	f_w	Failure mode
	mm	mm	N	N	MPa	
TUD-MAT-35a	208	99	20.10	122.39	0.15	B
TUD-MAT-35b	210	100	15.93	97.42	0.12	A
TUD-MAT-35c	208	99	16.13	48.64	0.06*	A
TUD-MAT-35d	209	99	20.05	88.96	0.11	B
TUD-MAT-35e	209	99	16.18	95.45	0.12	A
TUD-MAT-35f	208	99	16.38	155.06	0.20	A
TUD-MAT-35g	207	99	16.33	162.48	0.21	A
TUD-MAT-35h	209	98	16.18	190.17	0.24	A
TUD-MAT-35i	208	100	16.23	79.69	0.10	A
TUD-MAT-35j	209	100	16.28	14.80	0.02*	A
TUD-MAT-35k	210	99	16.03	78.16	0.10	A
TUD-MAT-35l	209	99	16.45	158.45	0.20	A
TUD-MAT-35m	209	99	16.23	106.68	0.13	A
TUD-MAT-35n	208	99	16.28	126.05	0.16	A
TUD-MAT-35o	208	99	20.10	122.39	0.15	B
Average					0.15	
st. dev.					0.05	
c.o.v.					0.32	
f_w/f_{x1}					0.94	

*Excluded from the average due to the incorrect application of the load

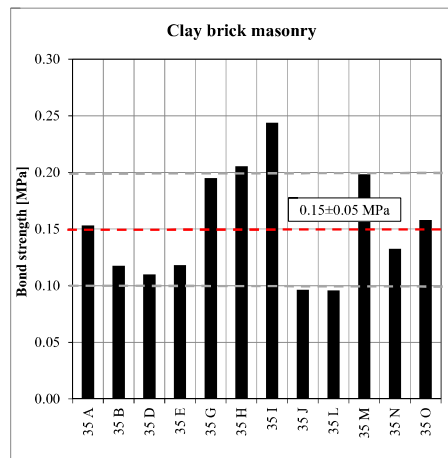


Figure 52 – Bond strength values of clay brick masonry: histogram representation.

11 Shear strength of masonry

The initial shear properties of masonry were determined in agreement with EN 1052-3:2002 [18]. However, a displacement control procedure was used, instead of the prescribed force control procedure, to evaluate the residual strength properties and the mode-II fracture energy.

11.1 Testing procedure

To investigate the possible effect of presence of mortar head joints on the shear properties, two types of specimens were adopted: standard triplet and modified triplet. The standard triplet is a three stacked bonded brick specimen (Figure 54a), while the modified triplet is formed by a full brick in the middle and two half bricks on the sides, see Figure 54b. Fourteen specimens for each type of triplet were prepared. Prior to testing, a layer of gypsum was applied to the external faces of the specimens.

Figure 53 shows the used test set-up. During the test, the specimen was rotated of 90 degrees with respect to the casting position. The specimen was kept under constant lateral pre-compression, while a shear load was applied at the mid masonry unit. Three different levels of pre-compression were investigated. Being the compressive strength of the masonry unit greater than 10 N/mm² [18], the pre-compression stresses applied were 0.2, 0.6 and 1.0 N/mm². For each pre-compression level, minimum two specimens were tested.

Two independently operated jacks were required to apply the shear and pre-compressive load. The shear load acted in a vertical direction using a displacement controlled apparatus. The apparatus had a 100 kN jack and a spherical joint. The displacement increased with a rate of 0.005 mm/s. During unloading, the displacement was decreased with a rate of 0.05 mm/s. The pre-compressive load was applied perpendicular to the bed joint plane by a manually operated hydraulic jack. The horizontal hydraulic jack was load controlled and applied different levels of transverse compressive load to the specimen. The jack was kept in position by means of four steel rods positioned on opposite sides of the specimen, which were in turn kept in position by steel plates (Figure 53). In order to keep the transverse compressive load constant ($\pm 2\%$), a spring system was used between the hydraulic jack and the load cell. The stiffness of the springs was defined on the basis of the required pre-compression level. Two types of the spring were used. A load cell was placed between the spring and the steel plate to measure the applied load.

Both on the front and the back side of the specimens, LVDTs were attached. Vertical LVDTs measured the relative vertical displacement of the middle brick with respect to the later ones. Horizontal LVDTs measured the horizontal displacement between the two external bricks. Their measuring range was 10 mm with an accuracy of 0.1% (Figure 54).

To get more information regarding the post-peak behaviour, a second phase of the test was performed in which the pre-compression load was increased and kept constant in the residual phases.



Figure 53 – Test set-up for the shear-compression test on masonry specimen.

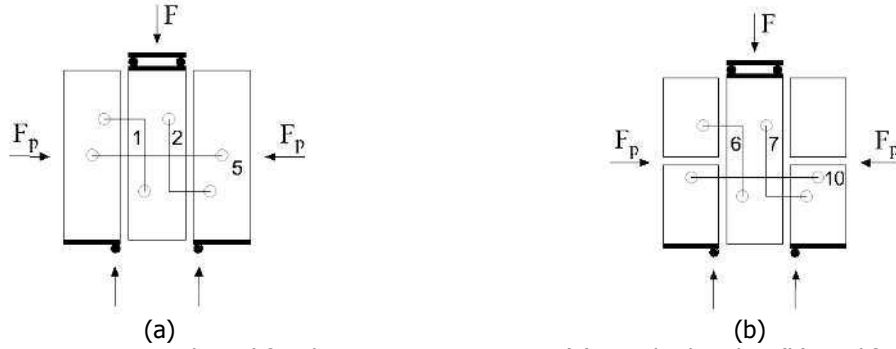


Figure 54 – Specimens adopted for shear-compression test: (a) standard triplet; (b) modified triplet.

11.2 Experimental results

The shear strength f_v was calculated for each specimen as follows [18]:

$$f_v = \frac{F_{\max}}{2A_s} \quad (16)$$

where F_{\max} is the maximum load, A_s is the cross sectional area of the specimen parallel to the bed joints. The pre-compression stress f_p can be calculated for each specimen as follows [18]:

$$f_p = \frac{F_p}{A_s} \quad (17)$$

where F_p is the pre-compression force.

The test was carried out in displacement control allowing for the determination of the post-peak behaviour. As a consequence, the residual shear strength $f_{v,res}$ was also determined. The residual strength occurred at an almost constant load where a plateau of large sliding displacement was observed. The resistance in the post-peak phase can be associated to friction only, since large relative displacement occurs.

The results of all the tests were plotted in a pre-compressive stress versus shear strength diagram. Considering a linear regression of the data, the initial shear strength f_{v0} and the initial coefficient of friction μ can be found such as the intercept with the vertical axis and the gradient of the line, respectively. The angle of internal friction α was determined as the angle between the regression line and the horizontal axis. Similar consideration can be applied to determine the residual shear strength $f_{v0,res}$ and the residual coefficient of friction μ_{res} . In the Coulomb friction formulation, the result is:

$$f_v = f_{v0} + \mu f_p \quad (18)$$

$$f_{v,res} = f_{v0,res} + \mu_{res} f_p \quad (19)$$

Table 21 and Table 22 list the results of standard triplet and modified triplet.

The shear stress versus relative displacement of the central brick of both standard triplets and modified triplets are shown in Figure 55 and Figure 56, respectively. The sliding of the middle unit was measured both from the LVDTs' reading and from jack's reading. The measuring range of LVDTs was 10 mm with an accuracy of 0.1%, beyond this range only the jack's measurement can be used to determine the residual strength.

It should be mention that due to the weak bond between the brick and mortar some of the specimens were debonded during the preparation or prior to testing; so at least two specimens for each pre-compression level were tested.

Table 21 - Maximum and residual shear strength and mode-II fracture energy of standard triplet.

$f_p = 0.2$ MPa				$f_p = 0.6$ MPa				$f_p = 1.0$ MPa			
Specimen name ^(*)	f_v	$f_{v,res}$	G_{f-II}	Specimen name ^(*)	f_v	$f_{v,res}$	G_{f-II}	Specimen name ^(*)	f_v	$f_{v,res}$	G_{f-II}
	MPa	MPa	N/mm		MPa	MPa	N/mm		MPa	MPa	N/mm
36A-f	0.36	0.18	0.15	36A-l**	-	0.39	-	36A-b	0.76	0.59	0.48
36A-e	0.28	0.17	0.09	36A-j	0.60	0.43	0.26	36A-g	0.99	0.70	0.66
No sample to be tested				36A-k	0.71	0.46	0.33	No sample to be tested			
Average	0.32	0.18	0.12	Average	0.65	0.49	0.30	Average	0.88	0.64	0.57
St. dev.	0.06	0.01	0.05	St. dev.	0.08	0.08	0.05	St. dev.	0.17	0.08	0.13
C.o.V.	0.17	0.04	0.40	C.o.V.	0.12	0.08	0.16	C.o.V.	0.19	0.13	0.22

^(*) Complete specimen name starting with TUD_MAT-.

^(**) Sample was debonded prior testing. Test was performed to find the residual properties.

Table 22 - Maximum and residual shear strength and mode-II fracture energy of modified triplet.

$f_p = 0.2$ MPa				$f_p = 0.6$ MPa				$f_p = 1.0$ MPa			
Specimen name ^(*)	f_v	$f_{v,res}$	G_{f-II}	Specimen name ^(*)	f_v	$f_{v,res}$	G_{f-II}	Specimen name ^(*)	f_v	$f_{v,res}$	G_{f-II}
	MPa	MPa	N/mm		MPa	MPa	N/mm		MPa	MPa	N/mm
36B-a	0.38	0.19	0.14	36B-f	0.54	0.42	0.12	36B-b	0.99	0.73	0.36
36B-c	0.26	0.13	-	36B-k	0.61	0.47	0.18	36B-e	0.96	0.73	0.30
36B-d	0.22	0.13	0.11	No sample to be tested				36B-h	0.84	0.64	0.27
Average	0.29	0.15	0.13	Average	0.58	0.45	0.15	Average	0.93	0.70	0.31
St. dev.	0.08	0.03	0.02	St. dev.	0.05	0.04	0.04	St. dev.	0.08	0.05	0.04
C.o.V.	0.29	0.22	0.19	C.o.V.	0.09	0.09	0.28	C.o.V.	0.08	0.08	0.13

^(*) Complete specimen name starting with TUD_MAT-.

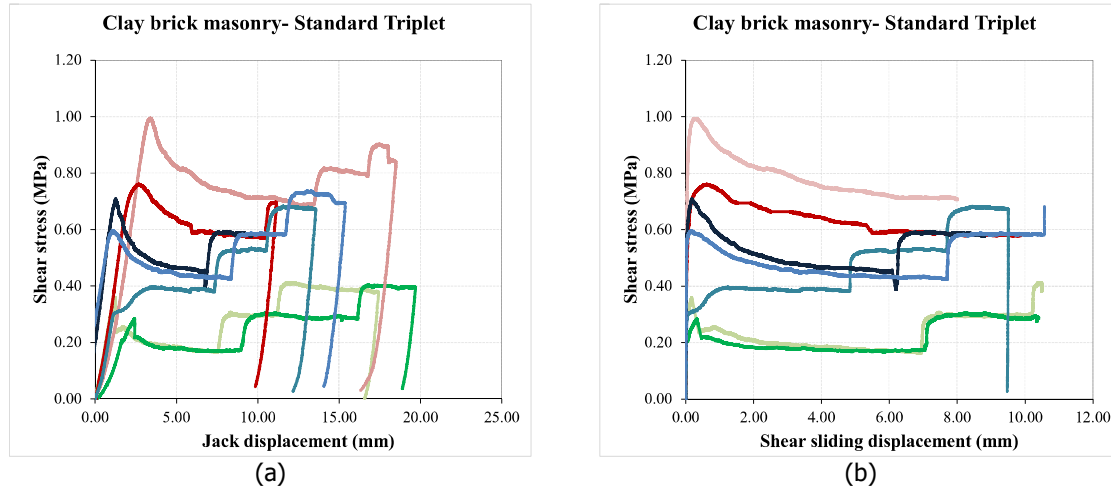


Figure 55 – Shear stress-displacement for the *standard* triplet: (a) relative displacement of the jack; (b) relative displacement of the central brick from LVDTs' readings.

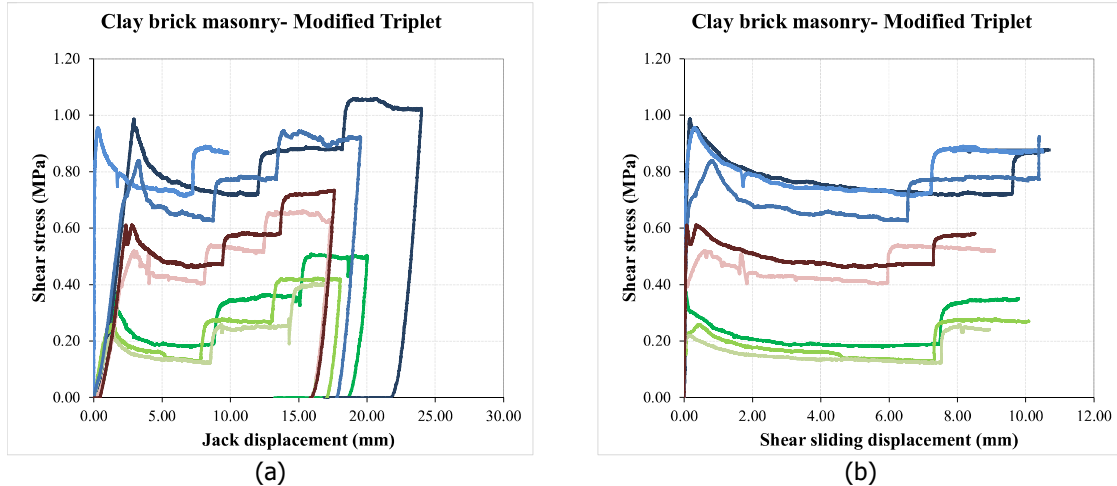


Figure 56 – Shear stress-displacement for the *modified* triplet: (a) relative displacement of the jack; (b) relative displacement of the central brick from LVDTs' readings.

Figure 57 and Figure 58 show the results of the shear strength versus pre-compression stress for standard triplets and modified triplet, respectively. To get a more precise envelope at residual state, a second phase of the test was performed where the pre-compression load was increased and kept constant at different levels in the residual phases. The data collected by increasing the level of pre-compression are shown in Figure 57b and Figure 58b with red filled dots. Passing a regression line through all the measured data, obtained in the second phase, the residual parameters can be obtained. It can be noted that the residual parameters obtained in the first (Figure 57a and Figure 58a) and second testing phase (Figure 57b and Figure 58b) are similar.

The standard triplet masonry showed an initial shear strength equal to 0.20 MPa and a coefficient of friction equal to 0.69. In the residual phase, the coefficient of friction decreased to 0.60. All the specimens presented a shear failure in the unit/mortar bond area. Figure 60 shows a typical crack pattern.

The modified triplet masonry showed an initial shear strength equal to 0.12 MPa and a coefficient of friction equal to 0.80. In the residual phase, the coefficient of friction decreased to 0.65. All the specimens presented a shear failure in the unit/mortar bond area. Figure 61 shows a typical crack pattern.

Figure 59 shows the mode II fracture energy G_{II} versus pre-compression for both standard triplet and modified triplet.

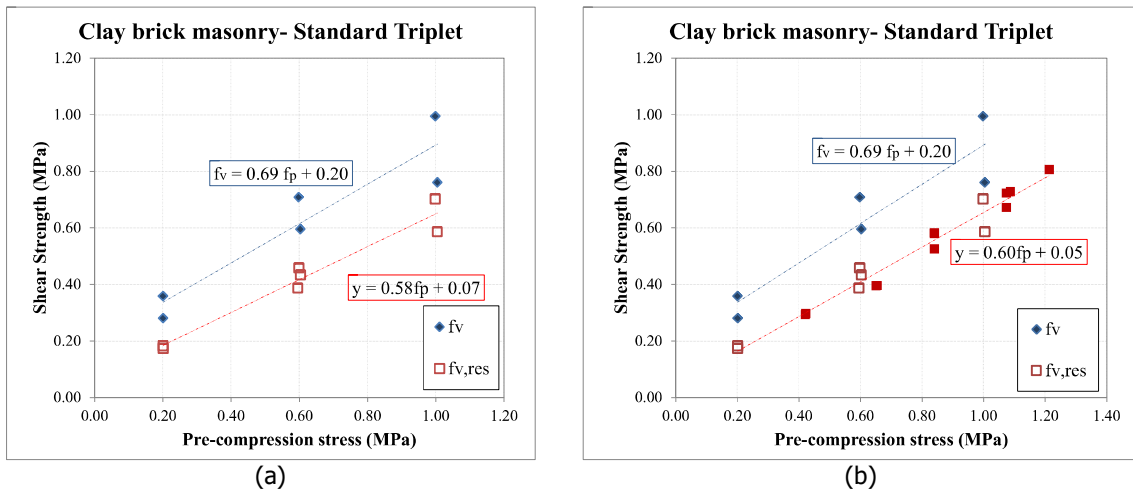


Figure 57 – Shear strength versus pre-compression stress for standard triplet: (a) data measured in the first phase; (b) data measured in the first and second phase of testing.

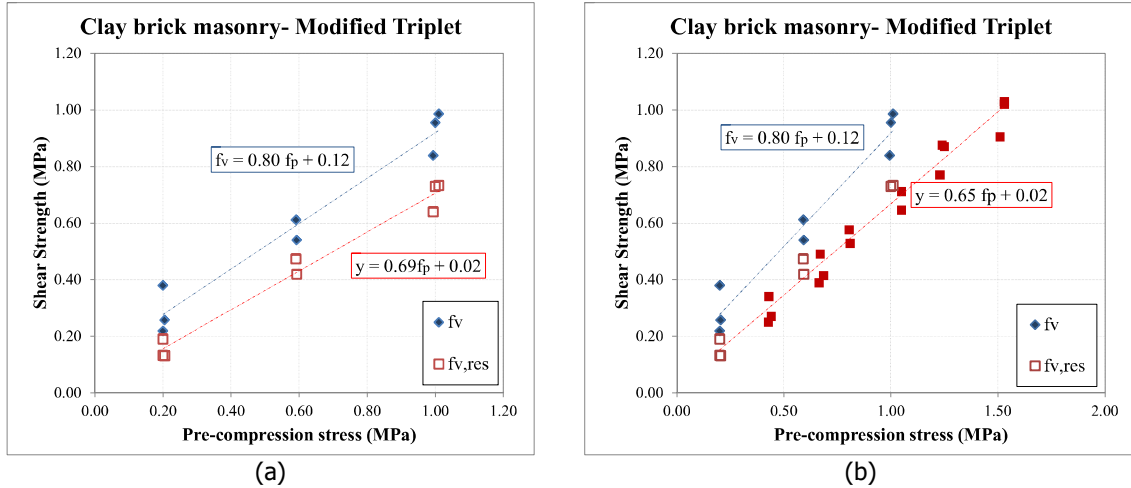


Figure 58 – Shear strength versus pre-compression stress for modified triplet: (a) data measured in the first phase; (b) data measured in the first and second phase of testing.

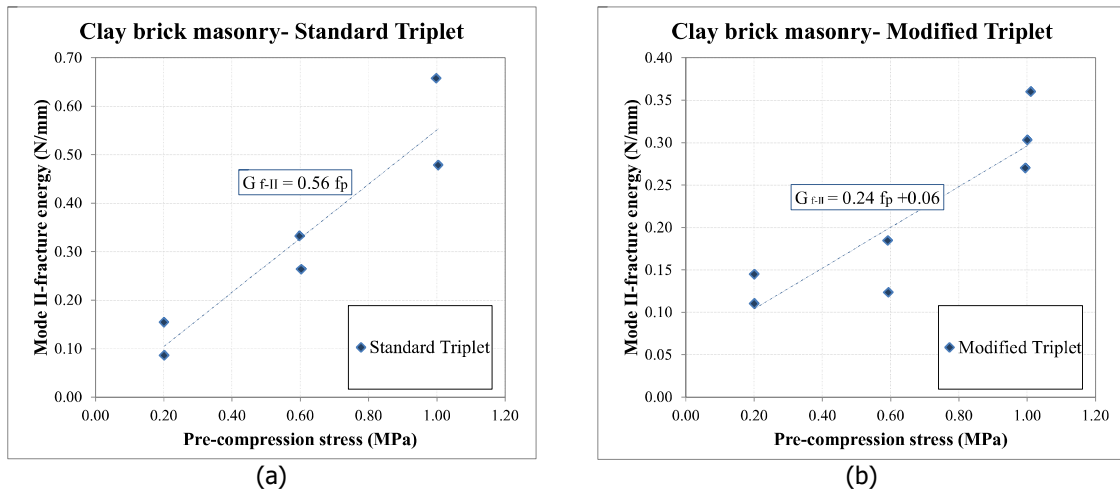


Figure 59 – Mode II-fracture energy versus pre-compression: (a) standard triplet (b) modified triplet.



Figure 60 – Crack pattern of standard triplet under shear test: (a) front-left joint; (b) front-right joint; (c) front view.

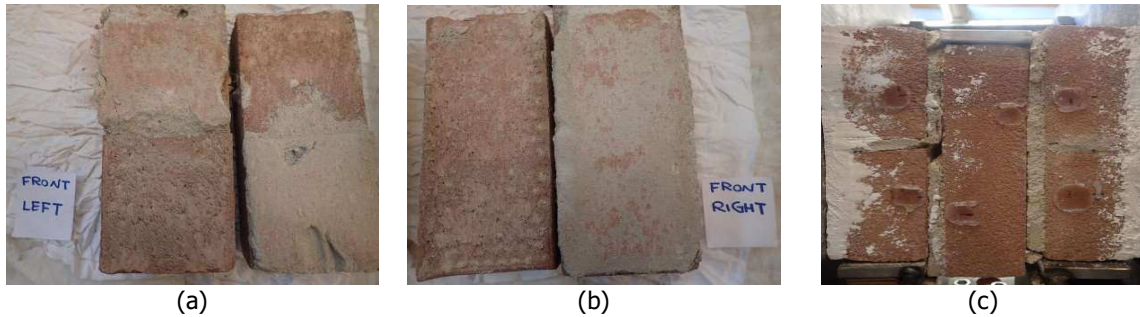


Figure 61 – Crack pattern of modified triplet under shear test: (a) front-left joint; (b) front-right joint; (c) front view.

Table 23 lists the shear properties for both the standard and modified triplet test. The initial shear strength obtained from the tests on the standard triplet was approximately 60% higher than the one obtained from the tests on the modified triplet. The coefficient of friction for the standard triplet was approx. 10% lower than the one obtained for the modified triplet. Approximately the same values of the residual coefficient of friction for the two types of the specimens were found.

Table 23 - Shear properties of standard triplet and modified triplet.

Property	Symbol	Unit	Standard triplets	Modified triplets
Number of specimens			7	8
Initial shear strength	f_{v0}	MPa	0.20	0.12
Initial coefficient of friction	μ		0.69	0.80
Angle of internal friction	α		34.61	38.66
Residual shear strength	$f_{res,v}$	MPa	0.05	0.02
Residual coefficient of friction	μ_{res}		0.60	0.65
Residual angle of internal friction	α_{res}		30.96	33.02

11.3 Comparison between the properties of standard triplet and modified triplet

To study the shear properties of brick-mortar interface, shear-compression test on the standard triplet can be conducted as suggested in the standard [18]. To study the possible effect of the head joint on the shear properties of masonry, tests on the modified triplet were carried out. The shear properties of the calcium silicate brick masonry both standard and modified triplet were investigated in the scope of WP1a [22]. While finding the shear properties of the clay brick masonry was pursued within WP1b. A comparison between the shear properties of standard and modified triplet for the clay brick masonry as well as calcium silicate brick masonry (in terms of histogram representation) is shown in Figure 62.

A slight difference between the shear properties of the standard triplet and modified triplet for the calcium silicate brick masonry was observed on the basis of the bond pattern, while for the clay brick a considerable difference between the shear properties of the standard and modified triplet was found. Due to the limited number of specimens tested, no conclusions can be drawn, so as a suggestion, further study should be carried out to investigate the possible effect of the presence of mortar head joint on the shear properties of the brick-mortar interface.

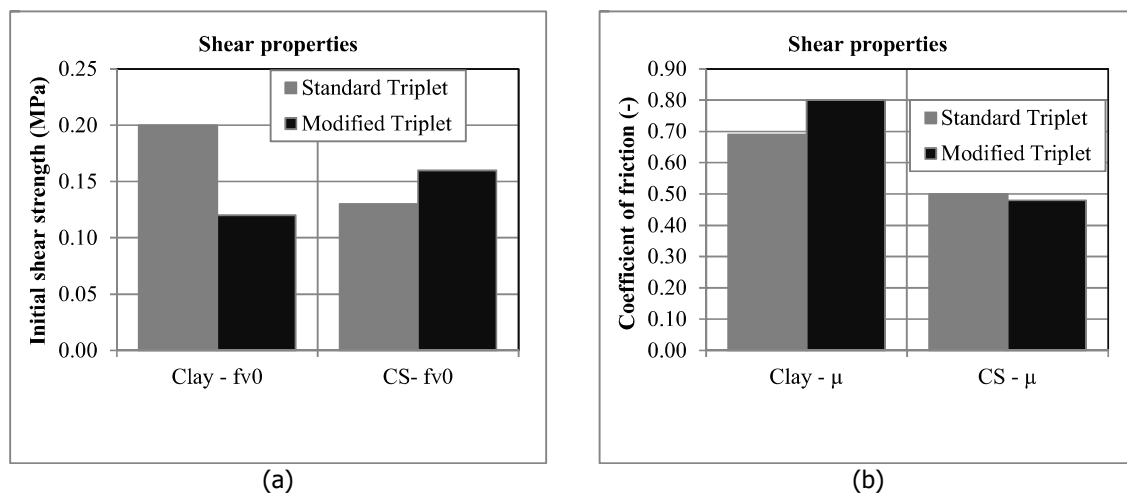


Figure 62 – Comparison between shear properties of standard triplet and modified triplet for the clay and calcium silicate brick masonry: (a) initial shear strength; (b) initial coefficient of friction.

12 Comparison with values proposed by standards

Eurocode 6 [2], National Annex to the Eurocode 6 [19], NPR 9096-1-1:2012 [20] and Section 9 in NPR 9998:2017 [21] propose characteristics value of masonry properties to be used in the design procedure. Additionally, the mean value of properties for the existing masonry including subdivision for masonry types and year of the construction are proposed in Table F.2 in NPR 9998:2017 [21]. In this section a comparison between experimental findings and the values proposed by these standards is presented. It should be pointed out that no distinction in the standards is made between the properties of masonry concerning the number of wythe. As a result, all the proposed values in the standards are considered to be applicable to both single and double wythe masonry.

12.1 Characteristic compressive strength of masonry

The compressive strength of masonry can be calculated by following Eurocode 6 and the national annex (Paragraph 3.6.1.2 [2], [20]):

$$f_{k,EC6} = K f_b^\alpha f_m^\beta \quad (20)$$

where f_b is the normalised mean compressive strength of the masonry unit, f_m is the compressive strength of mortar, and K, α, β are constants (Table NB-2 in [19]). The normalised mean compressive strength of the masonry unit f_b is determined by multiplying the measured value for the shape factor δ (Table B.1 in [2] or Table NB-A.1 in [19]).

Characteristic strength values of the compressive strength of masonry are also tabulated by the NPR 9096-1-1:2012 [21]. NPR 9998:2017 [21] prescribes minimum characteristics value on the basis of masonry type.

From the experiments, the characteristic compressive strength of masonry is calculated as [10]:

$$f_k = f_m' - 1.645\sigma \quad (21)$$

where f_m' is the mean measured compressive strength and σ is the standard deviation.

Table 24 lists the characteristics compressive strength value of single and double wythe masonry. The characteristic values prescribed by Eurocode 6 [2] and National Annex to the Eurocode 6 [19] have been obtained adopting the strength value of mortar and bricks as obtained from the tests. The calculations have been carried out by considering the properties of brick and mortar experimentally determined (Section 4 and Section 5). Additionally, a comparison with the values prescribes by NPR 9096-1-1:2012 and the minimum values proposed in NPR 9998:2017 (§ 9.3.2.3) is provided.

Experimentally, the compressive strength for the double wythe masonry is closer to the estimates prescribed by the standards. For the single wythe specimens, the experiments provide a higher characteristic value with respect to the standards prescriptions. From the experiments, for both single and double wythe masonry higher characteristic compressive strength were found with respect to the minimum values as proposed in NPR 9998:2017 (Section 9.3.2.3).

Table 24 – Characteristic values for the compressive strength of clay brick masonry.

			Clay single wythe	Clay double wythe
Compressive strength masonry mortar	f_m	MPa	3.81	
Compressive strength masonry unit	f_b	MPa	39.12	
Shape factor	δ		0.72	
Normalized compressive strength masonry unit	f_b	MPa	28.31	
Characteristic compressive strength masonry - Eurocode 6	K		0.55	
	α		0.70	
	β		0.30	
	$f_{k,EC6}$	MPa	8.53	
Characteristic compressive strength masonry - National annex to the Eurocode 6	K		0.60	
	α		0.65	
	β		0.25	
	$f_{k,N}$	MPa	7.36	
Characteristic compressive strength masonry - NPR 9096-1-1:2012	$f_{k,NPR9096}$	MPa	7.88	
Minimum value of the characteristic compressive strength masonry - NPR 9998:2017 in § 9.3.2.3	$f_{k,NPR9998}$	MPa	5.0	
Characteristic compressive strength masonry - Experiments	f_k	MPa	13.10	7.19

12.2 Elastic modulus of masonry

The national annex of Eurocode 6 [19] linearly correlates the elastic modulus of masonry (mean value) to its characteristic compressive strength with a constant factor $K_E = 700$.

The mean values of the elastic modulus (Table 9 and Table 16) for both single and double wythe masonry is correlated to the characteristic compressive strength as shown in Table 25. The characteristic compressive strength is evaluated from experiments following Eq. (21). The ratio between stiffness and characteristic compressive strength obtained from testing both single and double wythe masonry is less than 700. This ratio is approximately 350 and 400 for the single and double wythe masonry, respectively.

Table 25 – Ratio between elastic modulus and the characteristic compressive strength.

Clay brick masonry		Eurocode 6, national annex and NPR 9998:2017	Experiments		
			E_1/f_k	E_2/f_k	E_3/f_k
K_E	single wythe	700	334	311	350
	double wythe	700	386	368	411

12.3 Stress-strain relationship for masonry in compression

NPR 9998:2017 [21] proposes the following parabolic curve for the description of the stress-strain relationship in the pre-peak phase:

$$\sigma(\varepsilon) = \left[1 - \left(1 - \frac{\varepsilon}{0.0035} \right)^2 \right] \times f'_m \quad (22)$$

where σ is the compressive stress of masonry and ε is the corresponding strain. According to this expression the strain corresponding to compressive strength is 0.0035. Experimentally an average peak strain value for the single and double wythe masonry equal to 0.0043 and 0.0041 was found, respectively (Section 8).

12.4 Characteristic out-of-plane flexural strengths of masonry

Eurocode 6 [2] reports characteristic value for the out-of-plane flexural strengths, while NPR 9096-1-1:2012 [20] and NPR 9998:2017 [21] prescribe minimum characteristic values on the basis of the exposure zone and masonry types, respectively. From experiments, the characteristic value is determined by dividing the mean value by the factor 1.5, as prescribed by the testing standard [15].

Table 26 lists the characteristic values for the out-of-plane flexural strengths. The values proposed in NPR 9096-1-1:2012 and NPR 9998:2017 as minimum values for the characteristic strength are higher than those experimentally found, both for the single and double wythe masonry. The orthotropic flexural strength ratio both in Eurocode 6 and NPR 9998:2017 is prescribed as 2.0, while this ratio is proposed as 4.0 in NPR 9096-1-1:2012. Experimentally, a ratio equal to 4.1 and 2.9 is obtained for the single and double wythe masonry, respectively.

Table 26 - Characteristic values for the flexural strength of masonry.

Characteristic values for the flexural strength				Clay brick masonry	
				Single wythe	Double wythe
Flexural strength with the moment vector parallel to the bed joint and in the plane of the wall	EC6	$f_{x1k,EC6}$	MPa	0.10	
	Minimum characteristic value by NPR 9096-1-1:2012	$f_{x1,kNPR}$	MPa	0.20	
	Minimum characteristic value by NPR 9998:2017	$f_{x1,kNPR9998}$	MPa	0.30	
	Experiments	f_{x1k}	MPa	0.11	0.09
Flexural strength with the moment vector orthogonal to the bed joint and in the plane of the wall	EC6	$f_{x2k,EC6}$	MPa	0.20	
	Minimum characteristic value by NPR 9096-1-1:2012	$f_{x2k,NPR}$	MPa	0.79	
	Minimum characteristic value by NPR 9998:2017 in § 9.3.2.3	$f_{x2k,NPR9998}$	MPa	0.6	
	Experiments	f_{x2k}	MPa	0.43	0.27
Ratio f_{x2k} / f_{x1k}	EC6			2.0	
	NPR 9096-1-1:2012			4.0	
	NPR 9998:2017 in § 9.3.2.3			2.0	
	Experiments			4.1	2.9

12.5 Characteristic shear properties of masonry

Eurocode 6 [2] reports characteristics value for the initial shear strength, while and NPR 9096-1-1:2012 and NPR 9998:2017 [21] prescribe minimum characteristic value on the basis of the masonry types.

From experiment, the characteristic value of the initial shear strength is determined as the 80% of the mean measured value, as prescribed by the testing standard [18]. The characteristic initial shear strength obtained from experiments, both standard triplet and modified triplet are lower than the value prescribed by Eurocode 6 (Table 27). Experimentally, lower characteristic initial shear strength is found than those minimum characteristic values prescribed by NPR 9096-1-1:2012 and NPR 9998:2017.

Table 27 - Characteristic shear properties of clay brick masonry.

Clay brick masonry		Characteristic initial shear strength
		MPa
		$f_{v0,k}$
EC6		0.20
Minimum characteristic value by NPR 9096-1-1:2012		0.20
Minimum characteristic value by NPR 9998:2017 in § 9.3.2.3		0.20
Experiments	standard triplet	0.16
	modified triplet	0.10

12.6 Comparison with Table F.2 in NPR 9998:2017

The mean value of properties for the existing masonry including subdivision for masonry types and year of the construction are proposed in Table F.2 in NPR 9998:2017 [21]. This table was derived based on the laboratory test results obtained during the testing campaigns performed on existing masonry in 2014 and 2015 [7], from literature information, scientific judgment and some preliminary results of 2016 testing campaign on the replicated masonry (that were available until April 2017).

Table 28 lists the mean values from the experiments and the mean values proposed in Table F.2 for the clay brick masonry constructed before 1945. The mean values of masonry properties reported in Table F.2 NPR 9998:2017 are lower or approximately equal to the average values found from the experiments, with the exception of the Young's modulus and the initial shear strength for which the standard provides an overestimation. It should be mentioned that the fracture energy in shear for the experiment is calculated by considering pre-compression at level of 0.2 MPa.

Table 28 – Comparison between the masonry properties obtained from experiments and the mean values proposed in Table F.2 NPR9998:2018.

Masonry properties			Symbol	Unit	NPR 9998:2017 Table F.2	Experiment	
						Single wythe	Doubl e wythe
Compressive strength of masonry	vertical		f_m	MPa	8.5	14.0	9.3
	horizontal		$f_{m,h}$			13.1	9.2
Elastic modulus of masonry	vertical	E_1	E_1	MPa	5000	4380	2771
		E_2	E_2			4068	2646
		E_3	E_3			4590	2951
	horizontal	$E_{1,h}$	$E_{1,h}$			3332	4012
		$E_{2,h}$	$E_{2,h}$			3664	3954
		$E_{3,h}$	$E_{3,h}$			3207	4319
Flexural strength with the moment vector parallel to the bed joint and in the plane of the wall			f_{x1}	MPa	0.15	0.16	0.14
Flexural strength with the moment vector orthogonal to the bed joint and in the plane of the wall			f_{x2}	MPa	0.55	0.65	0.41
Initial shear strength	standard triplet		f_{v0}	MPa	0.3	0.20	
	modified triplet					0.12	
Masonry (bed joint) shear friction coefficient	standard triplet		μ		0.75	0.69	
	modified triplet					0.80	
Fracture energy in bending parallel to the bed joint			G_{R1}	N/m	10	4	12
Fracture energy in bending perpendicular to the bed joint			G_{R2}	N/m	35	168	53
Fracture energy in compression	vertical		G_{F_c}	N/m	20000	28500	34800
	horizontal		$G_{F_c,h}$			35100	28300
Fracture energy in shear	standard triplet		G_{RI}	N/m	100	112	
	modified triplet					108	

13 Comparison between the properties of single and double wythe specimens

A comparison between the compression and the bending properties obtained from tests on the single and double wythe masonry is presented in this section. The mean values of the compressive strength, Young's modulus and fracture energy for the single and double wythe masonry specimens subjected to vertical compression load are compared in terms of histogram representation in Figure 63. To make compelling comparison, the stress-strain and stress-displacement curves for one single wythe specimen (TUD-MAT-31F) and one double wythe specimen (TUD-MAT-41B-E) are presented next to the histogram. The following observations can be drawn:

- The double wythe masonry specimens showed a 45% lower values of the compressive strength with respect to the single wythe masonry specimens.
- The double wythe masonry specimens showed approximately 36% lower values of the Young's modulus with respect to the single wythe masonry specimens.
- The double wythe masonry specimens showed approximately 22% higher values of the fracture energy in compression with respect to the single wythe masonry specimens.

The mean values of the flexural strength of the single and double wythe masonry specimens subjected to vertical out-of-plane bending, horizontal out-of-plane bending and in-plane bending are represented by histograms in Figure 64. In addition, next to the histogram the force-mid span displacement for one single wythe specimen and one double wythe specimen are presented. The following observations can be drawn:

- The double and single wythe masonry specimens showed similar results in terms of vertical out-of-plane flexural strength f_{x1} . A good correspondence between these results and the flexural bond strength f_b was found.
- The double wythe masonry specimens showed a 37% lower values of the horizontal out-of-plane flexural strength f_{x2} with respect to the single wythe masonry specimens.
- The double and single wythe masonry specimens showed similar results in terms of in-plane vertical flexural strength f_{x3} .

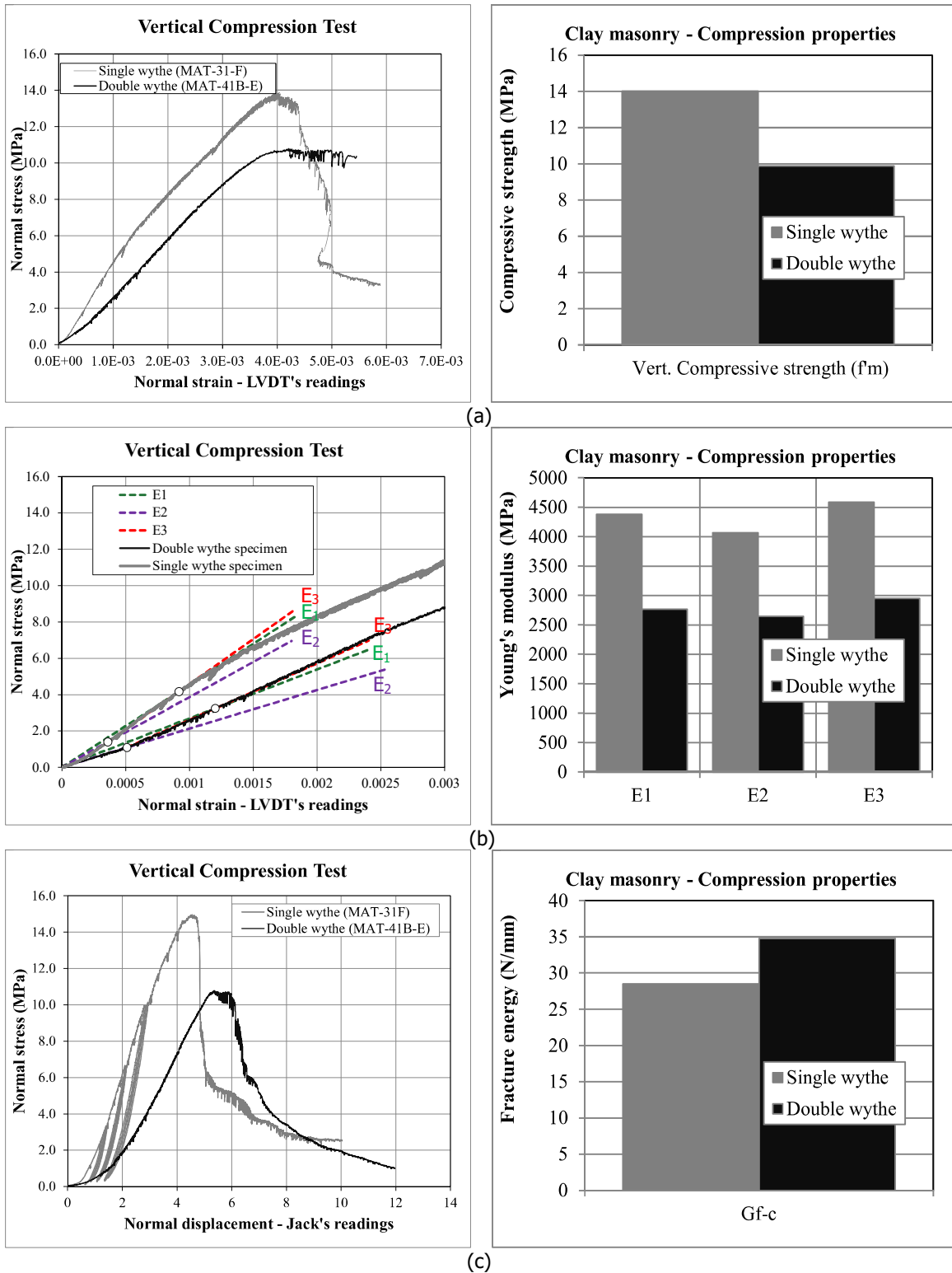


Figure 63 – Comparison between mean values of the compression properties of the single wythe and double wythe masonry: (a) compressive strength; (b) Young's modulus; (c) fracture energy in compression.

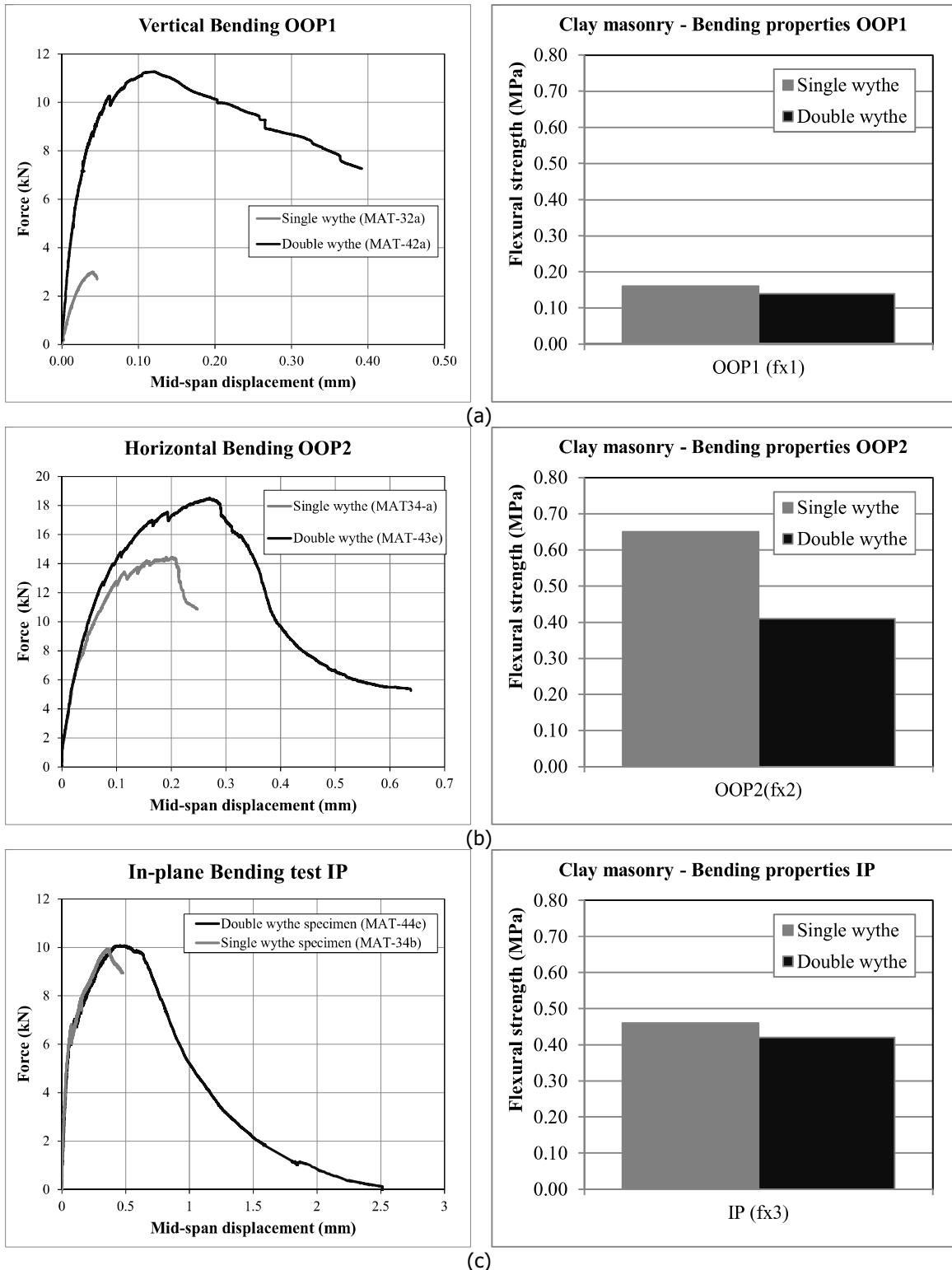


Figure 64 – Comparison between mean values of the bending properties of the single and double wythe masonry: (a) vertical out-of-plane bending (OOP1); (b) horizontal out-of-plane bending (OOP2); (c) in-plane bending (IP).

14 Summary and properties overview

This report concerns with characterisation of the solid clay brick masonry at material level. This material was frequently applied in the construction of the residential buildings before 1945. In these buildings the use of single and double wythe clay brick masonry is common. The masonry is made of general purpose mortar and solid clay brick. The knowledge regarding the behaviour of solid clay double wythe masonry at material level is limited in the literature. As a result, a complete characterisation of both solid clay single and double wythe was performed at material level. In spite of all the difficulties caused during the construction, handling and testing of double wythe specimens, conforming specimens were adopted in the current study. The material tests were performed within the WP1 of the large-scale testing campaign of 2016 at TU Delft. A characterisation at component level (in-plane and out-of-plane tests) was also performed in WP3 of the same testing campaign.

Adopting well-designed displacement-control testing set-ups is the privilege of the current study. The compression, bending and shear properties of masonry specimens were measured. The compression tests were performed in two orthogonal directions, perpendicular and parallel to the bed joints, aiming to investigate the orthotropic behaviour of masonry. The bending properties of the masonry were studied by performing four-point bending tests, both out-of-plane and in-plane, and bond wrench tests. Using the improved testing set-up, horizontal out-of-plane bending tests, where the plane of failure was perpendicular to the bed joints, and vertical out-of-plane bending tests, where the plane of failure was parallel to the bed joints, were performed. In-plane bending test was adopted where the moment vector was orthogonal to the plane of the specimen. In both in-plane and out-of-plane bending tests, the crack opening was used as a controlling parameter allowing an estimation of the post-peak behaviour. The shear properties of masonry were obtained by performing shear tests on triplets. By adopting a displacement-controlled procedure, the initial shear parameters, including initial shear strength and coefficient of friction was studied and the residual strength property, where a plateau was reached, was investigated. The initial and residual shear properties were found by applying the Coulomb friction criterion. To study the possible effect of the mortar head joint on the shear properties of the brick-mortar interface, two types of the triplet, without head joints and with head joints, were adopted. An overview of the material properties of solid clay brick masonry both single and double wythe is listed in Table 29.

Table 29 – Overview of mechanical properties of solid clay brick masonry.

Property	Symbol	Unit	Single wythe				Double wythe				
			Average	St. dev.	C.o.V.	Number of test	Average	St. dev.	C.o.V.	Number of test	
Compressive strength of mortar	f_m	MPa	3.81	0.34	0.09	108	Same as the single wythe				
Flexural strength of mortar	f_{mt}	MPa	1.40	0.17	0.12	54					
Normalised compressive strength of masonry unit	f_b	MPa	28.31	2.92	0.10	9					
Flexural strength of masonry unit	f_{bt}	MPa	6.31	0.72	0.11	8					
Elastic modulus of masonry unit	E_b	MPa	8049	423	0.05	2					
Density of masonry	ρ	Kg/m ³	1708	71	0.04	19					
Compressive strength of masonry in the direction perpendicular to bed joints	f_m	MPa	14.02	0.56	0.04	6	9.26	1.26	0.14	12	
Elastic modulus of masonry in the direction perpendicular to bed joints	E_1	MPa	4380	605	0.14		2771	496	0.18		
	E_2	MPa	4068	783	0.19		2646	970	0.37		
	E_3	MPa	4590	603	0.13		2951	431	0.15		
Fracture energy in compression for loading perpendicular to bed joints	G_{f-c}	N/mm	28.52	3.40	0.12		34.8	8.1	0.23		
Poisson ratio of masonry in compression for loading perpendicular to bed joints	ν		0.14	0.02	0.11		0.11	0.02	0.21		
Strain corresponding to peak strength in compression for loading perpendicular to bed joints	ϵ_p	‰	4.3	0.40	0.10	4.06	0.76	0.19			
Compressive strength of masonry in the direction parallel to bed joints	$f_{m,h}$	MPa	13.11	2.41	0.18	6	9.15	0.91	0.10	5	
Elastic modulus of masonry in the direction parallel to bed joints	$E_{1,h}$	MPa	3332	565	0.17		4012	676	0.17		
	$E_{2,h}$	MPa	3664	689	0.19		3954	516	0.13		
	$E_{3,h}$	MPa	3207	592	0.18		4319	1571	0.36		
Fracture energy in compression for loading parallel to bed joints	$G_{f-c,h}$	N/mm	35.06	6.63	0.19		28.3	4.3	0.15		
Strain corresponding to peak strength in compression for loading parallel to bed joints	$\epsilon_{p,h}$	‰	5.8	1.0	0.19		4.6	0.9	0.21		
Masonry flexural strength with the moment vector parallel to the bed joints and in the plane of the wall	f_{x1}	MPa	0.16	0.03	0.21	4	0.14	0.05	0.31	5	
Young's modulus in bending with the moment vector parallel to the bed joints and in the plane of the wall	E_{fx1}	MPa	3756	365	0.10		2570	692	0.27		
Fracture energy in bending with the moment vector parallel to the bed joints and in the plane of the wall	G_{fx1}	N/mm	0.0042	0.002	0.45		0.012	0.004	0.30		
Masonry flexural strength with the moment vector orthogonal to the bed joint and in the plane of the wall	f_{x2}	MPa	0.65	0.19	0.28	5	0.41	0.06	0.15	5	
Young's modulus in bending with the moment vector orthogonal to the bed joint and in the plane of the wall	E_{fx2}	MPa	7080	593	0.08		7155	1066	0.15		
Fracture energy in bending with the moment vector orthogonal to the bed joint and in the plane of the wall	G_{fx2}	N/mm	0.17	0.09	0.52		0.053	0.028	0.54		
Masonry flexural strength with the moment vector orthogonal to the plane of the wall	f_{x3}	MPa	0.46	0.10	0.22	7	0.42	0.02	0.05	4	
Young's modulus in bending with the moment vector orthogonal to the plane of the wall	E_{fx3}	MPa	2924	480	0.16		2385	438	0.18		
Fracture energy in bending with the moment vector orthogonal to the plane of the wall	G_{fx3}	N/mm	0.19	0.07	0.35		0.101	0.05	0.47		
Flexural bond strength	f_w	MPa	0.15	0.05	0.32	13					
Masonry (bed joint) initial shear strength	Standard	f_{v0}	MPa	0.20	-	-					7
	Modified			0.12	-	-					
Masonry (bed joint) initial shear friction coefficient	Standard	μ	-	0.69	-	-					8
	Modified			0.80	-	-					
Residual masonry (bed joint) initial shear strength	Standard	$f_{v0,res}$	MPa	0.05	-	-					
	Modified			0.02	-	-					
Residual masonry (bed joint) shear friction coefficient	Standard	μ_{res}	-	0.60	-	-					
	Modified			0.65	-	-					

In terms of characteristic values, the experimental results have been compared with the analytical formulation that are available in standards, such as Eurocode 6 [1], Dutch national annex to Eurocode 6 [19], NPR 9096-1-1:2012 [20] and NPR 9998:2017 (section 9.3.2.3) [21]. It is worth noting that the mean values of the mechanical properties for existing masonry for different masonry types are tabulated in the Table F.2 of NPR 9998:2017 [21]. The mean values of properties for the clay brick masonry made before 1945 are used for comparison.

A comparison between the results of the experiments and the values proposed in the standards, both for the characteristic and mean values is shown in Table 30. It should be noted that no distinction in the standards is made between the properties of masonry concerning the number of wythe. As a result, all the proposed values in the standards are considered to be applicable to both single and double wythe masonry. The higher values of the compression properties in terms of mean and characteristic compressive strength as well as the Young's modulus are established from the experiments obtained from the single wythe masonry rather than those values proposed in the standards. While the compressive strength of the double wythe masonry found from the experiments is approximately close to those values proposed in the standards.

Regarding the Young's modulus, an acceptable agreement between the results of the single wythe masonry and the value suggested in Table F.2 NPR 9998:2017 is established. However, a lower ratio between the Young's modulus and the characteristic compressive strength is found from the experiment both for the single and double wythe masonry, rather than those values prescribed in the standards.

Concerning the bending properties, an acceptable correspondence between the results obtained from the experiments and those mean values proposed in Table F.2 NPR 9998:2017 is found. The values proposed in standards as minimum values for the characteristic strength are higher than those experimentally found, both for the single and double wythe masonry.

Both the initial shear strength and characteristic initial shear strength obtained from the experiments are lower than those values suggested in the standards.

It should be noted that a limited number of the specimens were tested in the current research; therefore, the obtained results should be treated as indicative values.

Table 30 – Comparison between the masonry properties obtained from experiments and the characteristic and mean values proposed in the standards.

Masonry properties		Characteristic value						Mean value				
		Symbol	Eurocode 6	Dutch national annex	NPR 9096-1-1:2012	NPR 9998:2017 (§ 9.3.2.3)	Experiment		Symbol	NPR 9998:2017 Table F.2	Experiment	
							Single wythe	Double wythe			Single wythe	Double wythe
Compressive strength of masonry(MPa)		f_k'	8.5	7.4	7.9	5.0*	13.1	7.2	f_m'	8.5	14.0	9.3
Chord elastic modulus of masonry (MPa)		-	-	-	-	-	-	-	E_3	5000	4590	2951
Ratio between Young's modulus and characteristic/mean compressive strength		E_1/f_k'	700	700	700	700	334	386	E_1/f_m'	588	312	299
		E_2/f_k'					311	368	E_2/f_m'		290	286
		E_3/f_k'					350	411	E_3/f_m'		327	319
Flexural strength with the moment vector parallel to the bed joint and in the plane of the wall (MPa)		$f_{x1,k}$	0.1	-	0.2*	0.3*	0.11	0.09	f_{x1}	0.15	0.16	0.14
Flexural strength with the moment vector orthogonal to the bed joint and in the plane of the wall (MPa)		$f_{x2,k}$	0.2	-	0.79*	0.6*	0.43	0.27	f_{x2}	0.55	0.65	0.41
Ratio between horizontal out-of-plane bending and vertical out-of-plane bending		$f_{x1,k}/f_{x2,k}$	2	-	4.0	2.0	4.1	2.9	f_{x1}/f_{x2}	3.7	4.1	2.9
Initial shear strength (MPa)	Standard triplet	$f_{v0,k}$	0.2	-	0.2*	0.2*	0.16		f_{v0}	0.3	0.20	
	Modified triplet						0.10				0.12	
Initial coefficient of friction	Standard triplet	μ_k	-	-	-	-	-		μ	0.75	0.69	
	Modified triplet						-				0.80	
Fracture energy in bending parallel to the bed joint (N/m)									G_{fx1}	10	4	12
Fracture energy in bending perpendicular to the bed joint(N/m)									G_{fx2}	35	168	53
Fracture energy in compression (N/m)		loading direction perpendicular to the bed joint							G_{f-c}	20000	28500	34800
		loading direction parallel to the bed joint							$G_{f-c,h}$		35100	28300
Fracture energy in shear (N/m)		Standard triplet							G_{fII}	100	112	108
		Modified triplet										

* Minimum characteristic value prescribed by standard

References


- [1] Esposito, R., Meulman, E., Jafari, S. and Ravenshorst, G. (2016). Quasi-static cyclic tests on masonry components. Delft University of Technology. Report number C31B67WP3-3, version 2, 13 December 2016.
- [2] EN 1996-1-1+A1 (2013). Eurocode 6 – Design of masonry structures – Part 1-1: General rules for reinforced and unreinforced masonry structures. Nederlands Normalisatie-instituut (NEN).
- [3] Protocol for the construction of masonry, ver. 18-03-2015.
- [4] EN 1015-3 (1999). Method of test for mortar for masonry – Part 3: Determination of consistence of fresh mortar (by flow table). Nederlands Normalisatie-instituut (NEN).
- [5] EN 1015-11 (1999). Method of test for mortar for masonry – Part 11: Determination of flexural strength of hardened mortar. Nederlands Normalisatie-instituut (NEN).
- [6] EN 772-1 (2000). Methods of test for masonry units - Part 1: Determination of compressive strength. Nederlands Normalisatie-instituut (NEN).
- [7] Jafari, S., Panoutsopoulou, L. and Rots, J.G. Tests for the characterisation of original Groningen masonry. Delft University of Technology. Final report 18 December 2015.
- [8] Ad Vermeltfoort (2005). Brick-mortar interaction in masonry under compression, PhD thesis, Eindhoven University of Technology.
- [9] NEN 6790 (2005). Technical principles for building structures - TGB 1990 - Masonry structures - Basic requirements and calculation methods. Nederlands Normalisatie-instituut (NEN).
- [10] EN 1052-1 (1998). Method of test masonry – Part 1: Determination of compressive strength. Nederlands Normalisatie-instituut (NEN).
- [11] Esposito, R., Messali, F. and Rots J.G. (2016): Material characterisation of replicated masonry and wall ties. Delft University of Technology. Final report 18 April 2016.
- [12] Van Mier, J.G.M (1984). Strain softening of concrete under multiaxial loading conditions, PhD thesis, Eindhoven University of Technology.
- [13] Lourenco, P.B., De Borst, R. and Rots, J.G. (1997). A plane stress softening plasticity model for orthotropic materials. International Journal for Numerical Methods in Engineering 40(21), 4033-4057.
- [14] Vermeltfoort, A. D. (2005). Brick-mortar interaction in masonry under compression. Eindhoven, the Netherlands: Eindhoven University of Technology.
- [15] EN 1052-2 (1999). Method of test masonry – Part 2: Determination of flexural strength. Nederlands Normalisatie-instituut (NEN).
- [16] Pluijm R. Out-of-plane bending of masonry behaviour and strength: Technische Universiteit Eindhoven; 1999.
- [17] EN 1052-5 (2005). Method of test masonry – Part 5: Determination of bond strength by bond wrench method. Nederlands Normalisatie-instituut (NEN).
- [18] EN 1052-3 (2002). Method of test masonry – Part 3: Determination of initial shear strength. Nederlands Normalisatie-instituut (NEN).
- [19] NEN-EN 1996-1-1+C1/NB (2011). National Annex to NEN-EN 1996-1-1+C1 Eurocode 6: Design of masonry structures – Part 1-1: General rules for reinforced and unreinforced masonry structures. Nederlands Normalisatie-instituut (NEN) (in Dutch).
- [20] NPR 9096-1-1 (2012). Masonry structures – Simple design rules, based on EN 1996-1-1+C1. Nederlands Normalisatie-instituut (NEN) (in Dutch).
- [21] NPR 9998:2017. Assessment of structural safety of buildings in case of erection, reconstruction and disapproval – Basic rules for seismic actions: induced earthquakes (NEN).

- [22] Jafari, S. Esposito, R. (2016). Material tests for the characterisation of replicated calcium silicate brick masonry. Delft University of Technology. Report number C31B67WP1-9, version 01, 14 November 2016.

Appendix A


This appendix reports information on the brick and mortar used for the clay brick masonry as given by the producers. Table A.1 lists the characteristics of the clay bricks Euroa VB WF produced by Wienerberger. Table A.2 lists the composition of mortar BM2 version 2, having cement:lime:sand proportions equal to 1:2:9, produced by Remix.

Table A.1 – Declaration of performance of clay bricks (<http://wienerberger.nl/producten/euroa-vb#collapse-collapse1366232660485>, 28 July 2017).



Euroa VB WF

Euroa is een vormbak-sortering van Wienerberger Erlecom. Deze sortering is leverbaar in WF (exacte maten volgens fabrieksopgave). De precieze kleur van de steen kan afwijken van de getoonde afbeelding. Terca gevelbakstenen: kwalitatief hoogwaardige gevelbakstenen die bijdragen aan het creëren van een prettige, mooie en duurzame leefomgeving.

 Bestel monster

☐ Dit product selecteren voor vergelijking

Technische informatie

Gemiddelde maat	+/- 211 x 101 x 50 mm
Maattolerantie	T2
Maatspreiding	R1
Gemiddelde druksterkte \geq (N/mm ²)	35
Klasse vorstbestendigheid	F2 [D]
Initiële wateropzuigingscategorie	IW3 [normaal zuigend]
Bruto droge volumieke massa (kg/m ³)	1700
Vrijwillige wateropneming (Massa %)	20
Keurmerk	KOMO kwaliteitsverklaring en NL BSB productcertificaat
Toepassingsvoorwaarden	Dient te worden verwerkt overeenkomstig de geldende richtlijnen van Wienerberger.

Table A.2 – Composition of clay brick masonry mortar BM2 version 2 (Personal communication, 25 July 2016)

Raw material	Unit	Quantity
Cement CEM1 42.5R	kg	60
Limestone filler 0.09 mm	kg	40
Hydrated lime CL80S	kg	90
Sand (0.00-1.20 mm)	kg	630
Sand (1.20-3.55 mm)	kg	180
air entrained	kg	0.05